Stochastic Analysis of Medium Access Control in Wireless Ad Hoc Networks

無線アドホックネットワークにおけるメディアアクセス制御の統計学的解析

Thomas Bourgeois

Submitted to the Graduate School of Global Information and
Telecommunication Studies, Waseda University
in partial fulfillment of the requirements for the degree of

Doctor of Science in Global Information and Telecommunication Studies

WASEDA UNIVERSITY

February 2015

Thesis Supervisor: Shigeru Shimamoto
Title: Professor

Summary

An ad hoc network is composed of self-organizing radio transceivers communicating with one another. There is no hierarchy in an ad hoc network; therefore all nodes usually have the same characteristics and capabilities. Their practical applications include local device to device communications, sensor networks and environmental monitoring as well as emergency services.

Wireless ad hoc networks really emerged in the literature as a popular research topic at the early beginning of the 21st century and has remained an important part of the wireless field ever since. In a wireless ad hoc network, the medium access control protocol defines which transmitter-receiver pairs should be active at any given time. It attempts to find a trade-off between maximizing spatial reuse and minimizing interference. In large mobile wireless networks, the complexity of online algorithms for protocol parameter optimization becomes intractable. On the contrary, stochastic analysis based on the theory of point processes can provide design insights irrespectively of the network size. In this thesis, we present a stochastic analysis of various medium access control and communication mechanisms in wireless ad hoc networks. The analysis is based mathematically on the theory of multidimensional point processes. The mechanisms under study include a half-duplex single handshake, half-duplex multiple successive handshakes as well as a full-duplex two-way communication. The numerous closed form expressions derived enable to relate network and environment parameters to network performances. Their numerical analysis provides important practical insights regarding medium access control design and performance optimization in wireless ad hoc networks.

In more details, the presented doctoral work is composed of four main developments, each focusing on a different aspect of the subject. Those four parts are, namely: 1) the analysis of the performances of a link between a given node and its n-th closest neighbor given a deployment model with maximum entropy, 2) the analysis of the performances of a four-way handshake (i.e two successive handshakes) with control packet diversity, 3) the analysis of the impact of imperfect feedback on the performances of a handshake, and finally 4) the analysis of the performances of an in-band full-duplex simultaneous two-way transmission (as opposed to the other developments therein half-duplex operation is assumed). We now introduce in more details the research contributions of each of the developments mentioned above and which constitute each a distinct chapter of the thesis.

In chapter 2, we present the first stochastic analysis of link performances in an ad hoc network modelled by a single homogeneous Poisson point process (HPPP). According to the maximum entropy principle, the single HPPP model is mathematically the best model for random deployments with a given node density. However, previous works in the literature only consider a modified model which shows a discrepancy in the interference distribution with the more suitable single HPPP model. The main contributions of this chapter are as follows. 1) It presents a new mathematical framework leading to closed form expressions of the probability of success of both one-way transmissions and handshakes for a deployment modelled by a single HPPP. Our approach, based on stochastic geometry, can be extended to complex protocols and thus constitutes an important first step toward the accurate analysis of random ad hoc networks. 2) From the obtained results, all confirmed by comparison to simulated data, optimal PHY and MAC layer parameters are determined

and the relations between them is explained in details. This provides critical information directly applicable to practical protocol design. 3) The influence of the routing protocol on handshake performance is taken into account in a realistic manner, leading to the confirmation of the intuitive result that the effect of imperfect feedback is only negligible on the probability of success of a handshake between close neighbors.

Chapter 2 therefore considers a particular deployment model which is selected because it is mathematically the most able to predict actual network performances. However, more tractable models have the advantage to allow the study of more complex mechanisms. This is exemplified in the following chapters, the model thereof, although based on a HPPP, is not exactly a single HPPP.

In chapter 3, we present the stochastic analysis of a four-way handshake composed of a control handshake without spatial reservation and a traffic handshake, both preceded by a random test for medium access. Our framework takes into account time-varying channel impairments, the interference inherent to large ad hoc deployments and different decoding requirements for each packet as well as the influence of the routing protocol. Moreover, the proposed model also accounts for the impact of diversity in the control handshake. We obtain closed form expressions for the average frame success probability and the mean effective link throughput. Our results, confirmed by comparison to simulated data, provide the following twofold conclusions. In the presence of uncorrelated fading between control and traffic handshakes and given a fixed transmit-energy constraint: 1) as the diversity order increases, the diversity gain becomes counterbalanced by the loss due to increased control packet duration; hence the existence of an optimal diversity order value. 2) The design of throughput-optimal decoding requirements for the control packets is strongly influenced by the order of the control packet diversity.

In chapter 4, keeping the same framework as in chapter 3, we analyze the influence of imperfect feedback on the network performances using metrics taking into account the influence of both MAC and routing protocols. Throughout the chapter, we derive in closed forms the average link outage probability as well as the Average Spatial Density of Transport (ASDT) in a mobile multi-hop ad hoc network. All results are confirmed by comparison to simulated data and lead to two general conclusions. In the presence of fading uncorrelated between traffic and control handshakes, we observe the following. 1) Optimal contention is achieved by designing control packets decodable even in the presence of strong interference. 2) The impact of imperfect feedback on performances in an interference-limited mobile ad hoc network is not negligible.

Finally, in chapter 5, we extend our study of two-way network mechanisms to the case of In-Band Full Duplex (IBFD) operation. This mode of operation enables mobile radios to transmit and receive at the same time on the same frequency band; therefore, the average network throughput has the potential to be doubled. However, in an ad hoc setting, the implementation of IBFD would also result in a doubled density of interferers, a consequence so far overlooked in the literature. In this chapter, using a homogeneous Poisson point process-based deployment model, we determine an approximate yet accurate closed form for the joint probability of success of a two-way transmission in an IBFD ad hoc network. Both cases of ideal and imperfect Self-Interference Cancellation (SIC) are investigated. We then present a performance comparison of IBFD and its conventional counterpart In-Band Half Duplex (IBHD). Our study determines the environmental and network conditions in

which IBFD dominates in terms of spectral efficiency. Our theoretical results, confirmed by comparison to simulated data, provide key insights regarding the design of two-way transmissions in IBFD ad hoc networks. Notably, we observe that self-interference from reflections in the environment is particularly problematic for in-door applications using IBFD two-way transmissions but does not represent a key limiting factor in open, free space environments.

By extending the mathematical framework describing handshake-based medium access control and two-way communication mechanisms in wireless ad hoc networks, the present thesis provides an appreciable contribution to the related research areas. Notably, it provides important insights regarding the future development of such networks at the precise time when cellular networks are evolving toward more flexibility, smaller "ad hoc" network cells and device-to-device communication. This evolution supports the idea that large ad hoc networks are not simply an abstraction reserved to researchers, but actually an observable trend. Therefore, it is our belief that, in some cases, the work presented here may also find some application in predicting the behavior and performances of future 5G networks.

Acknowledgments

I would like to express my deepest gratitude to my supervisor, Professor Shigeru Shimamoto, who provided me with constant support and encouragement for my PhD course. I would like to thank Professor Sato, Professor Matsumoto, Professor Tsuda and Professor Nakajima for their reviews and comments. I would like to say my gratitude to the Ministry of Education, Culture, Sports, Science and Technology for its support through the MEXT scholarship. I am grateful to Ms. Miyagawa, Ms. Kishimoto and other GITS staff members, for their constant support and assistance. I would like to thank the fellow members of my laboratory, Dr.Liu Jiang, Zhenni Pan, Khourn Khemry and Mohamad Erick Ernawan for their useful discussions, comments and recommendations throughout my research. I am grateful to my friends who made my life in Japan a wonderful experience. Last but not least, I thank my wonderful family for their continuous love, blessing and respect.

Contents

List of Figures

List of Tables

Chapter 1

Introduction

1.1 Background and Definitions

1.1.1 Wireless Ad Hoc Networks

An ad hoc network is composed of self-organizing radio transceivers communicating with one another. There is no hierarchy in an ad hoc network, therefore all nodes usually have the same characteristics and capabilities (see figure 1-1 for an illustration). Their practical applications include local device to device communications, sensor networks and environmental monitoring as well as emergency services.

Wireless ad hoc networks is therefore a very broad category which includes simple two-node networks set up for device-to-device one-time file sharing as well as very large sensor networks operating for several hours or even days over a large region (e.g, a fleet of vehicles, building monitoring network, environment monitoring network, etc.). Consequently, the design of ad hoc networks has to account for this diversity of applications and scales as well as for the unplanned nature of their deployment.

Typically, mobile radios are battery-operated and therefore have limited resources to communicate with one another. Also, in a large deployment, given that the transmit power of each radio is limited, packets intended for an unreachable destination have to be sent through multiple hops. Consequently, the protocols ensuring the network performs its required tasks (i.e information transfer/exchange) have to deal with the issues of intra-

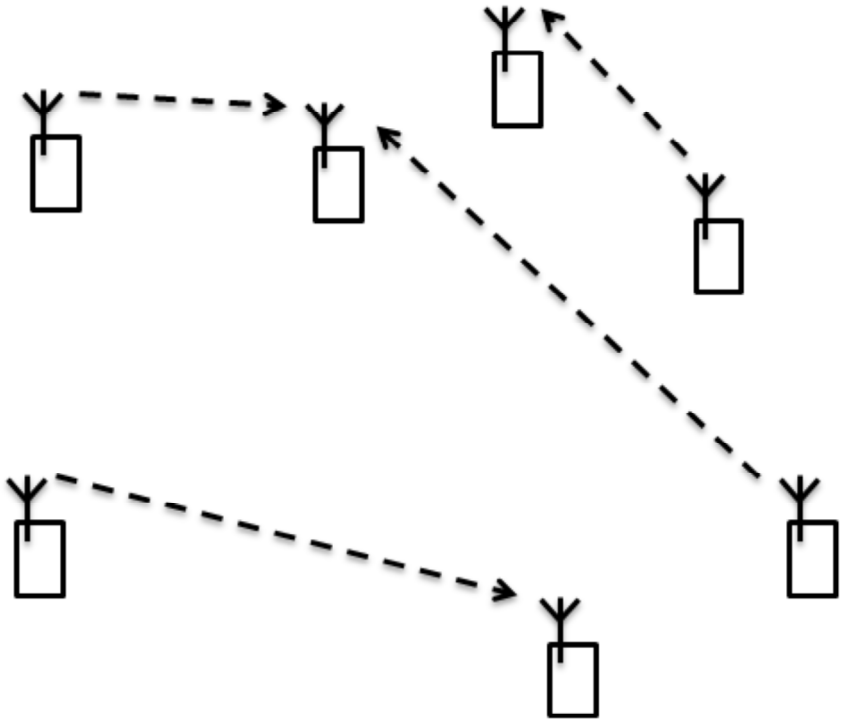

Figure 1-1: Illustration of a wireless ad hoc networks. Data transmissions are shown by arrows.

network interference and limited transmission and buffering resources.

These unique constraints on the design of protocols for wireless ad hoc networks call for new network control methods, different from those employed in the case of planned cellular networks or wired networks.

Wireless ad hoc networks really emerged in the literature as a popular research topic at the early beginning of the 21st century [39, 59, 14, 33, 45, 42, 23] and has remained an important part of the wireless field ever since. One can identify distinct research areas within this topic.

The first concerns networks of small to moderate size such as Wi-Fi networks with a mesh-type topology [40, 55, 58, 19] or even more simple Device-to-Device temporary links (e.g Bluetooth connection [22]). It is possible to create on-line self-optimizing MAC and routing protocols for such networks since the number of parameters to take into account in the process is finite and usually tractable. However, as the size of the network grows, the number of parameters becomes impractical to manage, especially in a mobile environment

where calculations need to be updated regularly.

Therefore, the second research area concerns such case therein the number of deployed nodes renders intractable any attempt of optimization of the network operation. Although it is impossible to determine the best control policy using on-line calculations based on measurements of the network state, it is still possible to obtain insights regarding the behavior of very large deployments using tractable analytical models. That is, a theoretical model of the network is used to predict its behavior in various scenarios. For instance, it can be used to analyze the influence on network performances of a particular MAC or routing protocol.

In the next subsection, we present in more details the notion of MAC protocol applied to wireless ad hoc networks, which is central to the present study.

1.1.2 Medium Access Control in Wireless Ad Hoc Networks

In a wireless ad hoc network, the MAC protocol defines which transmitter-receiver pairs should be active at any given time. It attempts to show a trade-off between maximizing spatial reuse and minimizing interference.

In its freest form, the MAC protocol allows nodes to transmit as soon as they have a packet ready. This is the principle which was introduced in the AlohaNET protocol, also simply known as ALOHA [1]. ALOHA is therefore the protocol providing maximum spatial reuse, since all nodes in the network may transmit at the same time. However, its total absence of interference control results in ALOHA showing very poor performances in large deployments.

A variant called Slotted-ALOHA was later introduced to reduce the impact of interference [15]. In Slotted-ALOHA, all network nodes are synchronized with one another and the time axis is divided into slots (see figure 1-2 for an illustration). Consequently, the chance that two transmissions interfere at least partially with each other is reduced.

Later, the principle of acknowledgment (ACK) packet used to confirm the reception of a previous packet was introduced as the notion of Quality of Service became increasingly preponderant in wireless networks.

This was quickly followed by the introduction of more complex MAC protocols able

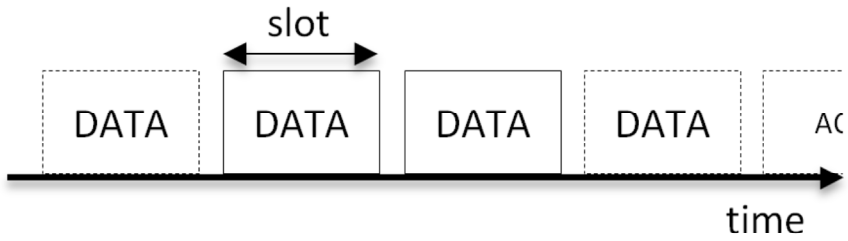

Figure 1-2: An illustration of the time structure of the Slotted-ALOHA protocol.

to control the level of interference in the network in a distributed manner. Popular examples of such protocol are Carrier Sense Multiple Access (CSMA) [36, 21, 41, 2] and its extension: CSMA/Collision Avoidance (CSMA/CA), popularized by the Distributed Coordination Function (DCF) which was implemented in networks based on the specification IEEE 802.11 [9].

In CSMA, network nodes sense the channel before transmitting each packet. If the power they receive during the sensing is greater than a certain threshold, they refrain from transmitting and wait for later opportunity. In CSMA/CA nodes sense the channel before transmitting as in CSMA. If a node detects a transmission opportunity, it transmits a control packet named Request-To-Send (RTS) to its intended receiver. The receiver upon detection of a RTS, replies with a packet named Clear-To-Send (CTS). Then the conventional exchange of Data and ACK packets follows. Other nodes in the surrounding detecting a RTS or a CTS automatically conclude that the channel is busy and refrain from transmitting. DCF is a variant of CSMA/CA in which nodes detecting a RTS or CTS not intended for themselves delay their transmission according to an exponential back-off mechanism.

Therefore in CSMA/CA, the RTS and CTS packets have what is called a spatial reservation effect. Indeed, nodes close enough to the transmitter of a RTS or CTS will remain silent for a certain duration after detecting such packet. CSMA/CA is effective in controlling the interference level in the network, but also has several drawbacks for large ad hoc networks which have been well documented [57]. In this thesis, we will therefore focus on MAC protocols which use control packets without spatial reservation effect.

1.2 Spatial Point Processes

1.2.1 Applications and Definition

A spatial point process is a random pattern of points in a d-dimensional space. It is useful to model scenarios where a large number of objects are located in space in a seemingly disorganized fashion. For instance, it can be used to model the position of a group of animals in a field ($d = 2$) or also to model the location of defects in a crystal ($d = 3$). In wireless communications, spatial point processes are used to model the deployment of wireless networks composed of a large number of radio equipments.

Mathematically, a spatial point process can be characterized by the distribution of the random number $\mathcal{N}(\mathcal{B})$ of nodes located in a given area $\mathcal{B} \subset \mathbb{R}^d$. Averaging $\mathcal{N}(\mathcal{B})$ over all possible realizations of a spatial point process, we obtain the intensity measure of the point process over $\mathcal{B}$ defined as $\Lambda(\mathcal{B}) = \mathbb{E}\{\mathcal{N}(\mathcal{B})\}$. The corresponding intensity function $\lambda(x)$ where $x \in \mathbb{R}^d$ is defined such that $\forall \mathcal{B} \subset \mathbb{R}^d, \Lambda(\mathcal{B}) = \int_{\mathcal{B}} \lambda(u)\, du$.

A spatial point process is said to be homogeneous if there exists a constant $\lambda \in \mathbb{R}^+$ such that, $\forall \mathcal{B} \subset \mathbb{R}^d$, $\Lambda(\mathcal{B}) = \lambda |\mathcal{B}|$ where $|.|$ denotes the Lebesgue measure on $\mathbb{R}^d$.

In practice, one often has to apply a particular transformation to each point of a spatial point process. In the case of a mapping transformation, the following theorem [29] characterizes the operation.

Theorem 1 (Mapping Theorem) *Let Φ be a spatial point process with intensity measure $\Lambda(.)$ and let $f : \mathbb{R}^d \to \mathbb{R}^s$ with $s \in \mathbb{N}^*$ be a measurable function such that $\Lambda(f^{-1}(\{y\})) = 0, \forall y \in \mathbb{R}^s$ and $\Lambda(f^{-1}(\mathcal{B})) < \infty, \forall \mathcal{B} \subset \mathbb{R}^d$. Then, the image of Φ by f is a spatial point process with intensity measure $\mu(\mathcal{B}) = \Lambda(f^{-1}(\mathcal{B}))$.*

In many applications, one is interested in the cumulative effect of some phenomenon taking place at each point of a spatial point process. In such cases, the Probability Generating Functional (PGFL) of the spatial point process often appears naturally as an important characteristic. The PGFL of a spatial point process is formally defined as follows [29].

Definition 1 (Probability Generating Functional) *For any mapping $v : \mathbb{R}^d \to \mathbb{R}^{*+}$ and a given spatial point process Φ, the PGFL of Φ is given by $\mathcal{G}(v) = \mathbb{E}\{\prod_{x \in \Phi} v(x)\}$.*

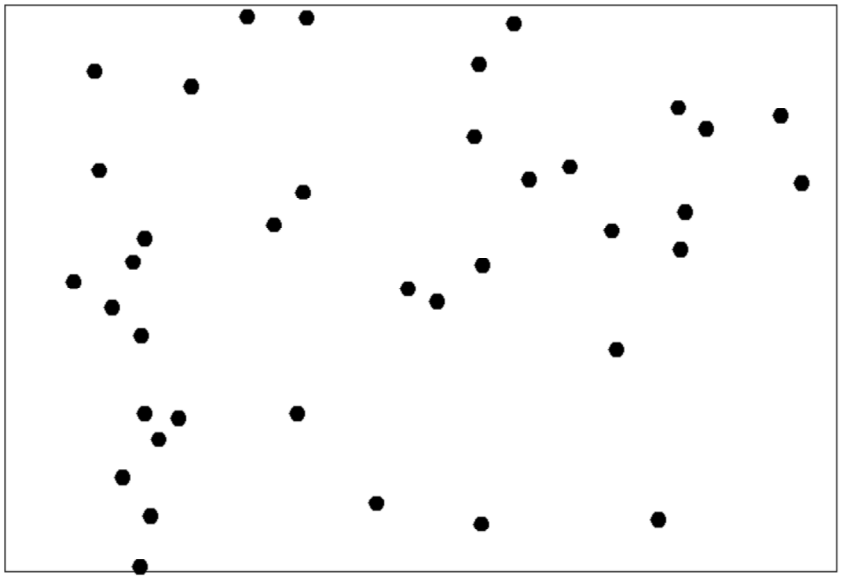

Figure 1-3: An example of two-dimensional point process.

In some other cases, instead of the product, the summation of all $v(x), \forall x \in \Phi$ will be of interest. In this case, Campbell's theorem provides the following useful integral form [29].

Theorem 2 (Campbell's Theorem) *For any application $v : \mathbb{R}^d \to \mathbb{R}^{*+}$ and a given spatial point process Φ over $\mathbb{R}^d$, we have*

$$\mathbb{E}\left\{\sum_{x\in\Phi} v(x)\right\} = \int_{\mathbb{R}^d} v(x)\,\Lambda(dx) \tag{1.1}$$

The most popular point process in the literature to model wireless ad hoc networks is the Homogeneous Poisson Point Process (HPPP) [16, 47, 7, 28, 48]. More point processes and their applications are described in [3], however in this thesis we focus our analysis on HPPP-based deployments. In the next subsection we provide a definition as well as the properties of the HPPP relevant to the understanding of this thesis.

1.2.2 The Homogeneous Poisson Point Process

In a HPPP of intensity λ, the number $\mathcal{N}(\mathcal{B})$ of nodes in a given region $\mathcal{B} \subset \mathbb{R}^d$ is Poisson-distributed with parameter $\lambda|\mathcal{B}|$.

Consequently, the HPPP has the highest entropy among all point processes of a given

average rate parameter (i.e, intensity λ) [16].

An important property of the HPPP is that its PGFL takes the following simple form [29].

Definition 2 (PGFL of a HPPP) *For a HPPP Φ with intensity λ and any application $v : \mathbb{R}^d \to \mathbb{R}^{*+}$, the corresponding PGFL is given by*

$$\mathcal{G}(v) = \exp\left(-\int_{\mathbb{R}^d} (1 - v(x))\, \Lambda(dx)\right) \tag{1.2}$$

In the following section, we introduce in more details how and why HPPP-based deployments are so popular in the literature on large wireless ad hoc networks.

1.3 Point Process-based Modelling of Wireless Ad Hoc Networks

In this section, we present how spatial point processes can be applied to the modelling of wireless ad hoc networks and describe the main models used up to now in the literature.

1.3.1 Criteria for Deployment Model Selection

The purpose of any deployment model is to represent actual deployments with as much accuracy as possible while preserving a certain degree of tractability for the purpose of analysis. The deployment of wireless ad hoc networks is intrinsically random, therefore this should be reflected in the choice of the deployment model; hence the importance of spatial point processes in this regard.

From the principle of maximum entropy, with no prior knowledge about the distribution of nodes in a wireless ad hoc network, it is best to choose a model with a minimum of prior information built in [34, 35]. Built-in information indicates any irregularity of the deployment, or, any feature of the deployment resulting from a conscious choice of construction. It is therefore reasonable to assume the deployment model to be homogeneous, so as to eliminate any such irregularity. The corresponding spatial point process therefore

has a constant intensity (which we may denote as λ). Moreover, among all point processes with a constant intensity, the HPPP is the one with maximum entropy. Therefore, modelling the deployment of an ad hoc network by a single HPPP is the most suitable choice, from a mathematical point of view.

Nevertheless, the selection of a certain model is worthless if the analysis based thereon eventually proves intractable.

1.3.2 Homogeneous Poisson Point Process-based Models

There exists several models in the literature constituting variants of the single HPPP. These models keep the main features of a single HPPP model but add also some noticeable modifications in order to dramatically reduce the complexity of analysis.

The main HPPP-based model used in the literature is as follows. The wireless ad hoc network is modelled by a HPPP of transmitters and a lone receiver located at a fixed distance from its intended transmitter. We denote this model as the "HPPP+1" model, as it consists of a HPPP and one additional node. An illustration is provided in figure 1-4.

The main interest of this model is to measure the cumulative interference at the receiver from all the transmitters except for the intended one. This is made possible through the use of a particular theorem specific to Poisson point processes. Indeed, from Slyvniak's theorem (see [29] for details), the distribution of a Poisson point process remains unchanged if a single point is removed from the process. A clear demonstration of this result necessitates the definition of several notions (e.g, the reduced Palm distribution of a point process) which are unused in the remainder of this thesis, hence the omission of a more advanced demonstration.

1.4 Organization of the Thesis

The remainder of the thesis is organized as follows. In chapter 2, we present the first stochastic analysis of link performances in an ad hoc network modelled by a single homogeneous Poisson point process (HPPP). This deployment model is the best model for a random deployment in a mathematical sense. However, its tractability is somehow limited

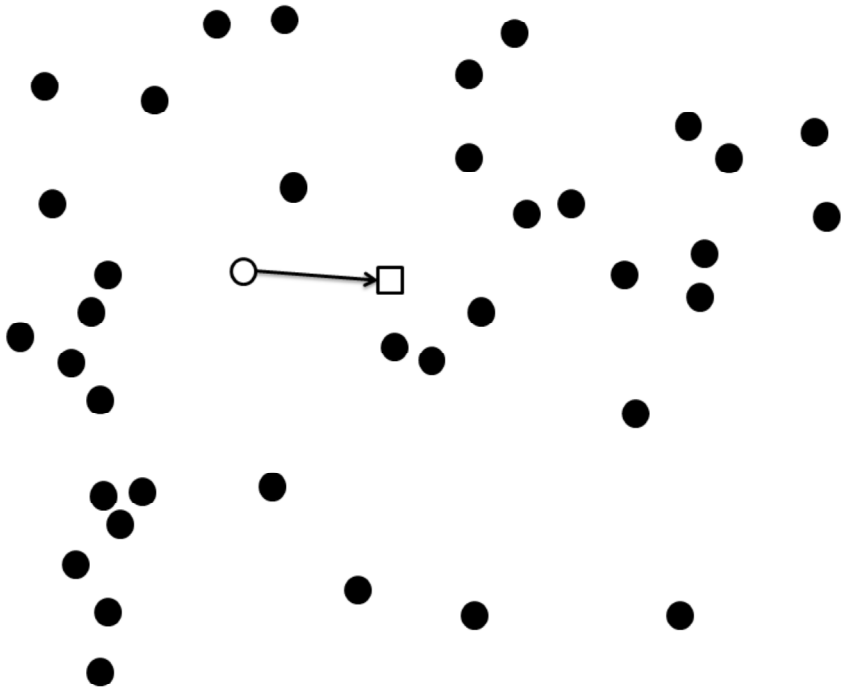

Figure 1-4: Illustration of the "HPPP+1" model. The receiver (square) receives a transmission from an intended transmitter (white circle) which is part of the HPPP of transmitters, like the interferers (black circles).

due to the complexity of the formulas obtained. In chapter 3, we present the stochastic analysis of a four-way handshake composed of a control handshake without spatial reservation and a traffic handshake, both preceded by a random test for medium access. The feedback packets are assumed error-free but the model accounts for the impact of diversity in the control handshake. In chapter 4, keeping the same framework as in chapter 3, we analyze the influence of imperfect feedback on the network performances using metrics taking into account the influence of both MAC and routing protocols. In chapter 5, we extend our study of two-way network mechanisms to the case of In-Band Full Duplex (IBFD) operation. We present a performance comparison of IBFD and its conventional counterpart In-Band Half Duplex (IBHD). Our study determines the environmental and network conditions in which IBFD dominates in terms of spectral efficiency. Finally, a conclusion summarizes the thesis.

Chapter 2

Stochastic Analysis of Random Ad Hoc Networks with Maximum Entropy Deployment

The conventional approach for the stochastic analysis of a one-way transmission in an ad hoc network consists in modelling the transmitter set (including the intended transmitter) as an HPPP while the intended receiver Rx is assumed to be located at a given distance from the intended transmitter Tx.[29, 26, 25, 6, 20, 4, 53]. Then, using the Probability Generating Functional (PGFL) of an HPPP combined with Slivnyak's theorem[29], one can determine the transmission success probability from Tx to Rx. The same method can be used to model two-way transmissions (see [54]). In that case, a HPPP of receivers is constructed by translation of the HPPP of transmitters and the method used for one-way transmissions is used in both transmit directions. However, Slivnyak's theorem states in substance that the effect of discarding Tx from the interferer set can be completely ignored. That is, the interference is treated as if all nodes including Tx caused interference to Rx. This result is valid to the conditions that Rx is **not** part of the HPPP of transmitters and is located at a **fixed** distance from Tx. We will later refer to this model as the "HPPP+1" model, as it is composed of an HPPP of transmitters and a lone receiver.

However, we stated earlier that mathematically the best statistical model for an ad hoc network is a **single** HPPP, which includes all nodes (i.e Tx, Rx and all transmitters and

receivers). Therefore, there is a discrepancy between the most natural statistical model for ad hoc networks (i.e the "single HPPP" model) and the conventional theoretical model used to derive their performances (i.e the "HPPP+1" model).

To the best of our knowledge, there is no work in the literature regarding the statistical analysis of the link performance in an ad hoc network using the "single HPPP" model, hence the motivation for the present work.

The main contributions of this chapter are as follows. 1) It presents a new mathematical framework leading to closed form expressions of the probability of success of both one-way transmissions and handshakes for a deployment modelled by a single HPPP. Our approach, based on stochastic geometry, can be extended to complex protocols and thus constitutes an important first step toward the accurate analysis of random ad hoc networks. 2) From the obtained results, all confirmed by comparison to simulated data, optimal PHY and MAC layer parameters are determined and the relations between them is explained in details. Therefore, they represent critical information directly applicable to practical protocol design. 3) The influence of the routing protocol on handshake performance is taken into account in a realistic manner, leading to the confirmation of the intuitive result that the effect of imperfect feedback is negligible on the probability of success of a handshake between close neighbors.

Parts of this work was presented in [10]. However, the present chapter provides complete, revisited proofs, more detailed explanations as well as additional simulation results. Throughout the chapter, we aim to obtain the probability of success of a transmission (one-way and handshake) to the k-th nearest neighbor in an ad hoc network modelled by a single HPPP in which nodes employ Slotted-ALOHA (without and with Acknowledgement, respectively). The remainder of this chapter is organized as follows. In section 2.1, we present our general system model and some preliminary results regarding interference modelling in a network modelled by a single HPPP. In section 2.2, exploiting results from section 2.1, we calculate the transmission success probability between two arbitrarily chosen nodes in the network. Reasonable approximations are used to render the analysis tractable. In section 2.3, we apply the results of the sections 2.1 and 2.2 to the cases of the MAC protocols S-ALOHA and S-ALOHA with ACK packet. In section 2.4, we vali-

date the approximate theoretical expressions obtained in the previous section by comparing them to computer simulation results and analyze the conditions for their validity. Finally, in section 2.5 a conclusion summarizes the chapter.

2.1 System Model and Preliminary Results

2.1.1 Deployment and channel models

In the remainder, independently of the protocols considered and before specific roles (i.e, transmitter or receiver) are attributed, node deployment is always assumed to be modelled by a d-dimensional HPPP with intensity λ.

The channel model incorporates path-loss and fast fading. The path-loss will follow the unbounded power law $l(r) = r^{-\alpha}$ where α is called the path-loss coefficient. Note that in general path-loss models should be bounded (i.e, the received power is at most equal to the transmitted one)[32]. The choice of an unbounded path-loss model is reasonable only if the distance between nodes is greater than a certain threshold (unity, in our case). Thus, our model will only be relevant for node density values such that the inter-node distance is greater than unity with high probability. More detailed conditions on the node density are discussed in section IV.

The fading will be Rayleigh distributed, the square thereof then following an exponential distribution with a rate parameter equal to one. Transmissions in the network will be slotted and the fading will be assumed to be constant over the duration of a slot and independent from one slot to another. Moreover, we will always assume fading coefficients of all links to be independent from one another, independent of node position and identically distributed.

Since our goal is to analyze the influence of a large number of simultaneous transmissions on the network performances, we will also assume the network to be interference-limited. Hence, as in [29, 5], a transmission will be considered successful if the received signal power S from the intended transmission is greater than the interference I generated by all other transmissions by a factor larger than a given threshold θ. That is, the inequal-

ity $\frac{S}{I} > \theta$ must be true for a transmission to be successful. The validity conditions for the combination of the interference-limited model with an unbounded path-loss model are presented in section 2.4.

2.1.2 Interference model

Let us consider a given network node denoted as Rx. For any realization of the HPPP, we can sort other nodes by order of distance to Rx. Let us define for a given slot the random squared fading coefficient G_i ($i = 1, ..., \infty$) of the channel between the i-th closest node and Rx, R_i the random distance from the i-th closest node to Rx. Furthermore, for all realizations of the HPPP, let us assume that the n-th closest node has a packet for Rx and that all nodes except Rx transmit during the slot. For a receiver threshold θ, the probability for this intended transmission to be successful is given by

$$p_{rx}^{n}(\theta) = \mathbb{E}\left\{\mathbb{P}\left(G_n > \theta R_n^{\alpha} \sum_{i=1, i\neq n}^{\infty} G_i R_i^{-\alpha} \left| \vec{R}_{1,\infty}, \vec{G}_{1,\infty\setminus n} \right.\right)\right\} \tag{2.1}$$

where $p_{rx}^{n}(\theta)$ denotes the transmission in a "receiver-centric" approach, with the n-th neighbor being the transmitter and $\mathbb{E}\{.\}$ is the expectation operator over the random vectors $\vec{R}_{1,\infty} = [R_1, ..., R_\infty]^T$ and $\vec{G}_{1,\infty\setminus n} = [G_1, ..., G_{n-1}, G_{n+1}, ..., G_\infty]^T$. Then, given that the Complementary Cumulative Distribution Function of an exponential variable with rate parameter one is $F^c(x) = e^{-x}$, we obtain from (2.1),

$$\begin{aligned} p_S(\theta) &= \mathbb{E}_{R_n, I}\left\{e^{-\theta R_n^{\alpha} I} | R_n, I\right\} \\ &= \mathbb{E}_{R_n}\left\{L_I\left(\theta R_n^{\alpha}\right) | R_n\right\} \end{aligned} \tag{2.2}$$

where $I = \sum_{i=1, i\neq n}^{\infty} G_i R_i^{-\alpha}$ is the interference term and $L_I(s) = \mathbb{E}_I\left\{e^{-sI}\right\}$ is its Laplace Transform. In the following subsections, we determine the Laplace Transform of the interference originating from two important node sets.

2.1.3 Interference from the $n-1$ closest interferers

Keeping the scenario from the last subsection, consider the $n-1$ closest nodes to Rx. These nodes are uniformly distributed over a d-dimensional ball with random radius R_n deprived from its center. However, given that the volume occupied by the center point (where Rx is located) is null, we may as well consider the $n-1$ nodes to be uniform over the whole ball. Thus, the $n-1$ nodes form a BPP with random intensity $\lambda = \frac{n-1}{c_d R_n^d}$ where c_d indicates the volume of a d-dimensional ball with unit radius. In these conditions, we have the following property.

Proposition 1 *Consider the annular region $\mathcal{A}(Rx, A, B)$ with center Rx, inner radius A and outer radius $B < R_n$. Also, given that there are exactly k interferers in the annular region $\mathcal{A}(Rx, A, B)$, the Laplace Transform of the interference they generate at Rx is given by:*

$$L_{I_{\mathcal{A}(Rx,A,B)|k}}(s) = \left(1 + \frac{B^d \Omega(s,B) - A^d \Omega(s,A)}{B^d - A^d}\right)^k \tag{2.3}$$

with

$$\begin{aligned}\Omega(s,X) = &\frac{F\left(1,1,1-\frac{d}{\alpha}, \frac{sX^{-\alpha}}{1+sX^{-\alpha}}\right)}{1+sX^{-\alpha}} \\ &- B\left(1-\frac{d}{\alpha}, 1+\frac{d}{\alpha}\right) s^{\frac{d}{\alpha}} X^{-d} - 1\end{aligned} \tag{2.4}$$

where $F(a,b,c,x)$ is the Gaussian hypergeometric function and $B(a,b)$ denotes the Beta function. To ease numerical computation, a simple approximation of $\Omega(s,X)$ is proposed in section IV.

***Proof* 1** *See appendix A.*

The Laplace Transform of the interference at Rx originating from all nodes in the ball, save the center, can be obtained by setting $B = R_n$, $k = n-1$ and making A converge toward zero. Then, to obtain a closed form expression, one may use (2.3) and the following proposition.

Proposition 2 *The limit of $A^d\Omega(s,A)$ for A converging toward zero is given by*

$$\lim_{A\to 0^+} A^d\Omega(s,A) = 0 \tag{2.5}$$

***Proof* 2** *See appendix B.*

Remark 1 *We note also that setting $s = \theta r^\alpha$, $A = ar$ and $B = br$ where $a,b > 0$ in (2.4) renders the Laplace Transforms in (2.3) independent of r, for any $r > 0$.*

The above property will prove useful when considering (2.2). Hence, for notational convenience, we will define the following function.

Definition 3 *For any positive real numbers a and b such that $a \leq b$,*

$$\Phi(\theta,a,b) = L_{I_{\mathcal{A}(O,ar,br)|1}}(\theta r^\alpha)$$

for all $r > 0$. Note that $\Phi(\theta,a,b)$ will be denoted as $\Phi(a,b)$ in the following for the sake of brevity when the threshold considered is clear from the context.

2.1.4 Interference from nodes beyond the *n*-th neighbor

Keeping the scenario presented in subsection 2.1.2, we now consider all nodes further away from *Rx* than the *n*-th closest node. In these conditions, we have the following property.

Proposition 3 *The Laplace Transform of the interference generated by all nodes away from Rx by a distance greater than R_n is given by*

$$L_{I_{\mathbb{R}^d/\mathcal{B}(Rx,R_n)}}(s) = e^{-\lambda c_d R_n^d\left(\Omega(s,R_n)+B\left(1-\frac{d}{\alpha},1+\frac{d}{\alpha}\right)s^{\frac{d}{\alpha}}R_n^{-d}\right)} \tag{2.6}$$

***Proof* 3** *See appendix C.*

In the following sections, we present general expressions of transmission success probabilities for various scenarios in the single HPPP model.

2.2 Transmission Success Probability in an ad hoc network modelled as a single HPPP

2.2.1 Neighbor index definition

In this subsection, we introduce the notion of neighbor index. As mentioned briefly in introduction, although employing the PGFL leads to a simple expression of the transmission success probability, it is only valid for a given transmitter-receiver distance. However, in the case of a single HPPP, this distance is random with an unknown distribution (since both nodes are part of the original generating HPPP). Conditioning transmitter and receiver on their mutual neighbour indexes allows to define the distance distribution and thus enables averaged results to be inferred.

The neighbour index is defined as follows.

Definition 4 *For two distinct network nodes Tx and Rx, Tx has neighbour index $n \in \mathbb{N}^*$ with respect to Rx, which we denote $\mathcal{I}_{Rx}(Tx) = n$, if there exists exactly $n-1$ nodes closer from Rx than Tx. If the identity of nodes is clear from the context, one may simply write $\mathcal{I} = n$.*

From this definition, two different approaches can be considered. In the receiver-centric approach, transmitters with a packet intended for a given receiver (namely, "intended transmitters", as opposed to "interferers") are conditioned on their neighbour index with respect to the considered receiver node. In the transmitter-centric approach, it is the receiver which is conditioned on its neighbour index with respect to the intended transmitter. The following conditional probability mass function (p.m.f) $\mathcal{F}(n,k)$ will prove useful in order to relate both approaches. For Tx and Rx being two distinct network nodes, we define

$$\mathcal{F}(n,k) = \mathbb{P}\left(\mathcal{I}_{Tx}(Rx) = n \,\middle|\, \mathcal{I}_{Rx}(Tx) = k\right) \tag{2.7}$$

When the identity of nodes is clear from the context, we will use simply $\mathcal{I}$ instead of $\mathcal{I}_{Tx}(Rx)$ and its symmetric $\mathcal{I}_{sym}$ instead of $\mathcal{I}_{Rx}(Tx)$ to denote neighbour indexes.

Proposition 4 *For points taken from a d-dimensional HPPP , the p.m.f in (2.7) is given by*

$$\mathcal{F}(n,k) = \sum_{l=0}^{m-1} w_{n,k}(l) \tag{2.8}$$

where

$$w_{n,k}(l) = \binom{k-1}{l}\binom{n+k-l-2}{k-1}\frac{\beta_d^l (1-\beta_d)^{n+k-2l-2}}{(2-\beta_d)^{n+k-l-1}}$$

and $m = \min(n,k)$. *Also, for* $\|TxRx\| = x \in \mathbb{R}^{*+}$ *and two d-dimensional balls* $\mathcal{B}_d(Tx,x)$ *and* $\mathcal{B}_d(Rx,x)$, $\beta_d = \beta_d$ *defined as* $\beta_d = \frac{\left|\mathcal{B}(Tx,x)\bigcap\mathcal{B}(Rx,x)\right|}{\left|\mathcal{B}(Tx,x)\right|} = B_{\frac{3}{4}}\left(\frac{d+1}{2},\frac{1}{2}\right)$ *with* $B_x(a,b)$ *denoting the incomplete Beta function.*

***Proof* 4** *The proof for (2.8), if slightly incorrect, was given in [46]. Indeed, in this reference, the author did not consider that the number of points in* $\mathcal{B}(Tx,x)\bigcap\mathcal{B}(Rx,x)$ *is at most* $\min(n,k)-1$. *Nevertheless, this is a minor error which does not invalidate the thought process of the proof provided, hence the omission of its presentation in this chapter. However, we provide in appendix the proof that the p.m.f as defined above does satisfy the normalization condition.*

Also, for notational convenience, we will define for the remainder $[y]_p = py + 1 - p$, which will prove useful when dealing with the expected value $\mathbb{E}\left\{y^X\right\}$ where $y \in \mathbb{R}$ and X is binomially distributed according to $X \sim \mathfrak{B}(N,p)$.

In the following subsections, we show how the preliminary results developed above may be used to obtain the transmission success probability in various contexts.

2.2.2 Receiver-centric approach for a single intended transmission

In this subsection, we consider the scenario described in subsection II-B.

Theorem 3 *Given that* $\mathcal{I}_{Rx}(Tx) = n$, *the probability of success for a transmission from* Tx *to* Rx *is given by*

$$p_{rx}^n(\theta) = \frac{\Phi(0,1)^{n-1}}{\left(1+\Omega(\theta x^\alpha,x)+B\left(1-\frac{d}{\alpha},1+\frac{d}{\alpha}\right)\theta^{\frac{d}{\alpha}}\right)^n} \tag{2.9}$$

Proof 5 *The proof relies on the observation that, according to the independence of the number of nodes in disjoint areas in a HPPP, the transmission success probability can be written as follows.*

$$p_{rx}^{n}(\theta) = \mathbb{E}_{R_n}\left\{\prod_{j=1}^{\infty} L_{I_{\mathcal{S}_j(R_n)}}\left(\theta R_n^{\alpha}\right)\right\} \tag{2.10}$$

where R_n is the distance from Rx to Tx and $\left\{\mathcal{S}_j(R_n)\right\}_{j=1,\ldots,\infty}$ is a complete partition of the d-dimensional space into disjoint areas functions of R_n and $I_{\mathcal{S}_j(R_n)}$ is the interference contribution from the nodes located in the area $\mathcal{S}_j(R_n)$. In the following, we find a tractable decomposition of the space.

The $n-1$ "close" interferers located in $\mathcal{B}(Rx, R_n)$ form an homogeneous BPP, while the "far" interferers (i.e, away from Rx by a distance greater than R_n) form an inhomogeneous PPP . Let us define the following regions:

$$\mathcal{S}_{n-} = \mathcal{B}(Rx, R_n)$$
$$\mathcal{S}_{n+} = \overline{\mathcal{B}(Rx, R_n)}$$

These two regions being disjoint, their node distributions are independent, thus the interference $I_{n-}(R_n)$ at Rx due to the "close" interferers and the interference $I_{n+}(R_n)$ at Rx due to the "far" interferers are independent. As a consequence, from (2.6) and from (2.3) for $A \to 0^{+}$, $B = R_n$ with $n-1$ nodes in $\mathcal{A}(Rx, A, B)$, we obtain that the success probability of a transmission from Tx to Rx can be expressed as

$$\begin{aligned} & p_S\left(\theta \middle| \mathcal{I}_{Rx}(Tx) = n\right) \\ &= \mathbb{E}_{R_n}\left\{L_{I_{n-}(R_n)}\left(\theta R_n^{\alpha}\right) L_{I_{n+}(R_n)}\left(\theta R_n^{\alpha}\right)\right\} \\ &= \mathbb{E}_{R_n}\left\{\Phi(0,1)^{n-1}\, e^{-\lambda c_d R_n^{d}\left(\Omega\left(\theta R_n^{\alpha}, R_n\right) + B\left(1-\frac{d}{\alpha}, 1+\frac{d}{\alpha}\right)\theta^{\frac{d}{\alpha}}\right)}\right\} \end{aligned} \tag{2.11}$$

From [46], the distance in a d-dimensional PPP from a node to its n-th nearest neighbour

is governed by the probability density function (p.d.f)

$$f_{R_n}(r) = d\frac{(\lambda c_d)^n}{\Gamma(n)} r^{dn-1} e^{-\lambda c_d r^d} \tag{2.12}$$

Taking the expectation of (2.11) with respect to $R_n = \|TxRx\|$ thus leads to an integral of the form $\int_0^{+\infty} r^{dn-1} e^{-\mu r^d} dr$ where $\mu > 0$, which can be solved easily by applying the variable substitution $y = \mu r^d$ and then recognizing in the ensuing integral the Gamma function $\Gamma(n)$. The final result follows then easily, which completes the proof.

2.2.3 Transmitter-centric approach for a single intended transmission

We now consider the transmitter-centric approach.[1]

Theorem 4 *The probability of a successful transmission from Tx to Rx, conditioned on $\mathcal{I}_{Tx}(Rx) = k$, can be approximated by*

$$p_{tx}^k(\theta) \approx \frac{\Phi(1,2)^{k-1}}{(1+K(\theta))^k} \tag{2.13}$$
$$\mathbb{E}_{\mathcal{I}}\left\{\Phi(0,1)^{\mathcal{I}-1}\left[\Phi(1,2)^{-1}\right]_{\beta_d}^{\min(\mathcal{I},k)-1} \middle| \mathcal{I}_{sym} = k\right\}$$

where $K(\theta) = 2^d \Omega(\theta x^\alpha, 2x) + B\left(1-\frac{d}{\alpha}, 1+\frac{d}{\alpha}\right)\theta^{\frac{d}{\alpha}}$
$+ \left(2^d - 2 + \beta_d\right)(1 - \Phi(1,2))$.

where $p_{tx}^k(\theta)$ denotes the transmission in a "transmitter-centric" approach, with the k-th neighbour being the receiver.

***Proof* 6** *Provided that $\mathcal{I}_{Tx}(Rx) = k$, $\mathcal{I}_{Rx}(Tx)$ is a random variable with distribution given by (2.7) and $R = \|TxRx\|$ is distributed according to (2.12) in which n is replaced by k.*

[1] The expectation in the expression of transmission success probability for the transmitter-centric approach is on the discrete random variable $\mathcal{I}$, which leads to an infinite sum. In practice, computing the first few terms produces values very close to the actual result.

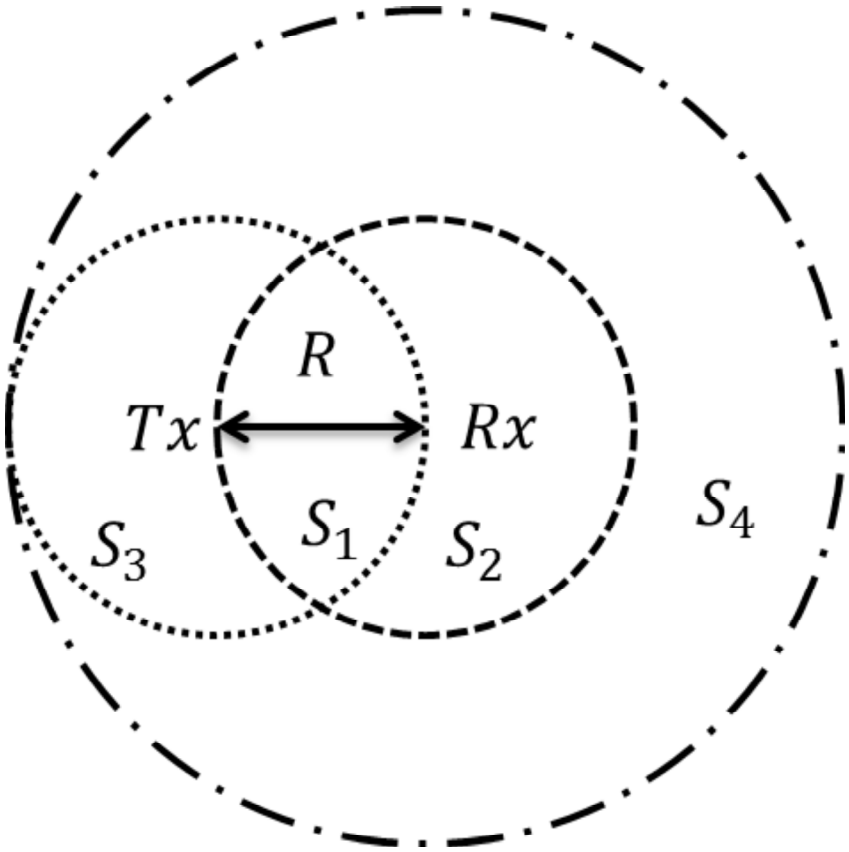

Figure 2-1: Illustration of the interference situation at a receiver Rx given an intended transmitter Tx located at distance R. The different zones in the figure are defined in (2.14).

Under these conditions, we consider the following partition of $\mathbb{R}^d$.

$$\begin{aligned}
\mathcal{S}_1(R) &= \mathcal{B}_d(Rx,R) \cap \mathcal{B}_d(Tx,R) \\
\mathcal{S}_2(R) &= \mathcal{B}_d(Rx,R) \cap \overline{\mathcal{B}_d(Tx,R)} \\
\mathcal{S}_3(R) &= \overline{\mathcal{B}_d(Rx,R)} \cap \mathcal{B}_d(Tx,R) \\
\mathcal{S}_4(R) &= \mathcal{A}(Rx,R,2R) \cap \overline{\mathcal{S}_3}
\end{aligned} \tag{2.14}$$

The geometry of these zones is illustrated in Fig.2-1. In the following, we simply denote $\mathcal{S}_j(R)$ *as* $\mathcal{S}_j$ *for the sake of brevity.*

We observe that $\mathcal{N}(\mathcal{S}_1)$ *is a binomially distributed random variable* $\mathfrak{B}(\mathcal{M}-1,\beta_d)$, *where* $\mathcal{M} = \min(\mathcal{I}_{Rx}(Tx), k)$.

Partitioning the space using the above-defined regions, the transmission success prob-

ability can be expressed as

$$
\begin{aligned}
& p_{tx}^{k}(\theta) = \\
& \mathbb{E}_{R,\mathcal{I}_{Rx}(Tx)}\left\{\Phi(0,1)^{\mathcal{I}_{Rx}(Tx)-1}\,\mathbb{E}_{\mathcal{N}(\mathcal{S}_1)}\left\{L_{I_{\mathcal{S}_3}}(\theta R^{\alpha})\right\}\right. \\
& \mathbb{E}_{\mathcal{N}(\mathcal{S}_4)}\left\{L_{I_{\mathcal{S}_4}}(\theta R^{\alpha})\right\} \\
& \left. e^{-\lambda c_d R^d\left(2^d\Omega(\theta R^{\alpha},2R)+B\left(1-\frac{d}{\alpha},1+\frac{d}{\alpha}\right)\theta^{\frac{d}{\alpha}}\right)}\right\}
\end{aligned}
\tag{2.15}
$$

We note that $L_{I_{\mathcal{S}_3}}(\theta R^{\alpha})$ is dependent on $\mathcal{N}(\mathcal{S}_1)$, through the relation $\mathcal{N}(\mathcal{S}_3) = k - 1 - \mathcal{N}(\mathcal{S}_1)$ while the remaining functions are only dependent on $\mathcal{I}_{Rx}(Tx)$ and R. From the properties of HPPPs , the number of nodes in $\mathcal{S}_4$ is Poisson distributed and independent of the number of nodes in other regions.

The distance from Rx to any node uniformly distributed in $\mathcal{S}_3$ (or in $\mathcal{S}_4$, respectively) follows a distribution with a non-trivial expression, rendering difficult any attempt to compute a closed form expression for the Laplace Transform of the interference contribution from nodes located in these regions.

Approximation 1 *The distribution of the distance from Rx to a node in the above-mentioned regions can be approximated by the distribution of the distance from Rx to a node uniformly deployed over the annular region $\mathcal{A}(Rx, R, 2R)$.*

A reasonable justification for this approximation is as follows. In order to obtain a simple approximation regarding a distribution, one may successively "forget" part of the constraints on the actual distribution and select the maximum-entropy distribution fitting the remaining constraints, if it exists. In our case, removing information regarding the shapes of $\mathcal{S}_3$ and $\mathcal{S}_4$, the only remaining knowledge we have is that both zones are inside $\mathcal{A}(Rx, R, 2R)$. However, the uniform distribution is the maximum entropy distribution among all continuous distributions supported in a bounded set, given that no other statistical characteristics are known about the actual distribution. Consequently, it is also the optimal distribution estimate for the actual distribution of nodes, according to the maximum entropy principle. [2]

[2]The actual distribution in our case can be calculated, but is of little interest for our analysis. The approx-

As a result, the interference generated by a given number of nodes in $\mathcal{S}_3$ (or $\mathcal{S}_4$) may be approximated by the interference due to the same number of nodes uniformly distributed in $\mathcal{A}(Rx, R, 2R)$.

Using the above lemma for $\mathcal{S}_3$, we obtain

$$\begin{aligned}
&\mathbb{E}_{\mathcal{N}(\mathcal{S}_1)}\left\{L_{I_{\mathcal{S}_3}}(\theta R^\alpha)\right\} \approx \\
&\sum_{i=0}^{\mathcal{M}-1}\binom{\mathcal{M}-1}{i}\beta_d^i(1-\beta_d)^{\mathcal{M}-1-i}\,\Phi(1,2)^{k-1-i} \\
&= \Phi(1,2)^{k-1}\left(\frac{\beta_d}{\Phi(1,2)}+1-\beta_d\right)^{\mathcal{M}-1}
\end{aligned} \tag{2.16}$$

where the last line follows from the binomial theorem.

Regarding $\mathcal{S}_4$, given that $|\mathcal{S}_4| = \left(2^d - 2 + \beta_d\right) c_d R^d$, we have from the definition of the Poisson distribution that

$$\begin{aligned}
&\mathbb{E}_{\mathcal{N}(\mathcal{S}_4)}\left\{L_{I_{\mathcal{S}_4}}(\theta x^\alpha)\right\} \approx \\
&e^{-\lambda\left(2^d-2+\beta_d\right)c_d R^d}\sum_{j=0}^{+\infty}\frac{\left(\lambda\left(2^d-2+\beta_d\right)c_d R^d\right)^j}{j!}\Phi(1,2)^j \\
&= e^{-\lambda c_d R^d\left(2^d-2+\beta_d\right)(1-\Phi(1,2))}
\end{aligned} \tag{2.17}$$

Further taking the expectation over $\mathcal{I}_{Rx}(Tx)$ and then taking the expectation over R in (2.15) leads to an integral that can be solved in the exact same way as the one leading to (2.9), which completes the proof.

In the next section, we show how results calculated up to now may be applied to the analysis of performances of some simple Medium Access Control protocols for ad hoc networks.

imation by a uniform distribution is first and formost a convenient mean to obtain closed-form expressions, which are of more practical interest than complicated, though accurate, integral forms.

2.3 Application to Slotted-ALOHA protocol analysis

In this section, we analyze the success probability of transmissions in an ad hoc network employing the MAC protocols Slotted-ALOHA with and without ACK packet. The system model used in the following is as described in subsection 2.1.1.

2.3.1 Case of S-ALOHA with constant Medium Access Probability

In previous sections, we considered that all nodes in the network were active transmitters, except for a single receiver Rx. However, node activity in real networks is controlled by the MAC protocol.

In a Slotted-ALOHA (S-ALOHA) protocol with fixed Medium Access Probability (MAP) p, each node in the network with a packet to transmit does so during the next slot if it passes a random test with success probability p, and stays silent otherwise.[5] We assume in the following that all silent nodes can act as receiver. Let us further assume that nodes always have at least one packet ready for transmission and that consequently all nodes passing the random test do transmit. Then, let us consider an ad hoc network modelled as an HPPP $\mathcal{X}$ with constant intensity λ. In this case, employing an S-ALOHA protocol with constant MAP p results, from the thinning properties of PPPs [29], in the separation of the original HPPP into two distinct HPPPs. Namely, $\mathcal{X}_1$ with intensity $p\lambda$ and $\mathcal{X}_0$ with intensity $(1-p)\,\lambda$, which correspond to active transmitters and silent nodes, respectively.

We now proceed to calculate the transmission success probability for both transmitter-centric and receiver-centric approaches.

Theorem 5 *Consider an intended transmitter $Tx \in \mathcal{X}_1$ being the n-th nearest neighbour in $\mathcal{X}$ of a receiver node $Rx \in \mathcal{X}_0$. In this receiver-centric model, the probability of success of a transmission from Tx to Rx is given by*

$$p_{rx}^{n}(\theta) = \frac{\left[\Phi(0,1)\right]_{p}^{n-1}}{\left(1 + p\Omega\left(\theta x^{\alpha}, x\right) + pB\left(1-\frac{d}{\alpha}, 1+\frac{d}{\alpha}\right)\theta^{\frac{d}{\alpha}}\right)^{n}} \tag{2.18}$$

Proof 7 *We firstly observe the following results. The independent thinning of the original*

process $\mathcal{X}$ has for consequence that, for any given bounded set $\mathcal{S} \subset \mathbb{R}^d$, the number of active transmitters $\mathcal{N}_1(\mathcal{S})$ in $\mathcal{S}$ is binomially distributed (i.e $\mathcal{N}_1(\mathcal{S}) \sim \mathfrak{B}(\mathcal{N}(\mathcal{S}), p)$). For unbounded regions of $\mathbb{R}^d$, active transmitters located in them form an inhomogeneous PPP with intensity $p\lambda$. It is easily verified that the Laplace Transform of their interference contribution may be obtained from the case treated in the previous section merely by changing λ into $p\lambda$ in the equations. Then, using the two results mentioned above, we obtain the transmission success probability

$$p_{rx}^{n}(\theta) = \mathbb{E}_{R_n}\left\{(p\Phi(0,1)+1-p)^{n-1} e^{-p\lambda c_d R_n^d\left(\Omega(\theta R_n^{\alpha},R_n)+B\left(1-\frac{d}{\alpha},1+\frac{d}{\alpha}\right)\theta^{\frac{d}{\alpha}}\right)}\right\} \tag{2.19}$$

Then, taking the expectation over R_n leads directly to the final result, which completes the proof.

Regarding the transmitter-centric approach, we have the following theorem.

Theorem 6 *Conditioned on $\mathcal{I}_{Tx}(Rx) = k$, the probability of success of a transmission from Tx to Rx can be approximated by*

$$p_{tx}^{k}(\theta) \approx \frac{[\Phi(1,2)]_p^{k-1}}{(1+pK(\theta))^k} \mathbb{E}_{\mathcal{I}}\left\{[\Phi(0,1)]_p^{\mathcal{I}-1}\left[[\Phi(1,2)]_p^{-1}\right]_{\beta_d}^{\min(\mathcal{I},k)-1}\right\} \tag{2.20}$$

***Proof* 8** *Very similar to the proof of the case without process thinning. The sole difference is that Laplace Transform terms for the interference contribution of each region are averaged over the random number of active transmitters.*

In the next subsection, we anayze the case of Slotted-ALOHA with Acknowledgement.

2.3.2 Case of constant MAP S-ALOHA with ACK slots

We now consider the same system as in the previous subsection, except that now each data transmission time slot is followed by a slot reserved for the transmission of ACK packets. Thus, nodes which receive successfully a packet intended for them during a data slot send an ACK packet during the following ACK slot.

Although interference in a HPPP is spatially correlated, we assume in the following that transmission successes on different links are independent so as to keep the derivations of handshake performances tractable. So as to show this assumption is reasonable, simulated data used for comparison will take into account the spatial correlation of interference.

An acknowledgement packet is considered successful if its SIR ratio is greater than the threshold θ'. If an intended data packet and the following ACK packet are both correctly received, then the handshake is considered successful. We assume that fading coefficients in data slots and ACK slots are independent.

Also, we define $q(\theta)$ the spatially averaged probability for any node in the network not transmitting during a given data slot to send a packet during the following ACK slot. That is, $q(\theta)$ can be seen as the spatially averaged probability that a node receives successfully a packet intended for itself during a given data slot, conditioned on its belonging to the receiver set. As a consequence, $q(\theta)$ not only depends on the MAP p, but also on the routing protocol employed (i.e, the way nodes in the network choose their packet destinations).

For a given receiver $Rx \in \mathcal{X}_0$, the general expression for $q(\theta)$ is given by

$$q(\theta) = p \sum_{n=1}^{\infty} \mathbb{P}(X_n \to Rx)\, p_{rx}^{n}(\theta) \tag{2.21}$$

in which X_n denotes the n-th nearest node to Rx, $X_n \to Rx$ means "X_n selects Rx as destination" and where $p_{rx}^{n}(\theta)$ is the transmission success probability from X_n to Rx and is given by (2.18). Consequently, provided that the routing protocol employed allows $\mathbb{P}(X_n \to Rx)$ to be known for all n, it is possible to determine $q(\theta)$ using the above equation. The particular case in which transmitters choose their destination uniformly among their N nearest neighbours will be covered in the next section.

For a given probability $q(\theta)$, which we denote simply as q, we have the following

theorem.

Theorem 7 *Conditioned on $\mathcal{I}_{Tx}(Rx) = k$, the probability for a data packet from a transmitter Tx to a receiver Rx and the following ACK packet from Rx to Tx to be both successfully received can be approximated by*

$$p_{tx}^{k}\left(\theta,\theta' \left| \mathcal{I}_{Tx}(Rx) = k\right.\right) \approx \Psi_2(\theta,\theta',1)^{k-1} \frac{\mathbb{E}_{\mathcal{I}}\left\{\Psi_1(\theta,\theta',1)^{\mathcal{I}-1}\left[\frac{\Psi_3(\theta,\theta',1)}{\Psi_1(\theta,\theta',1)\Psi_2(\theta,\theta',1)}\right]_{\beta_d(1)}^{\min(\mathcal{I},k)-1}\right\}}{\left(1+\sum_{i=2}^{\infty}\Upsilon(\theta,\theta',i)\right)^{k}} \tag{2.22}$$

where

$$\begin{aligned}
\Psi_1(\theta,\theta',i) &= \left[\Phi(\theta',i,i+1)\right]_q\left[\frac{\Phi(\theta,i-1,i)}{\left[\Phi(\theta',i,i+1)\right]_q}\right]_p \\
\Psi_2(\theta,\theta',i) &= \left[\Phi(\theta',i-1,i)\right]_q\left[\frac{\Phi(\theta,i,i+1)}{\left[\Phi(\theta',i-1,i)\right]_q}\right]_p \\
\Psi_3(\theta,\theta',i) &= \left[\Phi(\theta',i-1,i)\right]_q\left[\frac{\Phi(\theta,i-1,i)}{\left[\Phi(\theta',i-1,i)\right]_q}\right]_p \\
\Upsilon(\theta,\theta',i) &= \left(i^d-\right)\left(2-\Psi_1(\theta,\theta',i)-\Psi_2(\theta,\theta',i)\right) \\
&+\left(\beta_d(i)-2(i-1)^d+\beta_d(i-1)\right)\left(1-\Psi_3(\theta,\theta',i)\right)
\end{aligned} \tag{2.23}$$

and where $\beta_d(i) = \frac{\left|\mathcal{B}(Tx,ix)\cap\mathcal{B}(Rx,ix)\right|}{\left|\mathcal{B}(Tx,ix)\right|} = B_{\frac{1}{i}-\frac{1}{4i^2}}\left(\frac{d+1}{2},\frac{1}{2}\right)$.

Proof 9 *Given that $\mathcal{I}_{Tx}(Rx) = k$, let us consider the partition $\left\{\mathcal{S}_i^j(R)\right\}_{j=1,2,3;i=1,\ldots,\infty}$ of $\mathbb{R}^d$, which is illustrated in Figure.2-2. In this case the joint probability of success of a data transmission and its following ACK transmission is given by*

$$p_{tx}^{k}(\theta,\theta') = \mathbb{E}\left\{\prod_{j_1,i_1} L_{I_{\mathcal{S}_{i_1}^{j_1},Data}}(\theta R^{\alpha})\prod_{j_2,i_2} L_{I_{\mathcal{S}_{i_2}^{j_2},Ack}}(\theta R^{\alpha})\right\} \tag{2.24}$$

where the expectation is over R, $\mathcal{I}_{Rx}(Tx)$, $\left\{\mathcal{N}_1\left(\mathcal{S}_i^j\right)\right\}_{j=1,2,3;i=1,..,\infty}$ and $\left\{\mathcal{N}\left(\mathcal{S}_i^j\right)\right\}_{j=1,2,3;i=1,..,\infty}$. The first infinite product is actually the conditional probability of success of the data transmission, while the second product is that of the ACK transmission.

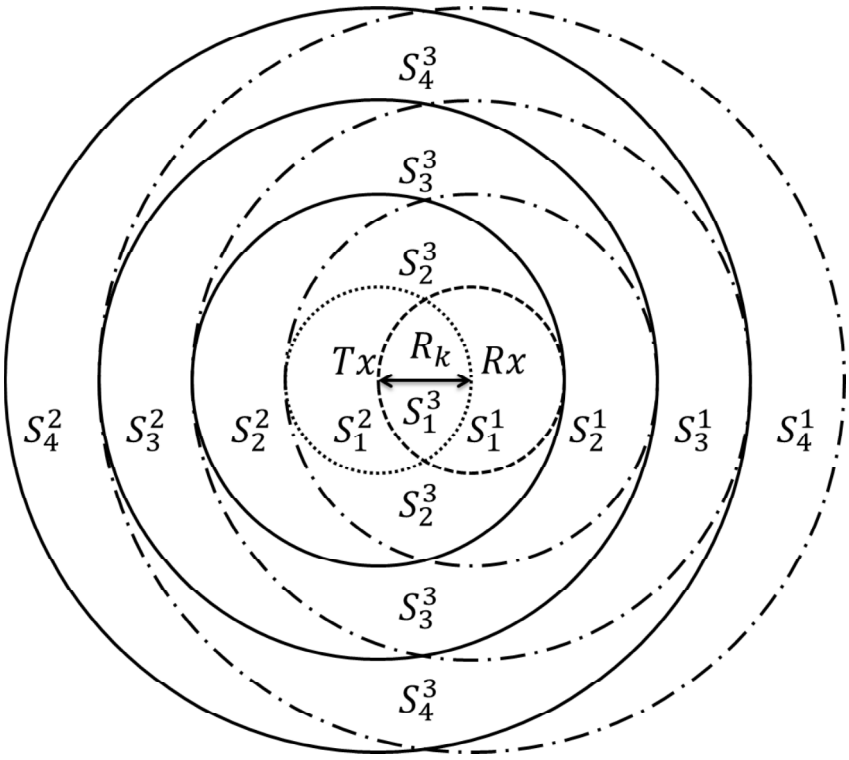

Figure 2-2: Illustration of the space partition used for the analysis of transmission success probability using Slotted-ALOHA protocol with Acknowledgement packet. The partition is composed of the disjoint regions resulting from the intersections of two infinite sets of concentric circles, centered on Tx and Rx, respectively. The figure only shows the regions closest to Tx and Rx. Regions further away are defined in the same way.

In [54], the authors employ product inequalities to separate the two transmit directions and derive lower and upper bounds. However, in our model, it is possible to treat directly the dependency between them. We can rewrite the handshake success probability using a single product as

$$p_{tx}^{n}(\theta,\theta') = \mathbb{E}\left\{\prod_{j,i} L_{I_{\mathcal{S}_i^j,Data}}(\theta R^{\alpha})\, L_{I_{\mathcal{S}_i^j,Ack}}(\theta R^{\alpha})\right\} \tag{2.25}$$

In order to keep the analysis tractable, we will use for each of the regions in the partition the same approximation on the distance distribution as we used to obtain (2.20). Note that according to the definition of q, the number of ACK packet transmitters in a given region $\mathcal{S}$

is binomially distribution according to $\mathfrak{B}\left(\mathcal{N}\left(\mathcal{S}\right)-\mathcal{N}_1\left(\mathcal{S}\right),q\right)$*. Consequently, we have*

$$
\begin{aligned}
&L_{I_{\mathcal{S}_i^1,Data}}\left(\theta R^{\alpha}\right)\approx\Phi\left(\theta,i-1,i\right)^{\mathcal{N}_1\left(\mathcal{S}_i^1\right)} \\
&L_{I_{\mathcal{S}_i^2,Data}}\left(\theta R^{\alpha}\right)\approx\Phi\left(\theta,i,i+1\right)^{\mathcal{N}_1\left(\mathcal{S}_i^2\right)} \\
&L_{I_{\mathcal{S}_i^3,Data}}\left(\theta R^{\alpha}\right)\approx\Phi\left(\theta,i-1,i\right)^{\mathcal{N}_1\left(\mathcal{S}_i^3\right)} \\
&L_{I_{\mathcal{S}_i^1,Ack}}\left(\theta R^{\alpha}\right)\approx\left[\Phi\left(\theta,i,i+1\right)\right]_q^{\mathcal{N}\left(\mathcal{S}_i^1\right)-\mathcal{N}_1\left(\mathcal{S}_i^1\right)} \\
&L_{I_{\mathcal{S}_i^2,Ack}}\left(\theta R^{\alpha}\right)\approx\left[\Phi\left(\theta,i-1,i\right)\right]_q^{\mathcal{N}\left(\mathcal{S}_i^2\right)-\mathcal{N}_1\left(\mathcal{S}_i^2\right)} \\
&L_{I_{\mathcal{S}_i^3,Ack}}\left(\theta R^{\alpha}\right)\approx\left[\Phi\left(\theta,i-1,i\right)\right]_q^{\mathcal{N}\left(\mathcal{S}_i^3\right)-\mathcal{N}_1\left(\mathcal{S}_i^3\right)}
\end{aligned}
\tag{2.26}
$$

Also, $\mathcal{N}_1\left(\mathcal{S}\right)$ *is binomially distributed according to* $\mathfrak{B}\left(\mathcal{N}\left(\mathcal{S}\right),p\right)$*. Thus, replacing the above terms into (2.25) and taking the expectation over* $\left\{\mathcal{N}_1\left(\mathcal{S}_i^j\right)\right\}_{j=1,2,3;i=1,..,\infty}$*, we obtain*

$$
\begin{aligned}
&p_{tx}^k\left(\theta,\theta'\right)\approx \\
&\mathbb{E}\left\{\prod_{i=1}^{\infty}\prod_{j=1}^{3}\Psi_j\left(\theta,\theta',i\right)^{\mathcal{N}\left(\mathcal{S}_i^j\right)}\right\}
\end{aligned}
\tag{2.27}
$$

Regarding the terms $\mathcal{N}\left(\mathcal{S}_i^j\right)$*, we observe that* $\mathcal{N}\left(\mathcal{S}_1^3\right)$ *is binomially distributed according to* $\mathfrak{B}\left(\min\left(\mathcal{I}_{Rx}\left(Tx\right),k\right)-1,\beta_d\left(1\right)\right)$*. Also,* $\mathcal{N}\left(\mathcal{S}_1^2\right)=\mathcal{I}_{Rx}\left(Tx\right)-1-\mathcal{N}\left(\mathcal{S}_1^1\right)$ *and* $\mathcal{N}\left(\mathcal{S}_1^3\right)=k-1-\mathcal{N}\left(\mathcal{S}_1^1\right)$*. Denoting* $\mathcal{I}=\mathcal{I}_{Rx}\left(Tx\right)$*, we then have*

$$
\begin{aligned}
&\mathbb{E}_{\mathcal{I},\mathcal{N}\left(\mathcal{S}_1^1\right)}\left\{\prod_{j=1}^{3}\Psi_j\left(\theta,\theta',1\right)^{\mathcal{N}\left(\mathcal{S}_1^j\right)}\right\}= \\
&\Psi_2\left(\theta,\theta',1\right)^{k-1} \\
&\mathbb{E}_{\mathcal{I}}\left\{\Psi_1\left(\theta,\theta',1\right)^{\mathcal{I}-1}\left[\frac{\Psi_3\left(\theta,\theta',1\right)}{\Psi_2\left(\theta,\theta',1\right)\Psi_2\left(\theta,\theta',1\right)}\right]_{\beta_d(1)}^{\min(\mathcal{I},k)-1}\right\}
\end{aligned}
\tag{2.28}
$$

The other terms $\left\{\mathcal{N}\left(\mathcal{S}_i^j\right)\right\}_{j=1,2,3;i>1}$ *are independent of* $\mathcal{I}_{Rx}\left(Tx\right)$*, independent of one another*

and Poisson distributed with parameter $\lambda\left|\mathcal{S}_i^j\right|$. *Consequently, for* $i>1$ *and any* $j\in\{1,2,3\}$,

$$\mathbb{E}_{\mathcal{N}\left(\mathcal{S}_i^j\right)}\left\{\Psi_j\left(\theta,\theta',i\right)\right\}=e^{-\lambda\left|S_i^j\right|\left(1-\Psi_j(\theta,\theta',i)\right)} \tag{2.29}$$

Also, the area of the regions $\left|S_i^j\right|$ *are given by*

$$\begin{aligned}\left|S_i^1\right|&=\left|S_i^2\right|=\left(i^d-\beta_d\left(i\right)\right)c_dR^d\\ \left|S_i^3\right|&=\left(\beta_d\left(i\right)-2\left(i-1\right)^d+\beta_d\left(i-1\right)\right)c_dR^d\end{aligned} \tag{2.30}$$

Consequently, using (2.30) and replacing (2.28) and (2.29) into (2.25) and then taking the expectation with respect to R, we obtain an integral of the same type as the one leading to (2.9). Solving this integral leads directly to the final result, which completes the proof.

Given that most of the important results calculated until now are actually approximations, it is reasonable to compare the obtained formulae with the results of computer simulations.

2.4 Results validation and applications

2.4.1 Simulation method

The method we use in our computer program to simulate an infinite HPPP is that proposed in [29]. It consists in creating a finite HPPP in a ball with a radius z large enough so that the mean $\mathbb{E}\{I\}$ of the sum of the interference contributions from all nodes in the network, calculated at the center using the bounded path-loss law $l_b\left(r\right)=\min\left(1,r^{-\alpha}\right)$, satisfies $\mathbb{E}\{I_z\}>\mathbb{E}\{I_\infty\}\left(1-\epsilon\right)$, where $\mathbb{E}\{I_\infty\}=\lim_{z\to\infty}\mathbb{E}\{I_z\}$. Given a path-loss exponent α, we have for unit transmit power [29]

$$\mathbb{E}\{I_z\}=\frac{\lambda c_d d}{\alpha-d}\left(1-\frac{1}{z^{\alpha-d}}\right) \tag{2.31}$$

It follows from (2.31) that the above-mentioned requirement is equivalent to constraining the radius z of the d-dimensional finite PPP to $z>\epsilon^{\frac{-1}{\alpha-d}}$. Then, for best results, one may

select the node used as reference for neighbour indexing among nodes close from the center of the finite PPP. In each simulation drop, we generate a random deployment then record the success/failure of a given link. Results are finally averaged over all the deployment realizations.

2.4.2 Conditions on assumptions validity

Note that the interference-limited model may be considered valid only if the mean interference power $\mathbb{E}\{I\}$ received by any node in the network is larger than the noise power W by a large factor, that is, $\frac{W}{\mathbb{E}\{I\}} < \epsilon$, where $\epsilon << 1$. Using (2.31) with $z \to \infty$ and assuming a transmit power P for all nodes, we see that this is equivalent to having $\lambda > \frac{(\alpha-d)W}{d\epsilon c_d P}$.

In order to determine the upper bound of the range of node density values for which the proposed model is well-behaved, we compare the respective influences of the previously mentioned unbounded path-loss function and the bounded path-loss function $l_{b'}(r) = (1+r^{\alpha})^{-1}$ on the link Mean Maximum Achievable Spectral Efficiency (MMASE).[3] We define the MMASE η_{tx}^{k} conditioned on $\mathcal{I}_{Tx}(Rx) = k$ as

$$\eta_{tx}^{k}(\theta,\theta') = p(1-p)\log_2(1+\theta)\, p_{tx}^{k}(\theta,\theta') \tag{2.32}$$

where the dependence on θ' disappears in the case no acknowledgement packet is used.

Numerically, we observed that in the 2-dimensional case, both path-loss functions led to indistinguishable results for all the investigated protocols when the node density satisfied $\lambda \leq 10^{-2}$ node per square meter. For the 3-dimensional case, both path-loss functions led to indistinguishable results for a node density $\lambda < 10^{-3}$ node per cubic meter.

2.4.3 Simulation results

In the following, we compare the theoretical results obtained in the previous sections with results from computer simulations. All theoretical results on figures are represented by

[3] The path-loss function $l_b(r) = \min(1, r^{-\alpha})$ can be seen as a close approximation of $l_{b'}(r) = (1+r^{\alpha})^{-1}$. It was used to derive a lower bound on the acceptable values of node density in the interference-limited model, for the sake of tractability. However, in simulations, the more realistic function (i.e, $l_{b'}(r)$) should be used.

solid lines, while dots are the simulated data. The node density is chosen so as to satisfy the conditions given in the previous subsection. The path-loss exponent is $\alpha = 4$ and $d = 2$. In order to ease the computation of theoretical expressions, we use the following approximation for the function $\Omega(s, X)$.

$$\tilde{\Omega}(s, X) = \left((1 + sX^{-\alpha})^{\frac{d}{\alpha}} - (sX^{-\alpha})^{\frac{d}{\alpha}}\right) B\left(1 - \frac{d}{\alpha}, 1 + \frac{d}{\alpha}\right) \tag{2.33}$$

A justification for this approximation is provided in Appendix E. On some figures (i.e when there was a noticeable difference), we plotted both theoretical results using the above approximation (solid lines) and using the expression with Hypergeometric function given in (2.4) (dashed lines).

Case of S-ALOHA without ACK In Fig.2-3 and Fig.2-4, we consider the case of S-ALOHA in a uniform RAHN modelled as a 2-dimensional HPPP. We observe a good agreement between the behaviors of simulated and approximate theoretical results. The latter appear as upper bounds of the simulated ones, which is to be expected since the approximation used in the derivation of (2.20) overestimates the distance between some interferers and the receiver.

Fig.2-3 illustrates the trade-off between decodability and bit rate. Note that the optimal MCS for transmissions to a given neighbour depends on the operating MAP p. Conversely, for a given receiver threshold, intuition suggests the existence of an optimal MAP. This is confirmed in Fig.2-4. Note that for $p > 0.5$, the number of receiver nodes is on average smaller than the number of transmitters, which implies that the optimal p lies between 0 and 0.5. We note that both theoretical and simulated results reach their respective maximum almost at the same abcissa, in both figures.

Regarding the influence of θ on optimal MAP p, further investigations have showed that increasing the data packet receiver threshold θ decreases the optimal p, which follows directly from the trade-off between the density of transmissions and the individual transmission rate.

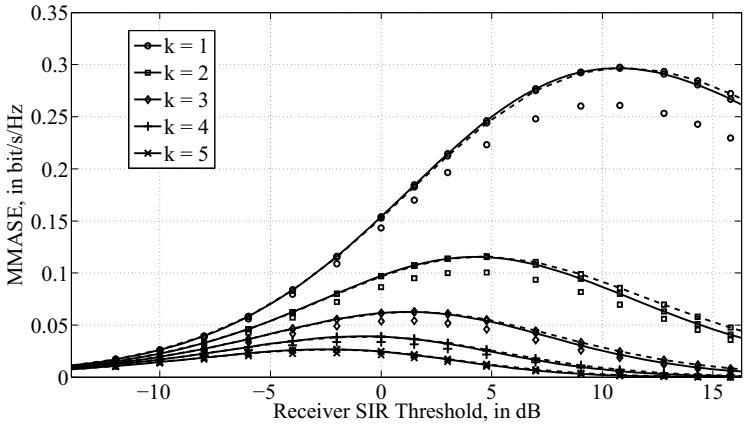

Figure 2-3: MMASE of transmissions to the k-th neighbour in a 2-dimensional uniform RAHN employing S-ALOHA with fixed MAP $p = 0.3$, against the receiver threshold (in dB). The curves are obtained from (2.20).

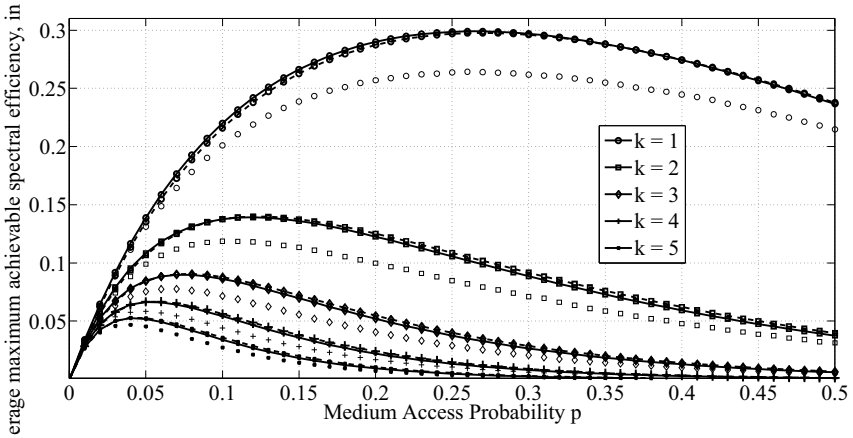

Figure 2-4: MMASE of transmissions to the k-th neighbour in a 2-dimensional uniform RAHN employing S-ALOHA, against the MAP p, for a given a receiver threshold $\theta = 10.4$. The curves are obtained from (2.20).

Case of S-ALOHA with ACK Regarding S-ALOHA with acknowledgement, we assume a routing protocol which makes transmitters select their packet destination uniformly among their N closest neighbours. In this particular case, $q(\theta)$ is given as follows.

$$q(\theta) = \frac{p}{N} \sum_{k=1}^{N} p_{tx}^{k}(\theta) \tag{2.34}$$

where $p_{tx}^{k}(\theta)$ denotes the success probability for a transmission to the k-th nearest neighbour and is given in (2.20). We assume $N = 2$ in the following.

The performances of S-ALOHA with ACK packet are described in Fig.2-5. The theoretical results are computed using (2.22) and (2.32). The denominator in (2.22) is approximated by computing the first thirty terms of the infinite sum (more terms did not provide any additional noticeable accuracy gain).

We observe again a good agreement between the behaviors of simulated and approximate theoretical results. The latter do not explicitely upper or lower bound simulated results, which can be explained by the diversity of shape of the regions on which the approximation for the distance from interferers to the receiver is used. The existence of optimal operating points can be noted, in a similar fashion to S-ALOHA. Again, both theoretical and simulated results reach their respective maximum at abcissa very close from each other.

Regarding the influence of θ' on optimal MAP p and θ, although it is not shown here due to the lack of space, increasing θ' also increases the optimal MAP p. This can be justified in the same way as the influence of θ on p in the case of S-ALOHA without acknowledgement, by considering that the number of interferers during the ACK packet slot is proportional to $1 - p$.

Also, by comparing Fig.2-5 and Fig.2-6, we observe that increasing θ' actually increases the value of the optimal θ, although the achieved maximum MMASE is lower than with a smaller θ'. One possible justification for this result is that a higher θ leads to less interference during the ACK slot, thus allowing a higher θ' to be used.

Finally, comparing Fig 2-3, Fig 2-5 and Fig 2-6, we observe that the transmission of the ACK packet has negligible influence for the case $k = 1$, even for high values of θ'. Note however, that for $k > 1$, the influence of imperfect feedback becomes stronger (e.g for $k = 3, \theta' = 0$dB, the MMASE in the case of S-ALOHA with ACK is 75% of the case without ACK). Our observations confirm the intuitive fact that imperfect feedback is only negligible for transmissions between close neighbours.

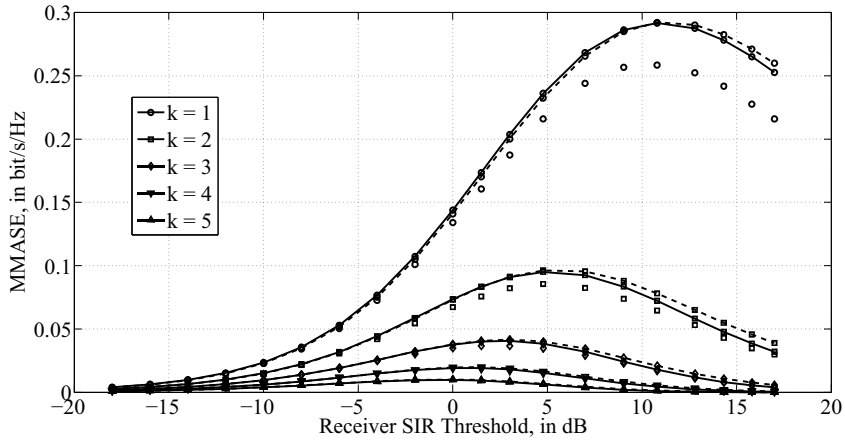

Figure 2-5: MMASE of transmissions to the k-th neighbour in a 2-dimensional uniform RAHN employing S-ALOHA with ACK and fixed MAP $p = 0.3$, against the receiver threshold θ (in dB). The curves are obtained from (2.22), for $\theta' = 0dB$.

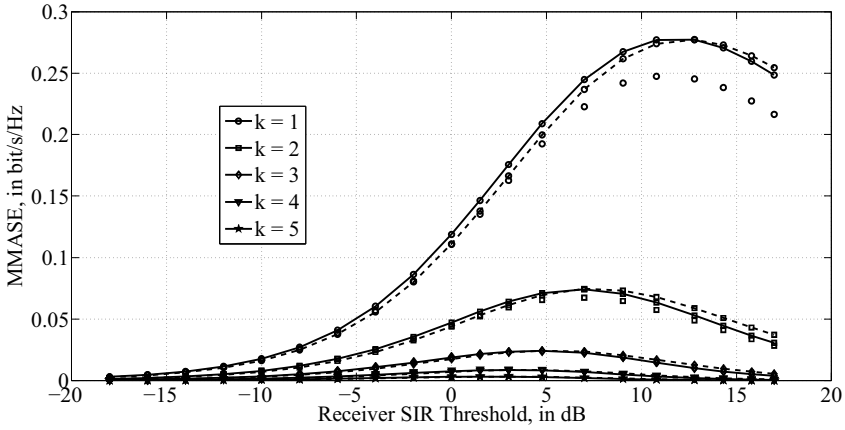

Figure 2-6: MMASE of transmissions to the k-th neighbour in a 2-dimensional uniform RAHN employing S-ALOHA with ACK and fixed MAP $p = 0.3$, against the receiver threshold θ (in dB). The curves are obtained from (2.22), for $\theta' = 9dB$.

2.5 Conclusion

In this chapter, we analyzed the probability of success of a transmission (one-way and handshake) to the k-th nearest neighbour in an ad hoc network modelled by a single homogeneous Poisson Point Process in which nodes employ the Slotted-ALOHA MAC protocol (without and with acknowledgement, respectively). The proposed approach enables to derive spatially averaged network performances at the routing level while tackling directly the dependency between both transmit directions in handshakes. We compared the devel-

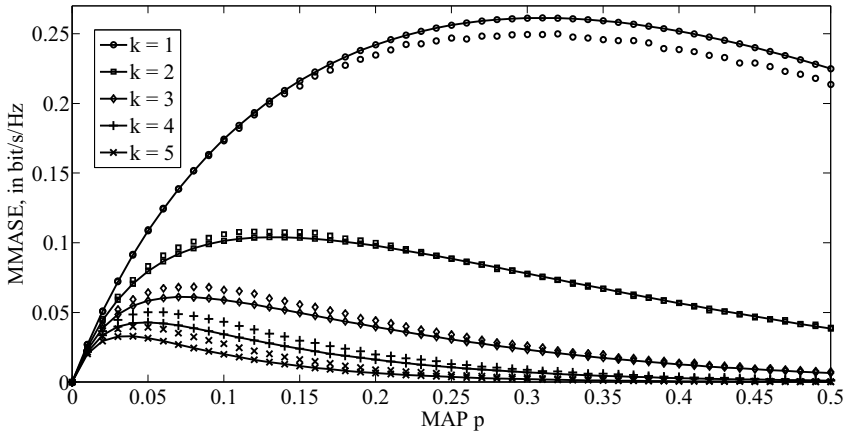

Figure 2-7: MMASE of transmissions to the k-th neighbour in a 2-dimensional uniform RAHN employing S-ALOHA with ACK packet, against the MAP p. The data packet threshold is $\theta = 8dB$ and the ACK packet threshold is $\theta' = 0dB$. The curves are obtained from (2.22).

oped closed form formula with computer simulation results and concluded that this work can find applications in the joint quantitative study of some MAC and routing protocols. Notably, exploiting the notion of neighbour index, we confirmed through our results the intuitive fact that imperfect feedback in handshakes is only negligible for transmissions to/from the closest neighbour. One limitation of the approach proposed in this chapter is the complexity of the derivations leading to the transmission success probability. In order to study more complex mechanisms, it is of interest to consider a modified deployment model leading to more tractable expressions. This will be the subject of the next chapters.

Chapter 3

Impact of Control Packet Diversity on Four-Way Handshaking Performance

In recent years, a new class of synchronous MAC protocols for ad hoc networks, based on handshakes without "spatial reservation" effect[1], has emerged. In such protocols, control handshakes are not used for spatial reservation of the channel, but solely to test the link quality. An example of such protocol is the Progressive Ramp-Up Algorithm (PRUA) protocol presented in [51]. However, to the best of our knowledge, the performances of such schemes have only been studied by means of simulations. Thus there lacks in the literature a mathematical model for such protocols. The closest work may be [54], which analyzes the performance of a two-way transmission in the case where interferer sets for each transmit direction have equal density and therefore is not applicable to four-way handshaking.

In this chapter, we propose a new mathematical framework based on point process theory which constitutes a first step toward the theoretical understanding of the above-mentioned protocols. The stochastic analysis we present focuses on a four-way handshake composed of a control handshake without spatial reservation and a traffic handshake, both preceded by a random test for medium access. Through this simple scheme, we can perform a tractable analysis with relevant conclusions for general protocol design. Our framework takes into account time-varying channel impairments, the interference inherent to large

[1] Spatial reservation means that the transmission of a control packet forces neighbor nodes to remain silent for a certain time window.

ad hoc deployments and different decoding requirements for each packet as well as the influence of the routing protocol. Moreover, the proposed model also accounts for the impact of diversity in the control handshake.

We obtain closed form expressions for the average frame success probability and the mean effective link throughput (MELT). Our results, confirmed by comparison to simulated data, provide the following important insights regarding contention in mobile ad hoc networks. In the presence of uncorrelated fading between control and traffic handshakes and given a fixed transmit-energy constraint: **1)** as the diversity order increases, the diversity gain becomes counterbalanced by the loss due to increased control packet duration; hence the existence of an optimal diversity order value. **2)** The design of MELT-optimal decoding requirements for the control packets is strongly influenced by the order of the control packet diversity.

The remainder of this chapter is organized as follows. In section 3.1, we introduce the system model used in our analysis. In section 3.2, we calculate the probability of success of a frame on a typical link for a given link distance. In section 3.3, we take into account the influence of the routing protocol and calculate the MELT in closed form. In section 3.4, we compare the developed theoretical results to simulated data. Finally, a conclusion summarizes the chapter in section 3.5.

3.1 System model

In this section, we describe the system model assumptions and the MAC scheme used in the remainder of this chapter.

3.1.1 Control Packet Diversity Model

The MAC scheme considered is structured so as to include the main features of the class of protocols targeted by our study while preserving analytical tractability. A frame is made of four successive slots, each corresponding to a packet: Forward Test packet (FWT), Feedback Test packet (FBT), Data and ACK. Similarly to PRUA [51], the control handshake of the scheme considered has no spatial reservation effect. It is simply an exchange of

packets between two nodes. The time/frequency resources are organized as in figure 3-1.[2] The spectrum available to the system is organized in K reserved bands interleaved with K shared bands. A given ad hoc network is attributed a single reserved band of bandwidth B in which it can transmit FBT, Data and ACK packets. FWT transmissions take place in the shared bands, which are used by different ad hoc networks in a time-division fashion.

In this work, we analyze link performances in a given network, without taking the influence of other networks into account. Within each reserved band, frequency division is used between forward and feedback slots. For each network, in the FWT slot, transmitters send a copy of the FWT packet on each of the K shared bands. Then the receiver considers the FWT slot a success if at least k out of K copies can be decoded. The full process of the protocol is illustrated in figure 3-2. As in [51], at the beginning of a frame, all nodes with a packet to transmit have to pass a random test with fixed success probability p, called Medium Access Test (MAT), to prevent congestion. MATs at different nodes are independent. Successful nodes become active transmitters while the remaining ones become silent and listen to the medium. After sending a forward packet (*i.e* FWT or Data), if an active transmitter does not decode any feedback packet (*i.e* FBT or ACK, respectively), it becomes silent. All control packets have the same payload: *i.e* the MAC address of the transmitter and the MAC address of the receiver. Therefore, we assume that $N_{fwt} = N_{fbt} = N_{ack}$, where N_{fwt} is the number of information bits carried by the FWT packet. In the remainder, we will refer to this MAC scheme as Multiple Test Packet-based MAC (MTPMAC), for brevity.

3.1.2 System Assumptions

We assume that time in the system is slotted. In a given network, all nodes always have a packet ready for transmission (i.e the network is in the saturated regime) and are synchronized with one another as in [51]. Each network is considered to be interference-limited and all nodes have unit transmit power. Nodes are considered to be mobile but moving slowly enough so that the path-loss on any link remains constant during a frame.

[2] OFDM or filter bank based systems can be adapted to support the time/frequency organization proposed in figure 3-1.

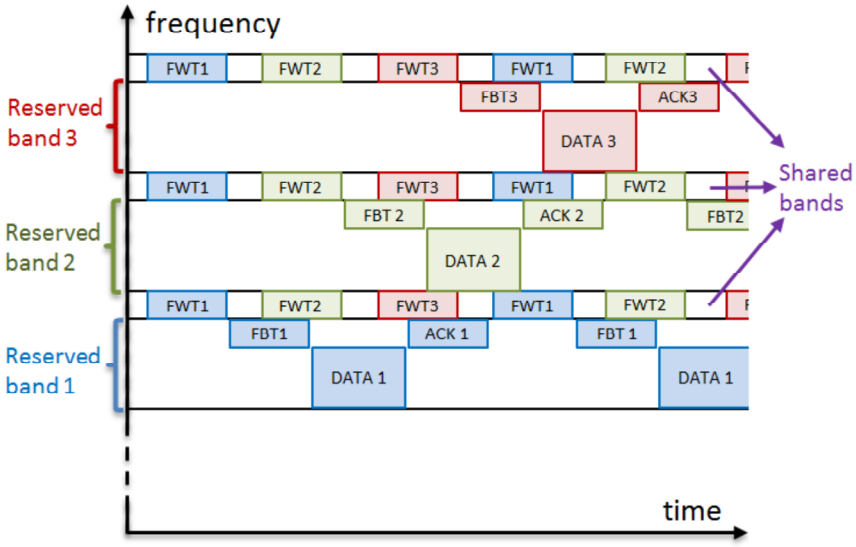

Figure 3-1: Illustration of the time/frequency structure of the system for the case $K = 3$. The numeral index in each packet indicates which network the packet belongs to.

We study the performances of a typical transmitter-receiver pair placed as follows. A first node Tx_0 is placed at the origin of the two-dimensional space and its target Rx_0 is placed at a distance r from it. We will later refer to these two nodes as the observed typical link. The deployment of the remaining nodes is modelled by an homogeneous Poisson point process (HPPP) Φ with density λ. We will later refer to Φ as the interferer set. After the initial MAT, the interferer set is divided into an active transmitter set Φ^1_{fwt} and a receiver set Φ^0_{fwt}. Here the index fwt is used because the two sets describe the roles of interferer nodes during the FWT slot, which immediately follows the MAT. Due to the thinning property of HPPPs, Φ^1_{fwt} and Φ^0_{fwt} are both HPPPs with density λp and $\lambda(1-p)$, respectively. Tx_0 and Rx_0 are equally subject to the MAT; however they are not part of the above-defined sets. As in [29], a transmission is considered successful if the Signal to Interference power Ratio (SIR) at the receiver is greater than a predetermined threshold $\theta = 2^{\eta} - 1$ where η is the spectral efficiency of the packet in bit/s/Hz. We define the decoding thresholds used in each type of slot by all nodes as follows: θ_{FWT}, θ_{FBT}, θ_D and θ_{ACK}.

The channel between nodes is composed of fast fading and path-loss modelled by a power law $l(r) = r^{-\alpha}$ where α is the path-loss exponent. A slot-by-slot block-fading channel model is used, therefore fading is constant over each slot. Also, the fading is

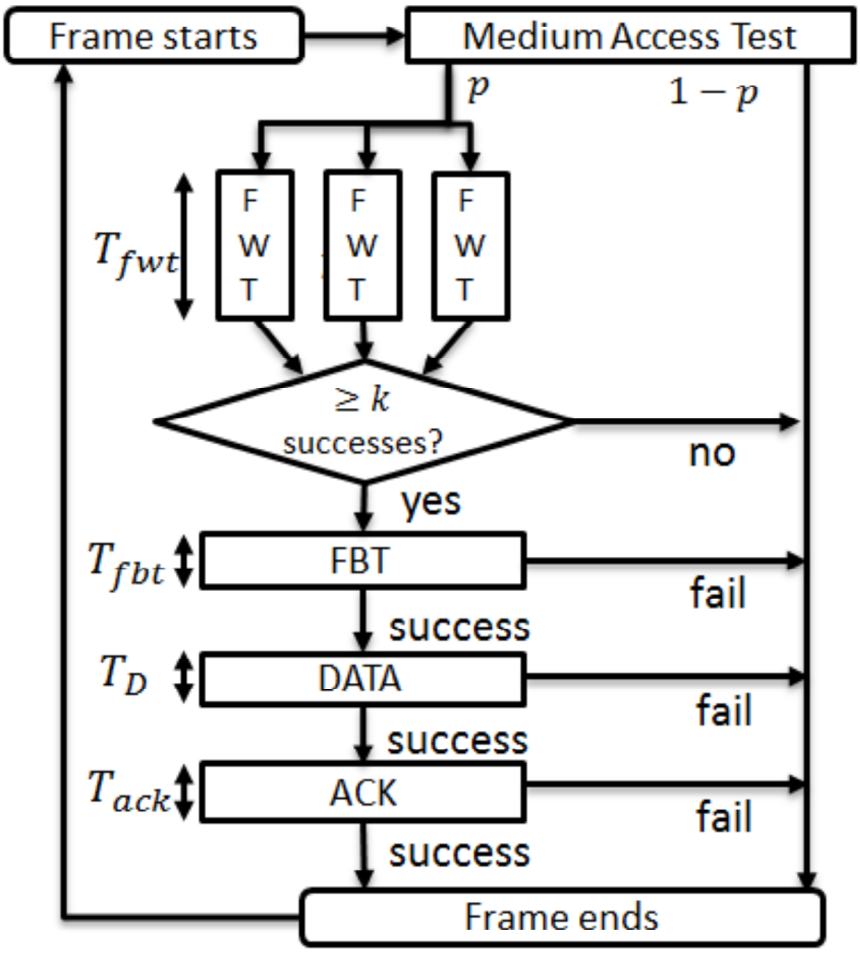

Figure 3-2: Frame structure of the MAC scheme used for the analysis for the case $K = 3$.

independent across links, time slots and across frequency bands. For each packet, the complex fading coefficient is assumed to be a circularly-Gaussian random variables with unit variance. Therefore, the squared norm of the fading is exponentially distributed with rate 1.

Remark: Note that the slot-by-slot block-fading channel model is a theoretical abstraction representing the worst case scenario for contention resolution, since the fading level during the control handshake does not provide any information about the fading during the traffic handshake. However, path-loss and interferer set are still constant during a frame. Based on this system model, we can study how the control packet diversity achieved through the use of multiple shared bands benefits to the performance of the contention process.

In order to keep the mathematical developments tractable, we incorporate the following commonly used features into our model (see e.g [52]). **1)** We consider that FBT and ACK packets are transmitted error-free for all links in the network. This assumption is actually reasonable in the sense that the densities of interferer during the FBT and ACK slots are much lower than during the FWT slot. Also, these small control packets have lower SIR requirements for detection at the receiver than the Data packet does. **2)** Although interference in a HPPP deployment is spatially correlated [27], we assume it is independent between nodes, for the sake of tractability. That is, successes in a given slot on two different links are independent. So as to show this assumption is acceptable, simulated data used for comparison will take into account the spatial correlation of interference. **3)** Since it is not tractable to consider simultaneously the situation of every link in the network, we assume that all active transmitters in Φ^1_{fwt} have the same transmission success probability $\bar{P}_{S,fwt}$ in the FWT slot. We define this probability as the average probability of success of a typical link during the FWT slot. This model is reasonable for an homogeneous deployment, as used in this chapter, in which all nodes experience in average the same interference level.

3.1.3 Mean Effective Link Throughput Definition

Let us assume that the success probability of a frame on the observed typical link is denoted as $P_S(r)$ for a given transmitter-receiver distance r. For a given routing protocol, this distance has a certain probability distribution. We can thus define $\bar{P}_S = \mathbb{E}_r\{P_S(r)\}$ the success probability averaged over the link distance given a combination of MAC and routing protocols. The MELT, which we define in details later in the chapter, is a function of this probability.

Therefore, as a first step, we calculate in the next section the probability of success of a frame $P_S(r)$ within the above-defined system model.

3.2 Transmission Success Probability

In this section, we aim to calculate the probability for a frame on the observed typical link to be successful given a fixed distance $\|Tx_0 - Rx_0\| = r$.

For any node $Tx_n \in \Phi^1$, $n = 1, ..., +\infty$, we define the distance $d_{0n} = \|Tx_n - Rx_0\|$ to the receiver Rx_0. Also, for a given frame, we define the squared fading coefficients $G_{0n,i}$ and $G_{D,0n}$ of the channel between Tx_n and Rx_0 during the FWT slot on the i-th shared band and during the Data slot, respectively. Let us define $G_{00,i}$ and $G_{D,00}$ the squared fading coefficients on the typical link during the FWT slot on the i-th shared band and during the Data slot, respectively. Given these definitions, if Tx_0 passes the MAT in a given frame and attempts a FWT transmission to Rx_0, then, the Signal to Interference Ratio $\gamma_{00,i}$ at Rx_0 of the i-th FWT packet (i.e, on the i-th shared band) is given by

$$\gamma_{00,i} = \frac{G_{00,i} r^{-\alpha}}{\sum_{Tx_n \in \Phi^1_{fwt}} G_{0n,i} d_{0n}^{-\alpha}} = \frac{G_{00,i} r^{-\alpha}}{I_{0,i}} \tag{3.1}$$

and in the same way for the data packet

$$\gamma_{D,00} = \frac{G_{D,00} r^{-\alpha}}{\sum_{Tx_n \in \Phi^1_D} G_{D,0n} d_{0n}^{-\alpha}} = \frac{G_{D,00} r^{-\alpha}}{I_{D,0}} \tag{3.2}$$

where $I_{0,i}$ and $I_{D,0}$ denote the interference at Rx_0 during the FWT slot on the i-th shared band and during the Data slot, respectively. In addition, if Rx_0 fails the MAT, then it listens to the medium and can potentially receive the transmission from Tx_0. In this case, we can write that the probability of success of a frame, conditioned on the two above results of the

MAT, is the following joint probability

$$
\begin{aligned}
&P_{S|Tx,Rx}\left(r,k,\theta_{fwt},\theta_D\right) = \qquad (3.3)\\
&\sum_{n=k}^{K}\sum_{\eta_n^1\in\mathcal{M}_n^1}\mathbb{P}\left(\bigcap_{j\in\eta_n^1}\gamma_{00,j}\geq\theta_{fwt},\bigcap_{i\in\bar{\eta}_n^1}\gamma_{00,i}<\theta_{fwt},\gamma_{D,00}\geq\theta_D\right)\\
&\overset{(a)}{=}\sum_{n=k}^{K}\binom{K}{n}\mathbb{P}\left(\bigcap_{i=1}^{n}\gamma_{00,i}\geq\theta_{fwt},\bigcap_{j=n+1}^{K}\gamma_{00,j}<\theta_{fwt},\gamma_{D,00}\geq\theta_D\right)\\
&\overset{(b)}{=}\sum_{n=k}^{K}\binom{K}{n}\mathbb{E}\left\{\prod_{i=1}^{n}e^{-\theta_{fwt}r^{\alpha}I_{0,i}}\prod_{j=n+1}^{K}\left(1-e^{-\theta_{fwt}r^{\alpha}I_{0,j}}\right)e^{-\theta_D r^{\alpha}I_{D,0}}\right\}\\
&\overset{(c)}{=}\sum_{n=k}^{K}\binom{K}{n}\mathbb{E}\left\{\prod_{i=1}^{n}e^{-\theta_{fwt}r^{\alpha}I_{0,i}}e^{-\theta_D r^{\alpha}I_{D,0}}\right.\\
&\left.\left(1+\sum_{l=1}^{K-n}(-1)^{l}\sum_{\eta_l^{n+1}\in\mathcal{M}_l^{n+1}}\prod_{j\in\eta_l^{n+1}}e^{-\theta_{fwt}r^{\alpha}I_{0,j}}\right)\right\}\\
&\overset{(d)}{=}\sum_{n=k}^{K}\binom{K}{n}\mathbb{E}\left\{e^{-\theta_{fwt}r^{\alpha}\sum_{i=1}^{n}I_{0,i}-\theta_D r^{\alpha}I_{D,0}}\right\}+\sum_{n=k}^{K}\binom{K}{n}\sum_{l=1}^{K-n}(-1)^{l}\\
&\sum_{\eta_l^{n+1}\in\mathcal{M}_l^{n+1}}\mathbb{E}\left\{e^{-\theta_{fwt}r^{\alpha}\sum_{j\in\eta_l^{n+1}}I_{0,j}-\theta_{fwt}r^{\alpha}\sum_{i=1}^{n}I_{0,i}-\theta_D r^{\alpha}I_{D,0}}\right\}\\
&\overset{(e)}{=}\sum_{n=k}^{K}\binom{K}{n}\mathbb{E}\left\{e^{-\theta_{fwt}r^{\alpha}\tilde{I}_0(n)-\theta_D r^{\alpha}I_{D,0}}\right\}\\
&+\sum_{n=k}^{K}\binom{K}{n}\sum_{l=1}^{K-n}(-1)^{l}\binom{K-n}{l}\mathbb{E}\left\{e^{-\theta_{fwt}r^{\alpha}\tilde{I}_0(n+l)-\theta_D r^{\alpha}I_{D,0}}\right\}
\end{aligned}
$$

where the notation $|Tx,Rx$ indicates that this is the frame success probability conditioned on the outcome of the MAT of the transmitter Tx_0 and the receiver Rx_0.

In the above equations, (a) is obtained by observing that SIR values of different FWT packets are independent and identically distributed, given a particular realization of the interferer set. Therefore, the order of successful and failed FWT packets is irrelevant. The term $\mathcal{M}_n^t$ denotes the set of all subsets of the integer set $\mathcal{K}_t=\{t,t+1,...,K\}$ with cardinality n while η_n^t is an element of $\mathcal{M}_n^t$ and $\bar{\eta}_n^t$ is the complementary set of η_n^t in $\mathcal{K}_t$. Expression (b) follows from the definition of the SIR terms and the fact that fading coefficients in different slots and/or shared bands are independent and identically distributed with complementary

cumulative distribution function $F_G(g) = \mathbb{P}(G > g) = e^{-g}$. Expression (c) follows by developing the second product in (b) into a sum. Expression (d) is obtained firstly by developing (c), then transforming the products of exponential terms into single exponentials with a sum in the exponent. As a next step, by linearity, the expectation operation can be moved inside the sums next to each exponential term. Finally, expression (e) is obtained by observing that, since all $I_{0,i}$s are identically distributed, sums over FWT interference terms are entirely characterized by the number of terms being summed. Consequently, two sums S_1 and S_2 with the same number of FWT interference terms but with distinct FWT packet index sets have the same Laplace Transform (*i.e* $\mathbb{E}\left\{e^{-sS_1}\right\} = \mathbb{E}\left\{e^{-sS_2}\right\}, \forall s$). Therefore, we can introduce the notation $\tilde{I}_0(n)$ as the sum of n distinct interference terms for FWT packets and adapt the summations over the FWT packet index sets accordingly.

Note that the term $\mathbb{E}\left\{e^{-\theta_{fwt} r^{\nu} \tilde{I}_0(n+l) - \theta_D r^{\nu} I_{D,0}}\right\}$ can be regarded as the joint probability of success of $n+l$ independent FWT packets and a Data packet. We denote it as $P_{n+l}(r)$ in the remainder of this chapter.

According to the system model defined in the previous section, the interferer set Φ^1_D is a subset of Φ^1_{fwt} obtained by independent thinning with a certain retention probability $\bar{P}_{fwt->D} = \mathbb{E}_d\left\{P_{fwt->D}(d)\right\}$, where d is the link distance and the index $fwt- > D$ denotes that it is the probability for a node in Φ^1_{fwt} to be also in Φ^1_D. Consequently, we can rewrite the interference at Rx_0 during the Data slot as follows.

$$I_{D,0} = \sum_{Tx_j \in \Phi^1_{fwt}} X_{D,j} G_{D,0j} d_{0j}^{-\alpha} \tag{3.4}$$

where $X_{D,j},\ j = 1, ..., +\infty$ are independent and identically distributed random variables taking value in $\{0,1\}$ and such that $\mathbb{P}(X_{D,j} = 1) = \bar{P}_{fwt->D}$. This probability will be evaluated in the next section, for a given routing protocol (*i.e* a given link distance distribution). Also, the interference term $\tilde{I}_0(n+l)$ can be written as follows.

$$\tilde{I}_0(n+l) = \sum_{i=1}^{n+l} \sum_{Tx_j \in \Phi^1_{fwt}} d_{0n}^{-\alpha} G_{0j,i} = \sum_{Tx_j \in \Phi^1_{fwt}} d_{0j}^{-\alpha} \tilde{G}_{0n}(n+l) \tag{3.5}$$

where the second equality is obtained by inverting the orders of the sums and defining

$\tilde{G}_{0n}(n+l) = \sum_{i=1}^{n+l} G_{0j,i}$. As the sum of $n+l$ i.i.d exponential variables, $\tilde{G}_{0n}$ is Gamma-distributed with shape parameter $n+l$ and scale parameter 1. Using (3.4), we can express $P_{n+l}(r)$ as follows.

$$
\begin{aligned}
& P_{n+l}(r) \overset{(a)}{=} \\
& \mathbb{E}\left\{ e^{-\theta_{fwt} r^{\alpha} \tilde{I}_0(n+l)} \prod_{Tx_j \in \Phi^1_{fwt}} \mathbb{E}_{X_{D,n}}\left\{ e^{-\theta_D r^{\alpha} X_{D,n} G_{D,0j} d_{0j}^{-\alpha}} \right\} \right\} \\
& \overset{(b)}{=} \mathbb{E}\left\{ e^{-\theta_{fwt} r^{\alpha} \tilde{I}_0(n+l)} \prod_{Tx_j \in \Phi^1_{fwt}} \left(\bar{P}_{fwt->D} e^{-\theta_D r^{\alpha} G_{D,0j} d_{0j}^{-\alpha}} + 1 - \bar{P}_{fwt->D} \right) \right\} \\
& \overset{(c)}{=} \mathbb{E}\left\{ \prod_{Tx_j \in \Phi^1_{fwt}} \left(\bar{P}_{fwt->D} e^{-r^{\alpha} d_{0j}^{-\alpha} \left(\theta_{fwt} \tilde{G}_{0j}(n+l) + \theta_D G_{D,0j} \right)} \right. \right. \\
& \left. \left. + (1 - \bar{P}_{fwt->D}) e^{-\theta_{fwt} r^{\alpha} \tilde{G}_{0j}(n+l) d_{0j}^{-\alpha}} \right) \right\} \\
& \overset{(d)}{=} \mathbb{E}\left\{ \prod_{Tx_j \in \Phi^1_{fwt}} \left(\bar{P}_{fwt->D} L_{\tilde{G}_{0j}(n+l)}\left(\theta_{fwt} r^{\alpha} d_{0j}^{-\alpha} \right) L_{G_{D,0j}}\left(\theta_D r^{\alpha} d_{0j}^{-\alpha} \right) \right. \right. \\
& \left. \left. + (1 - \bar{P}_{fwt->D}) L_{\tilde{G}_{0j}(n+l)}\left(\theta_{fwt} r^{\alpha} d_{0j}^{-\alpha} \right) \right) \right\}
\end{aligned}
\tag{3.6}
$$

The expression in (a) is obtained due to the independence assumption made on the transmission success of the interferers. Expression (b) is obtained by taking the expectation over each $X_{D,n}$. Expression (c) follows by replacing the term $\tilde{I}_0(n+l)$ by its definition given in (3.5), then expanding the exponential on the left of (b) into a product and associating together terms related to each interferer. Expression (d) is obtained by taking the expectation over all the squared fading coefficients, which are independent. Finally, we use the Laplace Transform notation $L_G(s) = \mathbb{E}\left\{e^{-sG}\right\}$ in each term of the expression. The Laplace Transform of $\tilde{G}_{0j}(n+l)$ is given by $L(s) = 1/(1+s)^{n+l}$ while the Laplace Transform of $G_{D,0j}$ is given by $\frac{1}{(1+s)}$. Using the Probability Generating Functional of a HPPP as in [29] (see eq.(3.20)), we obtain from (3.6) the following simple form for $P_{n+l}(r)$.

$$P_{n+l}(r) = exp\left(-p\lambda 2\pi \int_0^{+\infty} g(t)\, dt\right) \tag{3.7}$$

where

$$g(t) = t\left(\frac{\bar{P}_{fwt->D}}{\left(t^{\alpha}+\theta_{fwt}r^{\alpha}\right)^{n+l}\left(t^{\alpha}+\theta_{D}r^{\alpha}\right)} + \frac{1-\bar{P}_{fwt->D}}{\left(t^{\alpha}+\theta_{fwt}r^{\alpha}\right)^{n+l}}\right) \tag{3.8}$$

Finally, solving the integral above leads to the following result (the proof thereof is provided in appendix).

$$P_{n+l}(r) = exp\left(-p\lambda 2\pi r^2 h_{n+l}(\theta_{fwt},\theta_D)\right) \tag{3.9}$$

where

$$\begin{aligned} &h_{n+l}(\theta_{fwt},\theta_D) = \\ &\frac{\bar{P}_{fwt->D}\Gamma(n+l+\delta+1)\Gamma(1-\delta) f_{n+l}(\theta_{fwt},\theta_D)}{\Gamma(n+l+1)(\alpha(n+l)+2)} \\ &+\theta_{fwt}^{\delta}\sum_{i=0}^{n+l-1}\binom{n+l}{i}\frac{\Gamma(i+\delta+1)\Gamma(n+l-i-\delta)}{\Gamma(n+l)(\alpha i+2)} \end{aligned} \tag{3.10}$$

where $\delta = \frac{2}{\alpha}$ and

$$\begin{aligned} &f_{n+l}(\theta_{fwt},\theta_D) = \\ &\begin{cases} \theta_{fwt}^{\delta}\,{}_2F_1\left(n+l+\delta,1,n+l+1,1-\frac{\theta_{fwt}}{\theta_D}\right) & \theta_{fwt}\le\theta_D \\ \theta_D^{\delta}\frac{{}_2F_1\left(n+l+\delta\, n+l,n+l+1,1-\frac{\theta_D}{\theta_{fwt}}\right)}{\left(\frac{\theta_D}{\theta_{fwt}}\right)^{-n-l}} & \theta_{fwt}\ge\theta_D \end{cases} \end{aligned} \tag{3.11}$$

The expression in (3.3) provides us the probability that a frame on the observed typical link with inter-node distance r is successful in the case where the transmitter Tx_0 has passed the MAT and the receiver Rx_0 is listening (*i.e* failed its MAT). The probability of the combination of these two independent events is given by $p(1-p)$. Therefore, the probability of a successful frame on the observed typical link without any conditions on the outcome of the MAT of the transmitter Tx_0 and the receiver Rx_0 is simply given by

$$P_S(r) = p(1-p)P_{S|Tx,Rx}(r) \tag{3.12}$$
$$= p(1-p)\sum_{n=k}^{K}\binom{K}{n}\sum_{l=0}^{K-n}(-1)^l\binom{K-n}{l}P_{n+l}(r)$$

In the next section, we finally calculate $\bar{P}_{fwt->D}$ and derive performance metrics taking into account the influence of the routing protocol.

3.3 Link Distance-Averaged Performance Analysis

As mentioned previously, the routing protocol in multi-hop networks determines how transmitters select the next relay of a packet. For a random deployment, the link distance is equally random and its distribution is defined by the routing protocol. In this chapter, we consider the simple yet nearly-optimal "Nearest Neighbor in Cone" routing protocol [5].

Consider a network in which nodes are aware of the position of one another and use the "Nearest Neighbor in Cone" routing protocol with parameter ω. [5] Then, for a transmitter Tx_0 having a packet with final destination F_0, the next-hop Rx_0 of the packet will be the nearest neighbor to Tx_0 among all nodes located within a cone with angular width ω and directed from Tx_0 to F_0. In [5], it was shown that transmissions to the nearest neighbor located within a certain cone directed toward the final destination of the packet provided an almost optimal mean effective progress toward the final packet destination. In short, the reason is that the transmission success probability decreases exponentially with the link distance, while the spatial progress only increases linearly. Thus their product is maximized for short link distances. From [24], the distribution of the link distance for the above protocol is given by

$$f(r) = \lambda\omega r e^{-\lambda\frac{\omega}{2}r^2} \tag{3.13}$$

We are now ready to evaluate performance metrics averaged over the link distance. In the following, we calculate $\bar{P}_{fwt->D}$, the average frame success probability in (3.12) and the

MELT. The term $\bar{P}_{fwt->D}$ denotes the probability of success for a transmission from a node which has passed the MAT to a receiver for which the test result is unknown. Therefore, we can obtain $\bar{P}_{fwt->D}$ by averaging $(1-p)\,P_{S|Tx,Rx}\,(r)$ over the link distance r, in the special case where $\theta_D = 0$. Note that $P_{S|Tx,Rx}\,(r)$ is a function of r of the form $e^{-\lambda c r^2}$, where c is a fixed parameter independent of r. Consequently, for a network using the "Nearest Neighbor in Cone" routing protocol, taking the expectation over r leads to an integral of the form $\int_0^{+\infty} \lambda\omega r e^{-\lambda r^2\left(c+\frac{\omega}{2}\right)} dr$ which can be solved easily using the variable substitution $t = \lambda r^2\left(c+\frac{\omega}{2}\right)$. Thus, the average frame success probability can be expressed as

$$\bar{P}_S\,(k,\theta_{fwt},\theta_D) = \sum_{n=k}^{K}\binom{K}{n}\sum_{l=0}^{K-n}\frac{(-1)^l\binom{K-n}{l}p\,(1-p)\,\omega}{\omega + 4\pi p h_{n+l}\,(\theta_{fwt},\theta_D)} \tag{3.14}$$

and $\bar{P}_{fwt->D} = p^{-1}\bar{P}_S\,(k,\theta_{fwt},0)$.

Let us denote the bandwidth during the data slot as B_{TR} and the bandwidth in the FBT and ACK slots as B_{RT} such that $B_{TR}+B_{RT} = B$. We can now define the MELT $\bar{\mathcal{T}}$. Assuming that Gaussian signalling is used, $\bar{\mathcal{T}}$ can be expressed using the Shannon capacity formula for AWGN channel. That is,

$$\bar{\mathcal{T}} = B_{TR}\rho_{MAC}\log_2\left(1+\theta_D\right)\bar{P}_S\,(\theta_{fwt},\theta_D) \tag{3.15}$$

where $0 < \rho_{MAC} < 1$ is a factor accounting for the rate loss due to the fraction of time reserved for the transmission of control packets (*i.e*, FWT, FBT and ACK). Neglecting inter-slot intervals, we can write $\rho_{mac} = \frac{T_D}{T_{fwt}+T_{fbt}+T_D+T_{ack}}$. Note that in the case of Gaussian signalling, the duration of a control packet, *e.g*, the FWT packet, depends on its decoding threshold θ_{fwt} through the relation $T_{fwt} = \frac{N_{fwt}}{b(K)\log_2\left(1+\theta_{fwt}\right)}$, where $b\,(K)$ is the bandwidth of a shared band. In order to keep the energy consumed by the transmitter during the FWT slot constant for all values of K, we define the bandwidth of a shared band as $b\,(K) = \frac{B}{K}$.

We assume in the following that $\theta_{fbt} = \theta_{ack} = \theta_{fwt}$. Therefore, $T_{fbt} = T_{ack} = \frac{N_{fwt}}{B_{RT}\log_2\left(1+\theta_{fwt}\right)}$. Let us also define the occupancy ratio of the feedback bandwidth $\epsilon = \frac{B_{RT}}{B}$. Then we have $\theta_D = 2^{\frac{\tau}{(1-\epsilon)B}} - 1$, where τ is the target data-rate. Therefore, for fixed ω and K, the MELT is a function of τ, ϵ, k, θ_{fwt} and p.

In the next section, we compare theoretical results with simulated data and perform a

numerical analysis of the closed form expressions we developed.

3.4 Numerical Results

3.4.1 Simulation Method

In the following Monte-Carlo packet level simulation, nodes are distributed uniformly over a disk to approximate an HPPP according to the methodology in [29])[3]. Unlike the theoretical model used in the analysis, there is no observed typical link deployed additionally. All nodes are included in the HPPP. In each simulation drop, we generate a random deployment of the network, record the transmission successes of a randomly chosen link, then average results over all drops. The path-loss power law is defined as $1/\left(1+r^{\alpha}\right)$ to ensure that the power received is less than the transmitted one. Also, thermal noise is taken into account for a receiver temperature of $25^{o}C$. All other elements of the simulated model (e.g fading) are as described in section 2 and nodes strictly behave according to the MAC and routing protocols. Note that the assumption that FBT and ACK packets are transmitted error-free on all links in the network is maintained in the simulation.

3.4.2 Comparison to Simulated Data

Simulation parameters are given in table 3.1 and were set to values on the same order as those of conventional wireless sensor networks. Addresses of nodes are assumed to be 16 bits long. Control packets (i.e FWT, FBT and ACK) carry the addresses of both transmitter and receiver as well as 8 extra bits for other purposes.

The MELT is showed in figure 3-3 for various target data-rates. We observe a good qualitative agreement between theory and simulation. Theoretical curves acting as lower-bounds on the simulated data is due to the difference of deployment. In the simulation the observed link is chosen from the HPPP, while in the theoretical model it is not part of it. Thus, there are less interferers close to the observed link in the simulated system. Other simulation results for different values of ω, p, K and k consistently confirmed the satisfying

[3]The radius is set large enough so that approximately 10^3 nodes are deployed.

Table 3.1: Simulation Parameters

Parameter	Symbol	Value
path-loss exponent	α	4
node density	λ	10^3 node/km^2
reserved bandwidth	B	500 kHz
feedback ratio	ϵ	0.1
carrier frequency	f_c	2.4 GHz
control packet size	N_{fwt}	40 bit
data slot duration	T_D	2 ms
routing cone angle	ω	$\pi/3$ radian
MAT success probability	p	0.3
Number of shared bands	K	10
FWT success requirement	k	7

agreement between theoretical and simulated results.

3.4.3 Numerical Analysis

From the numerical analysis of (3.15), we obtain the three following important results. **1)** As illustrated in figure 3-4 for various T_D, there exists a certain number of shared bands K for which the MELT is maximum. As K increases, the MELT also increases at first. This is due to the improved information obtained during the control handshake thanks to the control packet diversity. However, increasing K also increases the time duration of FWT packets, due to $b(K) = \frac{B}{K}$, which in turn decreases ρ_{MAC}. Then, for high values of K, the diversity gain does not compensate the loss due to a lower ρ_{MAC}. Thus, the lower T_D, the faster ρ_{MAC} decreases with T_{fwt}, the lower the MELT-optimal K. **2)** For any value of K, the corresponding optimal number of FWT copies required for a FWT success is always $k = 1$. Therefore, as soon as the receiver decodes one of the FWT packets, it can discard the others and thus save energy. **3)** The MELT-optimal decoding threshold for the FWT packet is strongly influenced by the diversity order and the data packet duration T_D, as illustrated in figure 3-5.[4] The variations in θ_{fwt} for varying K and T_D are on the scale of several

[4]The non-smooth aspect of the curves is not due to a rough quantization of the search space for θ_{fwt}.

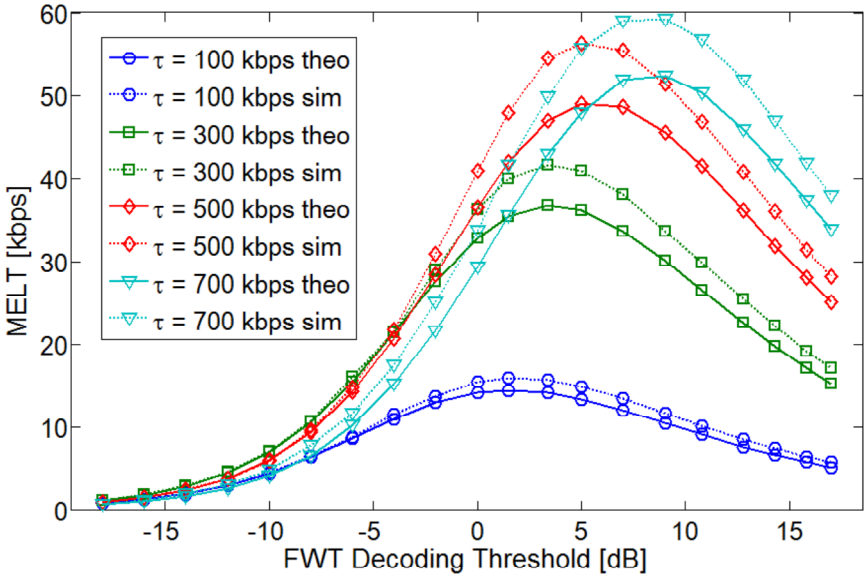

Figure 3-3: MELT against FWT decoding threshold, given various target data-rates. "Sim" denotes simulation and "Theo" denotes theory.

decibels and thus have a profound impact on the design of the decoding requirements of the FWT packet.

Note that the MELT-optimal values of the other parameters (i.e p, ϵ and τ) were almost invariant with respect to K and T_D. Practically, setting $0.13 < \epsilon < 0.16$, $0.36 < p < 0.39$ and $310 < \tau < 330$ kbps yielded an almost optimal MELT for any K and any $T_D \in \{1, 2, 3, 4\}$ ms.

3.5 Conclusion

In this chapter, we have presented a new theoretical framework based on point process theory as a first step toward the analysis of protocols based on handshakes without spatial reservation. Our study focused on a simple medium access control scheme composed of an initial random test followed by a four-way handshake. A closed forms expression for the mean effective link throughput was derived for the case with control packet diversity implemented through multiple frequency bands in a block-fading channel. Our results, confirmed by comparison to simulated data, provide the following important insights regarding contention in mobile ad hoc networks. In the presence of uncorrelated fading between control

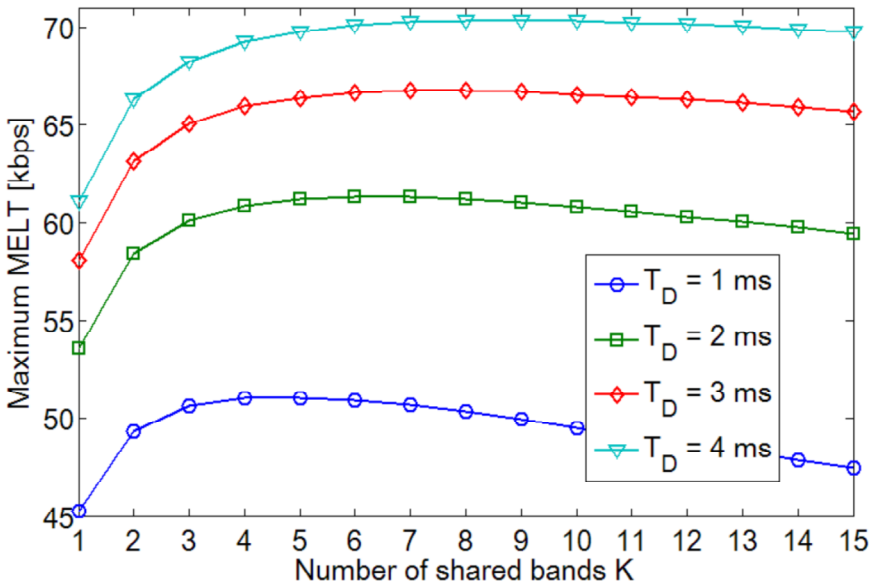

Figure 3-4: Maximum MELT against the number of shared bands used K, for various T_D. For each value of K, all the other parameters are set to their theoretically optimal value.

and traffic handshakes and given a fixed transmit-energy constraint: **1)** as the diversity order increases, the diversity gain becomes counterbalanced by the loss due to increased control packet duration; hence the existence of an optimal diversity order value. **2)** The design of MELT-optimal decoding requirements for the control packets is strongly influenced by the order of the control packet diversity. One limitation of the approach chosen in this chapter is that feedback packets are considered error-free, which is actually unrealistic. However, it is unclear whether this assumptions has an actual impact on performance; the the study of that latter case in the following chapter.

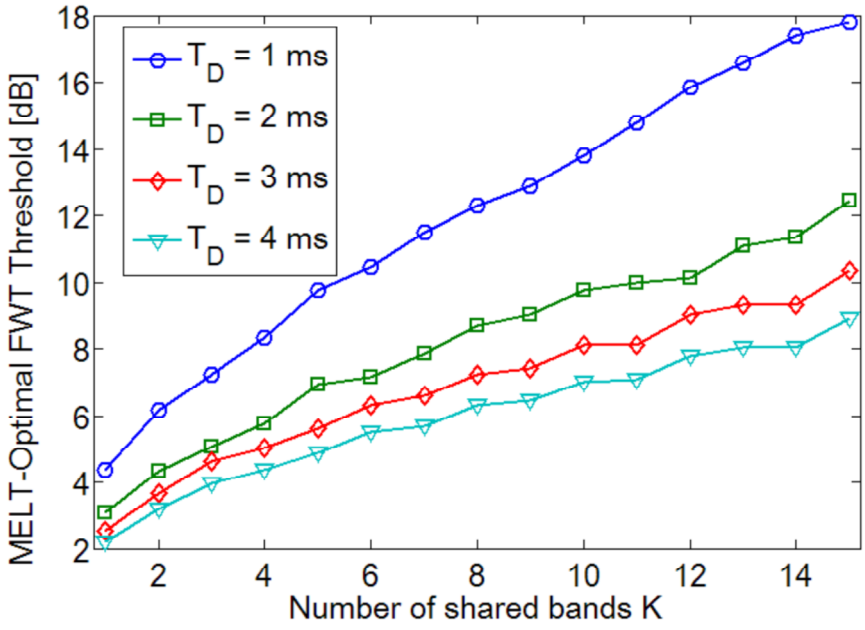

Figure 3-5: MELT-optimal decoding threshold θ_{fwt} against the number of shared bands K, for various T_D.

Chapter 4

Influence of Imperfect Feedback on Four-Way Handshake Performance

In this chapter, we propose a new mathematical framework based on point process theory applicable to the emerging contention mechanisms described above. Our analysis focuses on a simple MAC scheme including a random access test coupled with a four-way handshake (i.e one control handshake without spatial reservation effect and one traffic handshake). The theoretical model we present takes into account time-varying channel impairments, the interference inherent to large networks, different decoding requirements for each packet and the influence of the routing protocol. Moreover, in contrast with the majority of the literature, the influence of imperfect feedback is also considered in the analysis. Indeed, it is impractical to consider error-free feedback in an ad hoc network [38, 17], since the lack of coordination between nodes means that all links have to use a common feedback channel.

Throughout the chapter, we derive in closed forms the average link outage probability as well as the Average Spatial Density of Transport (ASDT) [5] in a mobile multi-hop ad hoc network. All results are confirmed by comparison to simulated data and lead to two general conclusions. In the presence of fading uncorrelated between traffic and control handshakes, we observe the following. 1) Optimal contention is achieved by designing control packets decodable even in the presence of strong interference. 2) The impact of imperfect feedback on performances in an interference-limited mobile ad hoc network is

not negligible.

The remainder of this chapter is organized as follows. In section 4.1, we introduce the system model used as a basis for our stochastic analysis. In section 4.2, we calculate a closed form approximation of the frame success probability for a given link distance. In section 4.3, we calculate the frame outage probability and the achievable spatial density of transport of the network, for the case of a progress-optimal routing protocol. Then, in section 4.4, we compare the presented theoretical results to realistic simulated data and perform a numerical joint optimization of the MAC/routing parameters. Finally, a conclusion summarizes the chapter.

4.1 System Model

In this section, we describe the system model used in the remainder of this chapter.

4.1.1 Imperfect Feedback Model

We consider that a frame is composed of four consecutive slots, each corresponding to a given packet, in the following order: Forward Test (FWT), Feedback Test (FBT), Data, ACK. At the beginning of a frame, all nodes with a packet to transmit have to pass a random test as in [51] (i.e a biased coin toss), which has a fixed success probability p. Successful nodes become active transmitters while the remaining nodes become silent and listen to the medium. In the remainder, we refer to the this random test as Medium Access Test (MAT). During the FWT slot, active transmitters send a FWT packet to their intended destination. If a silent node decodes a FWT packet intended for itself, it then replies to the sender with a FBT packet. If an active transmitter decodes a FBT packet intended for itself, then the link performs a conventional traffic handshake (Data then ACK). This process is illustrated in figure 4-1. In the remainder, when referring to the above-defined MAC scheme, we will use the abbreviation TPMAC (for Test Packet-based MAC). As in [29], a transmission is considered successful if the Signal to Interference power Ratio at the receiver is greater than a predetermined threshold, which is a function of the Modulation and Coding Schemes employed. Note this is a good approximation to the packet error rate if strong coding is

used [13]. We define the thresholds used in each type of slot as follows: θ_{FWT}, θ_{FBT}, θ_D and θ_{ACK}. We assume all links in the network use the same four above-mentioned thresholds.

4.1.2 System Assumptions

Time in the system is slotted and nodes are synchronized with one another as in [51]. The network considered is in the saturated regime, therefore each node has infinite backlog. All nodes use the same frequency band and therefore the network is also interference-limited (i.e the interference power at any given receiver is larger than the noise power by several orders). Finally, all nodes have unit transmit power and mobile but moving slowly enough so that path-loss on any link can be considered constant during a frame. The channel between nodes is composed of fast fading and path-loss, which is modelled by a power law $l(r) = r^{-\alpha}$ where α is the path-loss exponent. Regarding fast fading, we employ the slot-by-slot block-fading channel model. Therefore, fading is constant during a packet transmission but two fading coefficients on distinct packets are independent. The complex amplitude of the fading coefficient during each packet is defined as a circularly-Gaussian random variable with unit variance. Therefore, the squared norm of the fading is exponentially distributed with rate 1. The fading is also independent across links.

Remark: Note that in reality fading is correlated in time, which benefits the contention process since the fading level during the control handshake provides information about the fading level during the traffic handshake. The fading model used in the analysis represents a worst-case scenario in which only path-loss and interferer set are constant over a frame. Therefore, the results of our analysis provide lower-bounds on the actual performances of a mobile multi-hop ad hoc network.

We study the performances of a typical transmitter-receiver pair placed as follows. A first node Tx_0 is located at the origin of the two-dimensional space, while its target Rx_0 is placed at a distance r from it. We will later refer to these two nodes as the observed typical link. The deployment of the remaining nodes is modelled by an HPPP Φ with density λ. We will later refer to Φ as the interferer set. After the initial MAT, the interferer set is divided into an active transmitter set Φ^1 and a receiver set Φ^0. Due to the thinning property

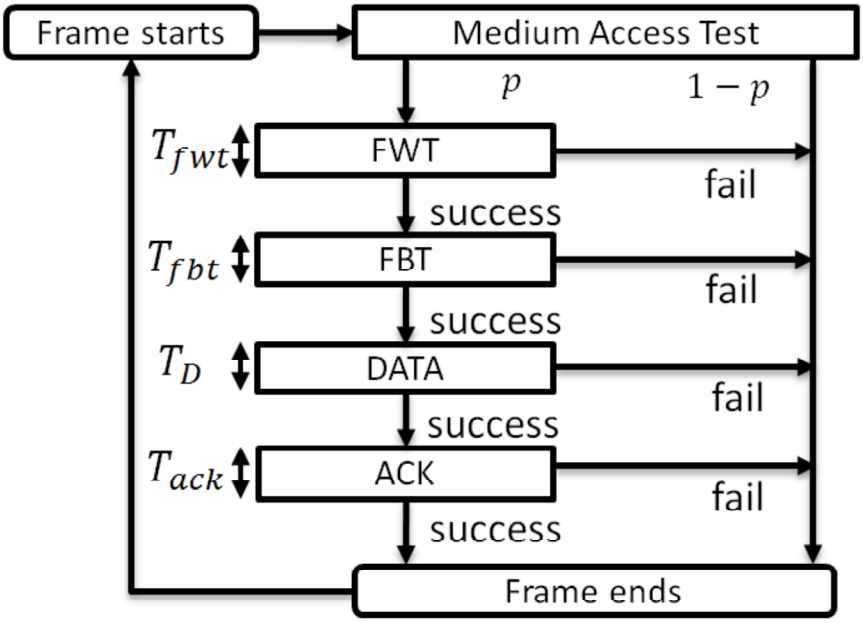

Figure 4-1: Process of the TPMAC scheme.

of the HPPP, Φ^1 and Φ^0 are both HPPPs with density λp and $\lambda(1-p)$, respectively. Tx_0 and Rx_0 are equally subject to the MAT, however they are not part of the above-defined sets. In order to keep the analysis tractable, we also incorporate the following features in our model, which are commonly used in the literature (see [52] and references therein). 1) Although interference in a HPPP deployment is spatially correlated [27], we assume it is independent between nodes, for the sake of tractability. That is, successes in a given slot on two different links are independent. So as to show this assumption is acceptable, simulations used for comparison take into account the spatial correlation of the interference. 2) Transmission success probabilities calculated on the typical link are used to approximate the same transmission success probabilities on each link of the interferer set. For instance, the probability of joint success of FWT and FBT packets on a link of the interferer set is approximated by the same probability obtained on the observed typical link. This assumption is reasonable for an homogeneous infinite network model, since every node in average experiences the same level of interference.

4.1.3 Achievable Spatial Density of Throughput Definition

The main goal of our analysis is to determine spatially-averaged results relevant to multi-hop transmissions (*i.e* averaged over all realizations of the interferer set and over the link distance). We firstly calculate the outage probability $\bar{P}_O$, defined as follows.

$$\bar{P}_O = 1 - \mathbb{E}_r \{P_S(r)\} \tag{4.1}$$

where $P_S(r)$ is the frame success probability for a fixed link distance r. Then, we calculate the ASDT $\bar{D}$, which can be regarded as the mean number of bit-meters transported per second per unit of space in the network [5]. Note that the probability distribution of the link distance r is determined by the routing protocol. In the next section, we investigate $P_S(r)$ with fixed r as a prerequisite to the analysis of routing-dependent metrics.

4.2 Outage Probability Calculation

In this section, we calculate the probability for a frame on the observed typical link to be successful, given that $\|Tx_0 - Rx_0\| = r$.

Given the system model of Section 2, the thinning property of HPPPs implies that the interferer set during each slot will be an HPPP. We thus define $\Phi_{ack} \subset \Phi_{fbt} \subset \Phi^0$ the interferer sets in the ACK and FBT slots, respectively, and $\Phi_D \subset \Phi_{fwt} = \Phi^1$ the interferer sets in the Data and FWT slots, respectively.

For any node $Tx_n \in \Phi^1$, $n = 1, ..., +\infty$, we define the distance $d_{0n} = \|Tx_n - Rx_0\|$ to Rx_0. Also, for a given frame, we define the squared fading coefficients $G_{fwt,0n}$ and $G_{D,0n}$ of the channel between Tx_n and Rx_0 during the FWT and Data slots, respectively. In the same way, for any node $Rx_l \in \Phi^0$, $l = 1, ..., +\infty$, we define the distance $d_{l0} = \|Rx_l - Tx_0\|$ to Tx_0 as well as $G_{fbt,0l}$ and $G_{ack,0l}$. Also, we define $G_{fwt,00}$, $G_{fbt,00}$, $G_{D,00}$ and $G_{ack,00}$ the squared fading coefficients on the typical link during the FWT, FBT, Data and ACK slots, respectively.

Given these definitions, if Tx_0 attempts a transmission to Rx_0 in a given slot, the Signal

to Interference Ratio $\gamma_{slot,00}$ at Rx_0 is given by

$$\gamma_{slot,00} = \frac{G_{slot,00} r^{-\alpha}}{\sum_{Tx_n \in \Phi_{slot}} G_{slot,0n} d_{0n}^{-\alpha}} = \frac{G_{slot,00} r^{-\alpha}}{I_{slot,0}} \tag{4.2}$$

where the index *slot* can denote either fwt, fbt, D or ack.

For any node U in the network, we define δ_U the random variable taking value in $\{0,1\}$ such that $\delta_U = 1$ if U passes the random MAT, and $\delta_U = 0$ otherwise. Conditioned on Tx_0 passing the MAT and Rx_0 failing to it, the frame success probability is given by

$$\begin{aligned}
&P_{S|Tx,Rx}(r) = \\
&\mathbb{P}\left(\gamma_{fwt,00} > \theta_{fwt}, \gamma_{fbt,00} > \theta_{fbt}, \gamma_{D,00} > \theta_D,\right. \\
&\left.\gamma_{ack,00} > \theta_{ack} \,\middle|\, \delta_{Tx_0} = 1, \delta_{Rx_0} = 0\right) \\
&\overset{(a)}{=} \mathbb{E}\left\{G_{fwt,00} > \theta_{fwt} r^{\alpha} I_{fwt,0}, G_{fbt,00} > \theta_{fbt} r^{\alpha} I_{fbt,0},\right. \\
&\left. G_{D,00} > \theta_D r^{\alpha} I_{D,0}, G_{ack,00} > \theta_{ack} r^{\alpha} I_{ack,0} \,\middle|\, \delta_{Tx_0} = 1, \delta_{Rx_0} = 0\right\} \\
&\overset{(b)}{=} \mathbb{E}\left\{e^{-\theta_{fwt} r^{\alpha} I_{fwt,0} - \theta_{fbt} r^{\alpha} I_{fbt,0} - \theta_D r^{\alpha} I_{D,0} - \theta_{ack} r^{\alpha} I_{ack,0}} \,\middle|\, \delta_{Tx_0} = 1, \delta_{Rx_0} = 0\right\}
\end{aligned} \tag{4.3}$$

where the notation $|Tx,Rx$ indicates it is the frame success probability conditioned on the outcome of the MAT of the transmitter Tx_0 and the receiver Rx_0. In the above equations, (a) is obtained by replacing (4.2) into the first line of (4.3). Then (b) follows from the fact that fading coefficients in different slots are independent and identically distributed with complementary cumulative distribution function $F_G(g) = \mathbb{P}(G > g) = e^{-g}$.

Let us consider a certain realization of the interferer set Φ. Then each node $Tx_n \in \Phi_{fwt}$ has a probability $P_{fwt->D}\left(d_{t(n)n}\right)$ to be also in Φ_D, where $d_{t(n)n}$ is the distance to its intended target. Therefore, we have

$$I_{D,0} = \sum_{Tx_n \in \Phi_{fwt}} X_{D,n} G_{D,0n} d_{0n}^{-\alpha} \tag{4.4}$$

where $X_{D,n}$, $n = 1, ..., +\infty$ are independent random variables taking value in $\{0,1\}$ and such that $\mathbb{P}(X_{D,n} = 1) = P_{fwt->D}\left(d_{t(n)n}\right)$. In the same way, every node $Rx_l \in \Phi^0$ has a probability $P_{0->fbt}(\mathbf{d}_l)$ to be also in Φ_{fbt}. Note that this is the probability for a node in Φ^0 to decode a FWT packet intended for itself, from any transmitter. Therefore, it is a function

of the distances to all the transmitters of FWT packet, *i.e*, a function of the vector $\mathbf{d}_l = [d_{l1}, d_{l2}, ..., d_{ln}, ...]^T$, where d_{ln} is the distance from the n-th node in Φ_{fwt} to Rx_l. We define the corresponding activity indicator random variables $X_{fbt,l}$, $l = 1, ..., +\infty$. Finally, every node in Φ_{fbt} has a probability $P_{fbt->ack}\left(d_{lc(l)}\right)$ to be also in Φ_{ack}, where $d_{lc(l)}$ is the distance to its target. We thus define the corresponding activity indicator random variables $X_{ack,l}$, $l = 1, ..., +\infty$. Note that the above random variables are defined for a certain realization of Φ. Therefore, link successes are only random due to the random fading coefficients. We can thus conclude that $X_{fbt,l}$, $X_{ack,l}$ and $X_{D,n}$ are pairwise independent, $\forall l, n \in \mathbb{N}^*$. Now we are ready to develop the conditioned frame success probability as follows. For the sake of

brevity, we drop the notation $\left|\delta_{Tx_0}=1,\delta_{Rx_0}=0\right.$ in the following expressions.

$$
\begin{aligned}
&P_{S|Tx,Rx}\left(r\right)= \qquad (4.5)\\
&\mathbb{E}\left\{e^{-r^{\alpha}\sum_{Tx_n\in\Phi^1}d_{0n}^{-\alpha}\left(\theta_{fwt}G_{fwt,0n}+\theta_D X_{D,n}G_{D,0n}\right)}\right.\\
&\left.e^{-r^{\alpha}\sum_{Rx_l\in\Phi^0}d_{0l}^{-\alpha}\left(\theta_{fbt}X_{fbt,l}G_{fbt,0l}+\theta_{ack}X_{ack,l}X_{fbt,l}G_{ack,0l}\right)}\right\}\\
&\overset{(a)}{=}\mathbb{E}\left\{\prod_{Tx_n\in\Phi^1}\left(P_{fwt->D}\left(d_{t(n)n}\right)e^{-r^{\alpha}d_{0n}^{-\alpha}\left(\theta_{fwt}G_{fwt,0n}+\theta_D G_{D,0n}\right)}\right.\right.\\
&+\left(1-P_{fwt->D}\left(d_{t(n)n}\right)\right)e^{-r^{\alpha}d_{0n}^{-\alpha}\theta_{fwt}G_{fwt,0n}}\Big)\\
&\prod_{Rx_l\in\Phi^0}\left(P_{0->fbt}\left(\mathbf{d}_l\right)P_{fbt->ack}\left(d_{lc(l)}\right)e^{-r^{\alpha}d_{0l}^{-\alpha}\left(\theta_{fbt}G_{fbt,0l}+\theta_{ack}G_{ack,0l}\right)}\right.\\
&+P_{0->fbt}\left(\mathbf{d}_l\right)\left(1-P_{fbt->ack}\left(d_{lc(l)}\right)\right)e^{-r^{\alpha}d_{0l}^{-\alpha}\theta_{fbt}G_{fbt,0l}}\\
&\left.\left.+\left(1-P_{0->fbt}\left(\mathbf{d}_l\right)\right)\right)\right\}\\
&\overset{(b)}{=}\mathbb{E}\left\{\prod_{Tx_n\in\Phi^1}\left(\bar{P}_{fwt->D}e^{-r^{\alpha}d_{0n}^{-\alpha}\left(\theta_{fwt}G_{fwt,0n}+\theta_D G_{D,0n}\right)}\right.\right.\\
&+\left(1-\bar{P}_{fwt->D}\right)e^{-r^{\alpha}d_{0n}^{-\alpha}\theta_{fwt}G_{fwt,0n}}\Big)\\
&\prod_{Rx_l\in\Phi^0}\left(\bar{P}_{0->ack}e^{-r^{\alpha}d_{0l}^{-\alpha}\left(\theta_{fbt}G_{fbt,0l}+\theta_{ack}G_{ack,0l}\right)}\right.\\
&\left.\left.+\left(\bar{P}_{0->fbt}-\bar{P}_{0->ack}\right)e^{-r^{\alpha}d_{0l}^{-\alpha}\theta_{fbt}G_{fbt,0l}}+\left(1-\bar{P}_{0->fbt}\right)\right)\right\}\\
&\overset{(c)}{=}\mathbb{E}\left\{\prod_{Tx_n\in\Phi^1}\left(\bar{P}_{fwt->D}L_{\tilde{G}_1}\left(r^{\alpha}d_{0n}^{-\alpha}\right)\right.\right.\\
&+\left(1-\bar{P}_{fwt->D}\right)L_{G_{fwt}}\left(r^{\alpha}d_{0n}^{-\alpha}\theta_{fwt}\right)\Big)\\
&\prod_{Rx_l\in\Phi^0}\left(\bar{P}_{0->ack}L_{\tilde{G}_0}\left(r^{\alpha}d_{0l}^{-\alpha}\right)\right.\\
&\left.\left.+\left(\bar{P}_{0->fbt}-\bar{P}_{0->ack}\right)L_{G_{fbt}}\left(\theta_{fbt}r^{\alpha}d_{0l}^{-\alpha}\right)+\left(1-\bar{P}_{0->fbt}\right)\right)\right\}
\end{aligned}
$$

In the above, expression (a) is obtained by developing the exponential terms into products. Expression (b) is obtained by taking the expectation over all the link distances from each node of the interferer set, assuming they are independent. That is, we strictly apply the simplification stated in the previous section regarding the independence of suc-

cess probabilities on distinct links. The notation used is $\bar{P} = \mathbb{E}\{P\}$. The term $\bar{P}_{0->ack}$ is the average probability for a node in Φ^0 to be also in Φ_{ack}. It is obtained first by observing that $P_{0->ack}(\mathbf{d}_l) = P_{0->fbt}(\mathbf{d}_l) P_{fbt->ack}\left(d_{lc(l)}\right)$ which follows from Baye's theorem, then by taking the expectation over the link distances. To obtain expression (c) we firstly define the random variables $\tilde{G}_1 = \theta_{fwt}G_{fwt} + \theta_D G_D$ and $\tilde{G}_0 = \theta_{fbt}G_{fbt} + \theta_{ack}G_{ack}$ where $G_{ack}, G_D, G_{fwt}, G_{fbt}$ are independent and identically distributed exponential random variables with rate parameter 1. Then we simply apply the Laplace Transform notation $L_G(s) = \mathbb{E}\left\{e^{-sG}\right\}$ to the expression.

The Laplace Transform of an exponential random variable with rate 1 is given by $L(s) = 1/(1+s)$. Also, the Laplace Transform of $\tilde{G}_1$ is given by $\frac{1}{\left(1+\theta_{fwt}s\right)(1+\theta_D s)}$ and that of $\tilde{G}_0$ is given by $\frac{1}{\left(1+\theta_{fbt}s\right)(1+\theta_{ack}s)}$. Consequently, we can rewrite the conditioned frame success

probability as

$$
\begin{aligned}
&P_{S|Tx,Rx}\left(r\right) = \qquad (4.6)\\
&\mathbb{E}\left\{\prod_{Tx_n\in\Phi^1}\left(\frac{\bar{P}_{fwt->D}}{\left(1+\theta_{fwt}r^{\alpha}d_{0n}^{-\alpha}\right)\left(1+\theta_{D}r^{\alpha}d_{0n}^{-\alpha}\right)}\right.\right.\\
&\left.\left.+\frac{\left(1-\bar{P}_{fwt->D}\right)}{\left(1+\theta_{fwt}r^{\alpha}d_{0n}^{-\alpha}\right)}\right)\right\}\\
&\mathbb{E}\left\{\prod_{Rx_l\in\Phi^0}\left(\frac{\bar{P}_{0->ack}}{\left(1+\theta_{fbt}r^{\alpha}d_{l0}^{-\alpha}\right)\left(1+\theta_{ack}r^{\alpha}d_{l0}^{-\alpha}\right)}\right.\right.\\
&\left.\left.+\frac{\left(\bar{P}_{0->fbt}-\bar{P}_{0->ack}\right)}{\left(1+\theta_{fbt}r^{\alpha}d_{l0}^{-\alpha}\right)}\right)\right\}\\
&\overset{(a)}{=}e^{-\int_{\mathbb{R}^2}1-\frac{\bar{P}_{fwt->D}}{\left(1+\theta_{fwt}r^{\alpha}\|x-Rx_0\|^{-\alpha}\right)^{n+l}\left(1+\theta_{D}r^{\alpha}\|x-Rx_0\|^{-\alpha}\right)}-\frac{1-\bar{P}_{fwt->D}}{\left(1+\theta_{fwt}r^{\alpha}\|x-Rx_0\|^{-\alpha}\right)^{n+l}}\Lambda_1(dx)}\\
&e^{-\int_{\mathbb{R}^2}1-\frac{\bar{P}_{0->ack}}{\left(1+\theta_{fwt}r^{\alpha}\|x-Tx_0\|^{-\alpha}\right)^{n+l}\left(1+\theta_{D}r^{\alpha}\|x-Tx_0\|^{-\alpha}\right)}-\frac{\bar{P}_{fbt->ack}-\bar{P}_{0->ack}}{\left(1+\theta_{fwt}r^{\alpha}\|x-Tx_0\|^{-\alpha}\right)^{n+l}}\Lambda_0(dx)}\\
&\overset{(b)}{=}exp\left(-p\lambda 2\pi\int_0^{+\infty}\left(1-\frac{\bar{P}_{fwt->D}}{\left(1+\theta_{fwt}r^{\alpha}t^{-\alpha}\right)^{n+l}\left(1+\theta_{D}r^{\alpha}t^{-\alpha}\right)}\right.\right.\\
&\left.\left.-\frac{1-\bar{P}_{fwt->D}}{\left(1+\theta_{fwt}r^{\alpha}t^{-\alpha}\right)^{n+l}}\right)tdt\right)\\
&exp\left(-\left(1-p\right)\lambda 2\pi\int_0^{+\infty}\left(1-\frac{\bar{P}_{0->ack}}{\left(1+\theta_{fwt}r^{\alpha}t^{-\alpha}\right)^{n+l}\left(1+\theta_{D}r^{\alpha}t^{-\alpha}\right)}\right.\right.\\
&\left.\left.-\frac{\bar{P}_{fbt->ack}-\bar{P}_{0->ack}}{\left(1+\theta_{fwt}r^{\alpha}t^{-\alpha}\right)^{n+l}}\right)tdt\right)
\end{aligned}
$$

The first line is obtained by replacing the Laplace Transform terms and then observing that the product on Φ^1 and the product on Φ^0 are independent. Expression (a) follows by identifying the Probability Generating Functional of an HPPP (see Definition A.5 in [29]) in the first line. In the resulting two-dimensional integral, x is a point in space, while the function $\Lambda_1(.)$ (resp. $\Lambda_0(.)$) is the intensity measure of the HPPP Φ^1_{fwt} (resp. Φ^0_{fwt}). It can be thought of as the expected number of nodes in the region $dx \subset \mathbb{R}^2$. Then (b) follows immediately from the mapping theorem (see Theorem A.1 in [29]). The theorem is used to project Φ^1_{fwt} (resp. Φ^0_{fwt}) on $\mathbb{R}^+$, which simplifies the integration domain. To calculate

the integrals in (b), we use the following result, which can be obtained by recognizing Appell hypergeometric function in the integral below when taken from 0 to any $z > 0$, then by letting z tend toward infinity and using Appell's function relation to the Gauss hypergeometric function. The derivation is tedious but straightforward and so is omitted in this chapter due to limited space.

$$\int_0^{+\infty} \frac{t^u dt}{\left(t^\alpha + \left(\theta_{fwt} r^\alpha\right)\right)^v \left(t^\alpha + \left(\theta_D r^\alpha\right)\right)^w} = \tag{4.7}$$
$$\begin{cases} \frac{\Gamma\left(\frac{u+1}{\alpha}+1\right)\Gamma\left(v+w-\frac{u+1}{\alpha}+1\right){}_2F_1\left(\frac{u+1}{\alpha},w,v+w,1-\frac{\theta_{fwt}}{\theta_D}\right)}{\Gamma(v+w)(u+1)\left(\theta_{fwt} r^\alpha\right)^{v-\frac{u+1}{\alpha}}\left(\theta_D r^\alpha\right)^w} & \theta_{fwt} \leq \theta_D \\ \frac{\Gamma\left(\frac{u+1}{\alpha}+1\right)\Gamma\left(v+w-\frac{u+1}{\alpha}+1\right){}_2F_1\left(\frac{u+1}{\alpha},v,v+w,1-\frac{\theta_D}{\theta_{fwt}}\right)}{\Gamma(v+w)(u+1)\left(\theta_{fwt} r^\alpha\right)^{v}\left(\theta_D r^\alpha\right)^{w-\frac{u+1}{\alpha}}} & \theta_{fwt} \geq \theta_D \end{cases}$$

In the above u, v, w must satisfy $u - \alpha(v + w) < -1$ and the function ${}_2F_1$ is the Gauss hypergeometric function. Solving the above expression for the parameters in (4.6) leads, after some algebraic manipulations, to the following result

$$P_{S|Tx,Rx}(r) = \tag{4.8}$$
$$exp\left(-\lambda\pi r^2 C(\alpha)\left(h_{TR}\left(\theta_{fwt},\theta_D\right) + h_{RT}\left(\theta_{fbt},\theta_{ack}\right)\right)\right)$$

where $C(\alpha) = \pi\delta \csc(\pi\delta)$ with $\delta = \frac{2}{\alpha}$ and

$$h_{TR}\left(\theta_{fwt},\theta_D\right) = p\theta_{fwt}^\delta + \frac{p\theta_D \bar{P}_{fwt->D}\left(\theta_{fwt}^\delta - \theta_D^\delta\right)}{\theta_{fwt} - \theta_D} \tag{4.9}$$

and

$$h_{RT}\left(\theta_{fbt},\theta_{ack}\right) \tag{4.10}$$
$$= \begin{cases} (1-p)\left(\bar{P}_{0->fbt}\theta_{fbt}^\delta + \frac{\theta_{ack}\bar{P}_{0->ack}\left(\theta_{fbt}^\delta - \theta_{ack}^\delta\right)}{\theta_{fbt}-\theta_{ack}}\right) & \text{if } \theta_{fbt} \neq \theta_{ack} \\ (1-p)\,\theta_{fbt}\left(\bar{P}_{0->fbt} + \bar{P}_{0->ack}\delta\right) & \text{if } \theta_{fbt} = \theta_{ack} \end{cases}$$

We are now left with the tasks of evaluating in closed form the average probabilities $\bar{P}_{fwt->D}, \bar{P}_{0->ack}, \bar{P}_{0->fbt}$ and calculating the other routing-dependent metrics (*i.e* the aver-

age outage probability and the ASDT). To proceed, we have to consider a particular routing protocol so as to define the link distance distribution.

4.3 Joint MAC-Routing Performance Analysis

In this section, we evaluate in closed form the average outage probability and the ASDT, for the case of the routing protocol "Nearest Neighbor in Cone". In this protocol, nodes forward packets to the closest neighbor located within a cone of angle ω directed toward the final packet destination. It was shown in [5] that the "Nearest-Neighbor in Cone" routing protocol is almost optimal in terms of packet progress toward the final destination. The main reason is that, as the link distance increases, the outage probability increases faster than the progress made toward the final destination.

From [24], we have that the corresponding probability density function of the link distance r is defined as

$$f(r) = \lambda \omega r e^{-\lambda \frac{\omega}{2} r^2} \tag{4.11}$$

However, setting the data-rate arbitrarily low obviously allows to transmit reliably even to very distant receivers. Therefore, the achievable throughput on each hop is also a metric of interest. The concept of transport, expressed as the product of the number of bits and the number of meters associated with a transmission, captures both of the above notions. Therefore, the ASDT, which is the achievable transport of the network per unit of space, emerges as the most relevant metric to quantify the performance of a multi-hop ad hoc network. Mathematically, the ASDT can be defined as follows.

$$\bar{D} = \lambda \rho_D \log_2(1+\theta_D)\, \mathbb{E}\{\cos(\Psi)\}\, \mathbb{E}_r\{r P_S(r)\} \tag{4.12}$$

In the above expression, $\rho_D \log_2(1+\theta_D)$ is the spectral efficiency of the transmission, where $\rho_D = \frac{1}{1+\epsilon}$ with $\epsilon = \frac{T_{fwt}+T_{fbt}+T_{ack}}{T_D}$ is a factor that account for the throughput loss due to the fraction of time in a frame reserved for control packets (*i.e* FWT, FBT and ACK).[1] Note

[1]The interval between slots, which is commonly on the order of the microsecond, is assumed negligible compared to slot durations.

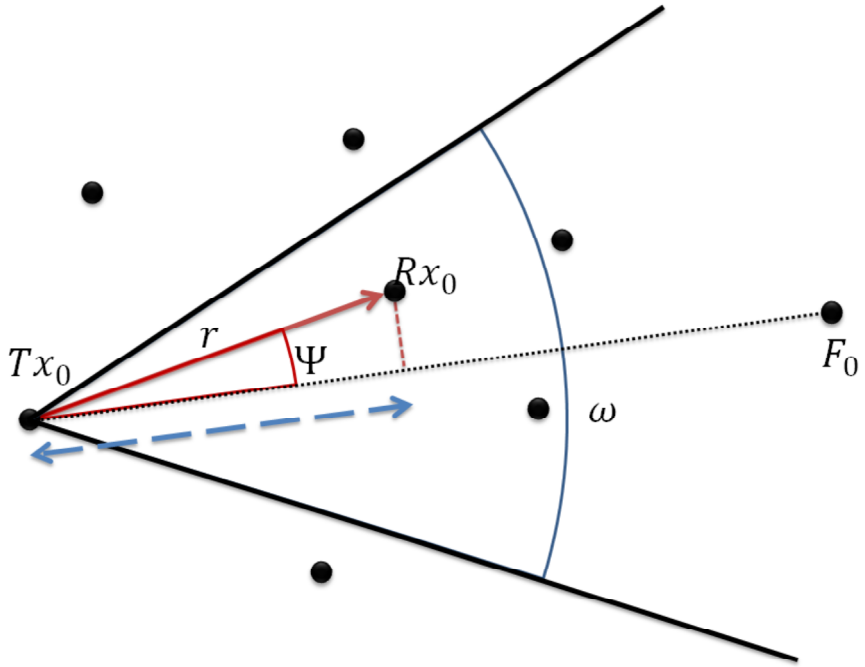

Figure 4-2: Selection of the next relay with the "Nearest Neighbor in Cone" routing protocol. In the figure Tx_0 is the transmitter, Rx_0 is the receiver and F_0 is the final destination of the packet.

that ϵ is a function of the decoding thresholds of these control packets. To illustrate this fact, consider for instance a desired FWT decoding threshold θ_{fwt}, then, assuming Gaussian signalling, the duration of the FWT packet is given by $T_{fwt} = \frac{N_{fwt}}{Blog_2\left(1+\theta_{fwt}\right)}$, where N_{fwt} is the number of information bits in a FWT packet and B is the bandwidth used for transmission.

The term $\mathbb{E}\{\cos(\Psi)\}\mathbb{E}_r\{rP_S(r)\}$ is the mean effective progress made by the packet toward its final destination. The term Ψ is the random angle between the direction toward the receiver and the direction toward the final destination (see figure 4-2 for an illustration). We assume in the remainder that for each node in the network, the direction toward the final destination of each packet is uniformly distributed and independent across nodes and packets. It follows that Ψ is uniformly distributed between $-\frac{\omega}{2}$ and $\frac{\omega}{2}$. Therefore, we have $\mathbb{E}\{\cos(\Psi)\} = \frac{2}{\omega}\sin\left(\frac{\omega}{2}\right)$ (see [47]). Then, given (4.8), taking the expectation over r in (4.12) leads to an integral of the form

$$\int_0^{+\infty} r^2 e^{-cr^2} dr = \frac{\int_0^{+\infty} \sqrt{t} e^{-t} dt}{2c^{\frac{3}{2}}} = \frac{\Gamma\left(\frac{3}{2}\right)}{2c^{\frac{3}{2}}} \tag{4.13}$$

where c is independent of the integration variable. It then follows that

$$\bar{D} = \frac{\rho_D \log_2(1+\theta_D)\, p(1-p)\, \lambda^{\frac{1}{2}} \sin\left(\frac{\omega}{2}\right) \frac{\sqrt{\pi}}{2}}{\left(\frac{\omega}{2} + \pi C(\alpha)\left(h_{TR}(\theta_{fwt}, \theta_D) + h_{RT}(\theta_{fbt}, \theta_{ack})\right)\right)^{\frac{3}{2}}} \tag{4.14}$$

Similarly, we can evaluate the outage probability averaged over the link distance, given by $\bar{P}_O = p(1-p)\left(1 - \mathbb{E}_r\left\{P_{S|Tx,Rx}(r)\right\}\right)$. Using (4.11) and (4.8), we obtain a well-known integral of the form $\int_0^{+\infty} re^{-cr^2}dr$ which is equal to $\frac{1}{2c}$ for some constant c. It then follows that

$$\bar{P}_O = \frac{p(1-p)\, 2\pi C(\alpha)\left(h_{TR}(\theta_{fwt}, \theta_D) + h_{RT}(\theta_{fbt}, \theta_{ack})\right)}{\omega + 2\pi C(\alpha)\left(h_{TR}(\theta_{fwt}, \theta_D) + h_{RT}(\theta_{fbt}, \theta_{ack})\right)} \tag{4.15}$$

This expression can be regarded as the average probability in a given frame to fail the transmission of the packet at the top of the buffer.

Note that we still have to calculate the terms $\bar{P}_{fwt->D}$, $\bar{P}_{0->ack}$, $\bar{P}_{0->fbt}$ in order for the a

2, we evaluate these probabilities on the typical link Tx_0, Rx_0 and use the result as an approximation of the actual probability. The term $\bar{P}_{fwt->D}$ is the probability for a node which has sent a FWT to also transmit during the Data slot. Therefore, for any link

$$\begin{aligned}
\bar{P}_{fwt->D} &= (1-p)\,\mathbb{E}\left\{\mathbb{P}\left(\gamma_{fwt} \geq \theta_{fwt}, \gamma_{fbt} \geq \theta_{fbt}\right)\right\} \qquad (4.16)\\
&\overset{(a)}{=} (1-p)\,\mathbb{E}\left\{\prod_{Tx_n \in \Phi^1} e^{-\theta_{fwt} d_{0n}^{-\alpha} G_{fwt,0n}} \prod_{Rx_l \in \Phi^0} e^{-\theta_{fbt} d_{l0}^{-\alpha} G_{fbt,0l} X_{fbt,l}}\right\}\\
&\overset{(b)}{=} (1-p)\,\mathbb{E}\left\{\prod_{Tx_n \in \Phi^1} e^{-\theta_{fwt} d_{0n}^{-\alpha} G_{fwt,0n}}\right\}\\
&\mathbb{E}\left\{\prod_{Rx_l \in \Phi^0} P_{S,fwt}\left(d_{lc(l)}\right) e^{-\theta_{fbt} d_{l0}^{-\alpha} G_{fbt,0l}}\right\}\\
&\overset{(c)}{=} \mathbb{E}\left\{(1-p)\, e^{-\lambda r^2 \pi C(\alpha)\left(p\theta_{fwt}^{\delta} + (1-p)\bar{P}_{S,fwt}\theta_{fbt}^{\delta}\right)}\right\}\\
&\overset{(d)}{=} \frac{(1-p)\,\omega}{\omega + 2\pi C(\alpha)\left(p\theta_{fwt}^{\delta} + (1-p)\,\bar{P}_{S,fwt}\theta_{fbt}^{\delta}\right)}
\end{aligned}$$

In the above, (a) is obtained from the definition of γ_{fwt} and γ_{fbt}. Expression (b) follows from taking the expectation over $X_{fbt,l}$ for $l = 1, ... + \infty$, then observing that the resulting

random products over Φ^1 and Φ^0 are statistically independent. Expression (c) follows from using the same steps as used to obtain equation (4.6). Finally, (d) is obtained by taking the expectation over the link distance r.

The term $\bar{P}_{0->fbt}$ represents the probability for a node in Φ^0 (*i.e* listening to the channel during the FWT slot) to successfully receive at least one packet intended for itself. Therefore, its calculation requires to take all transmitters in the network into account, which makes it a difficult problem. However, it is possible to obtain a simple upper-bound on this probability. Let us consider the ideal case where for any two nodes in Φ^1, the FWT packet destinations chosen are different. In this case, FWT transmissions never compete for a same receiver. Let $\bar{P}_{S,fwt|Tx,Rx}$ be the average probability of success on the typical link conditioned on the transmitter being in Φ^1 and the receiver being in Φ^0. Since a unique receiver is associated to each transmitter, we have in this case $\bar{P}_{0->fbt} = p\bar{P}_{S,fwt|Tx,Rx}$. In the general case where FWT transmissions may compete with one another for a single receiver, we have $\bar{P}_{0->fbt} \leq p\bar{P}_{S,fwt|Tx,Rx}$. In the remainder we will use this upper-bound as an approximation of the actual probability.

The term $\bar{P}_{0->ack}$ is the average probability that a node in Φ^0 is active during both FBT and ACK slots. To calculate this probability exactly is very challenging. Nevertheless, using the same reasoning as for the upper-bound on $\bar{P}_{0->fbt}$, we can write $\bar{P}_{0->ack} \leq \bar{P}_{S,fwt+fbt+D|Rx}$, which is the average joint probability of success of the FWT, FBT and Data slots on the typical link, given that the receiver is listening to the channel. Therefore, we have

$$\begin{aligned}\bar{P}_{0->ack} &\leq \bar{P}_{S,fwt+fbt+D|Rx} \\ &= \frac{p\omega}{\omega + 2\pi C(\alpha)\left(h_{TR}(\theta_{fwt},\theta_D) + \bar{P}_{0->fbt}(1-p)\theta_{fbt}^{\delta}\right)}\end{aligned}$$

which is simply obtained by setting $\theta_{ack} = 0$ in (4.15) and then removing the assumption that the transmitter has passed the MAT successfully. We now have a closed form expression for $\bar{P}_{fwt->D}$ and upper bounds on $\bar{P}_{0->fbt}$ and $\bar{P}_{fbt->ack}$. Therefore, we can calculate and exploit numerically the theoretical results developed above, which is the subject of the next section.

4.4 Numerical Results

4.4.1 Simulation Method and Assumptions

In each drop of the Monte-Carlo packet level simulation, we generate a random deployment and record the transmission successes/failures of a randomly chosen link during one frame. We then average over all drops to estimate the outage probability. Nodes behave as described in section 2. Each node selects its next hop according to the "Nearest-Neighbor in Cone" routing protocol, then uses the TPMAC scheme to transmit the packet. However, the three following points of the simulated system are different. 1) The simulated network is modelled by a single HPPP (i.e all network nodes are in the point process, there is no "typical link" deployed additionally as in the theoretical model). 2) We employ the bounded path-loss model $l(r) = 1/(1 + r^{\alpha})$, so that the received power is always less than the transmitted one. 3) The receiver noise is taken into account for the calculation of SINR values.[2]

4.4.2 Simulation Parameters

The numerical values of the simulation parameters, listed in table 4.1, are chosen to fit the scenario of a large sensor network. The deployment area is a disk chosen large enough so that the network approximates an HPPP [29]. We assume that MAC addresses of nodes are 16 bits long, as in IEEE 802.15.4-based sensor networks [8]. Then FWT, FBT and ACK packets all carry $N_{fwt} = 40$ information bits (32 bits for addressing, plus 8 extra bits for other purposes).

To confirm that different fading levels between successive packets is realistic in the above system, we determine the condition on the node velocity v to obtain a coherence time shorter than the duration of two successive packets (i.e around 1ms with the given settings). Given that the 50% coherence time is $T_{coh} = \frac{9c}{16\pi f_c 2v}$ ms [44] where c is the speed of light in vacuum and $2v$ is the maximum relative speed between two nodes, we obtain the condition $v \geq 36$ km/h, which is a realistic vehicular speed.

[2]The temperature of the receivers is set to 25^oC.

Table 4.1: Simulation Parameters

Parameter	Symbol	Value
path-loss exponent	α	4
node density	λ	10^3 node/km^2
bandwidth	B	500 kHz
carrier frequency	f_c	2.4 GHz
control packet size	$N_{fwt}, N_{fbt}, N_{ack}$	40 bit
data slot duration	T_D	1 ms
routing cone angle	ω	$\pi/3$ radian
MAT success probability	p	0.3^3

4.4.3 Exploitation of Numerical Results

The frame outage probability as a function of the Data decoding threshold is plotted in figure 4-3 for $\theta_{fwt} = -2$dB, $\theta_{ack} = -15$dB and various values of θ_{fbt}. Theoretical results fit qualitatively with simulated ones, but act as upper bounds. The reason is that the density of interferers in the vicinity of the observed link is relatively higher in the theoretical deployment model, hence a higher outage probability. Other simulations with different values of p, ω and decoding thresholds exhibited a similar fitting, thus confirming the accuracy of the analysis.

Through numerical research, we determine the solution maximizing numerically the ASDT given by (4.14). The following optimal combination is obtained in the case of imperfect feedback: $(\theta_{fwt} = -0.6\text{dB}, \theta_{fbt} = 2.1\text{dB}, \theta_D = 14.8\text{dB}, \theta_{ack} = 3.4\text{dB}, p = 0.35, \omega = 0.57\pi\Big)$. This indicates that, in the absence of correlation between the fading levels of successive packets, control packets designed for detection even in the low SINR regime are optimal in terms of ASDT.

In figure 4-4 and figure 4-5, we treat each decoding threshold as a variable while keeping the other parameters set to their theoretically optimal values and plot the corresponding ASDT. We observe in both figures that the maximum of ASDT is reached in both theoretical and simulated cases for very similar decoding threshold values, which confirms the optimal parameter combination calculated above.

To understand the influence of imperfect feedback, we also determine the optimal com-

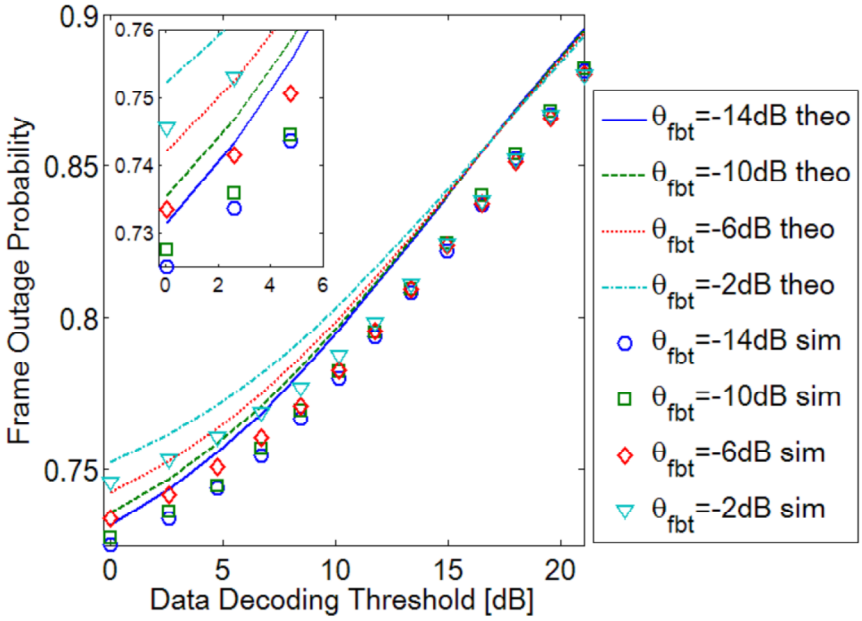

Figure 4-3: Frame success probability against Data decoding threshold. "Theo" indicates theory and "sim" indicates simulation.

bination of parameters for the case of error-free feedback (i.e feedback thresholds set to 0 and $T_{fbt} = T_{ack} = T_{fwt}$). It is given by $(\theta_{fwt} = 1.7\,\text{dB}, \theta_D = 13.3\text{dB}, p = 0.27, \omega = 0.6\pi)$, which shows noticeable differences with the case of imperfect feedback stated earlier in this section. We conclude that imperfect feedback cannot be neglected in the network optimization process. To confirm this result, considering error-free feedback, we let the data decoding threshold vary while other parameters are optimal and plot the corresponding ASDT in figure 4-4. We observe that the optimal ASDT is overestimated by 9% as compared to the imperfect feedback case, which is also non negligible.

4.5 Conclusion

In this chapter, we presented a stochastic analysis based on the theory of point processes of a simple medium access control scheme including a random test followed by a four-way handshake (one control handshake without spatial reservation and one traffic handshake). This combination of contention mechanisms which recently appeared in the literature had so far been studied only by means of simulation. Our new mathematical framework takes

[3]The same value is used in [51].

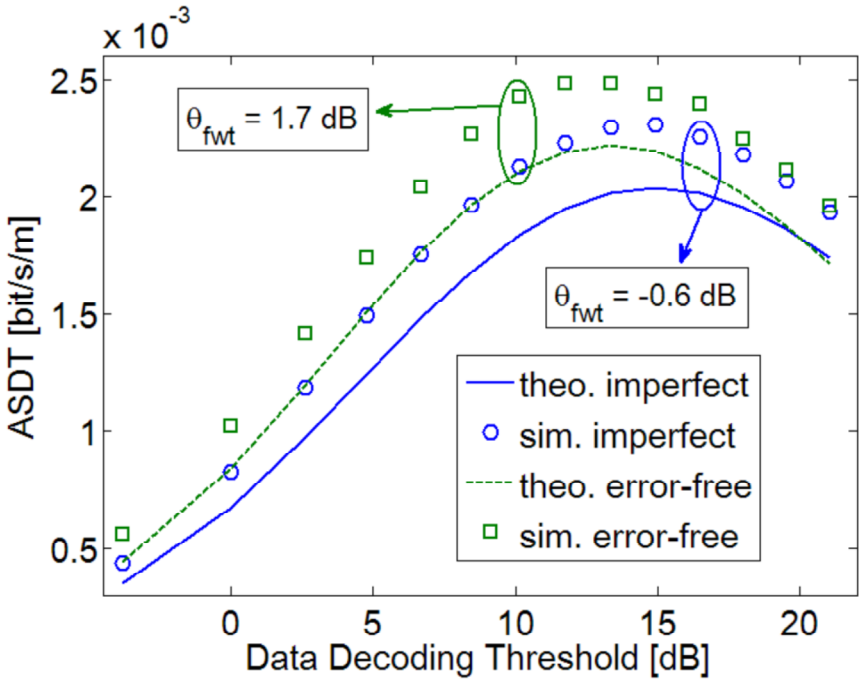

Figure 4-4: Achievable Spatial Density of Transport against Data decoding threshold, all other parameters being set to their theoretically optimal values. "Theo" indicates theory and "sim" indicates simulation.

into account time-varying channel impairments, interference, distinct decoding requirements for each packets as well as imperfect feedback. All our results were confirmed by comparison to simulated data and led us to two general conclusions. In the presence of fading uncorrelated between traffic and control handshakes, we observe the following. 1) Optimal contention is achieved by designing control packets decodable even in the presence of strong interference. 2) The impact of imperfect feedback on performances in an interference-limited mobile ad hoc network is not negligible. So far in the previous chapters our analysis has focused on networks operating in half duplex. However, full duplex communication is attracting more and more attention from researchers. It is therefore relevant to analyze its performance in the context of ad hoc networks as well; hence the treatment of this topic in the next chapter.

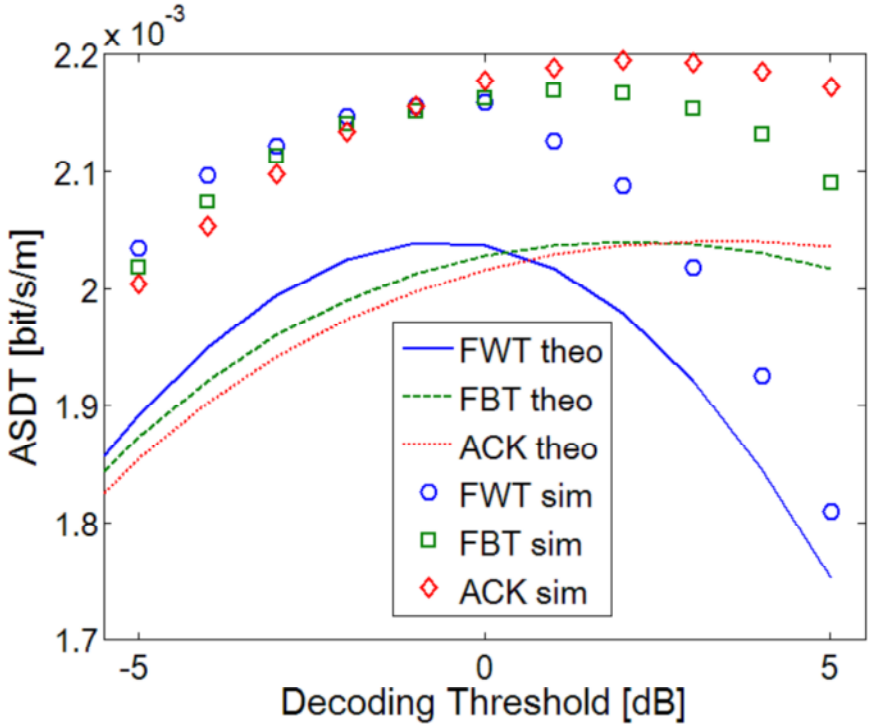

Figure 4-5: Achievable Spatial Density of Transport against decoding thresholds of control packets. For each curve, non-varying parameters are set to their theoretically optimal values. "Theo" indicates theory and "sim" indicates simulation.

Chapter 5

Stochastic Analysis of Two-Way Transmissions in an In-Band Full Duplex Ad Hoc Network

Until now, In-Band Half Duplex (IBHD) operation has been considered the norm in ad hoc networks (i.e in a given frequency band at a given time, a node can either transmit or receive). Revolutionizing this concept, In-Band Full Duplex (IBFD) communications [31] has recently attracted much attention as a possible way to increase spectral efficiency in wireless networks. IBFD radios can transmit and receive at the same time on the same frequency band. Therefore, the average network throughput has the potential to be doubled. However, in an ad hoc deployment, this would also result in a doubled interference level. This straightforward consequence questions the viability of IBFD in ad hoc deployments. Nevertheless, it has so far been overlooked in the literature, although numerous works regarding IBFD in ad hoc networks have appeared during the last few years (see e.g [49, 50, 12, 11]). One of the important features of IBFD is the ability for network nodes to perform a simultaneous two-way transmission. Thanks to this, both ends of a link could gain almost instantaneous channel state information (CSI) and packet acknowledgments, which could in turn dramatically influence the design of channel coding and medium access control [31]. To the best of our knowledge, there still lacks a point process-based mathematical framework enabling the analysis of a two-way transmission in a large IBFD

ad hoc deployment. The only related work[1] is [37]. However, this reference has the following drawbacks: 1) it treats both transmit directions independently instead of considering their joint success and neglects the correlation of interference levels at both ends of a link, 2) it does not take into account the impact of self-interference on performance and 3) it does not consider any IBFD/IBHD performance comparison.

In the present chapter, we propose a new tractable mathematical framework based on the theory of point processes which enables the analysis of two-way transmissions in an interference-limited IBFD ad hoc network. As compared to existing works [37], the analysis presented here has the following advantages: 1) the success of a two-way transmission is treated as a single event taking into account both transmit directions simultaneously and accounts for the interference correlation intrinsic to IBFD two-way transmissions, 2) the impact of self-interference on performances at each receiver is modelled explicitly and also 3) the performance of the IBFD case is compared in details to the conventional IBHD case.

Using a HPPP-based deployment model, we determine a tight lower bound on the joint probability of success of a two-way transmission in an IBFD ad hoc network. Both cases of ideal and imperfect Self-Interference Cancellation (SIC) are investigated. All theoretical results are confirmed by means of comparison to simulated data. Using tractable expressions, we then present a performance comparison of IBFD and its conventional half-duplex counterpart, assuming optimal medium access contention is used in each case. Our study determines the environmental and network conditions in which IBFD dominates in terms of spectral efficiency. Notably, we find that the influence of the path-loss exponent on the predominance of either technology is a function of the level of residual (i.e, post-SIC) self-interference.

The remainder of this chapter is organized as follows. In section 5.1, we present the system model used in our study. In section 5.2, we derive the joint distribution of the Signal to Interference Ratio (SIR) of both receivers involved in an IBFD two-way transmission with ideal SIC. In section 5.3, we extend the analytical results of section 5.2 to the general case with imperfect SIC. We describe in details how SIC performance is related to other system parameters and define the notion of two-way spectral efficiency. In section 5.4, we

[1]Only related work to the best of our knowledge, at the time of writing.

present an in-depth comparison of IBFD and IBHD for the case of two-way transmissions in an ad hoc network, assuming optimal medium access control (MAC). Finally, a conclusion summarizes the chapter in section 5.5.

5.1 System Model

5.1.1 Deployment and MAC Scheme Assumptions

We study the performance of a two-way transmission between two nodes denoted as O and M (i.e O transmits to M and M transmits to O, simultaneously). Node O is assumed to be located at the origin of $\mathbb{R}^2$ while M is at a distance $\|OM\| = d$ from it. The deployment of the other nodes in the network is modelled by a two-dimensional HPPP denoted Φ with density λ. We assume that all the nodes in Φ are also arranged in pairs (also referred to as links).

All nodes operate in the same frequency band, therefore the network is assumed to be interference-limited (i.e the interference power at any node is larger than its thermal noise power by several orders). Time in the system is slotted and the duration of a slot is equal to the duration of a transmission, which is the same for all links. All nodes are synchronized with one another; therefore, they start their transmissions simultaneously at the beginning of each slot.

The MAC scheme selects a subset of links randomly so that a fraction $0 < p < 1$ of them is active in any given slot. We assume that, prior to this selection process, each link in Φ is formed by selecting two nodes randomly.[2] This is equivalent to Φ being partitioned into two independent HPPPs Φ_1 and Φ_2, both of density $\lambda/2$, such that $X_n^1 \in \Phi_1$ and $X_n^2 \in \Phi_2$ form the n-th link in Φ. Then, the selection of active links according to the MAC protocol is equivalent to performing an independent thinning of both Φ_1 and Φ_2, which produces the HPPPs Φ_1^p and Φ_2^p. Let us denote Φ^p the superposition of Φ_1^p and Φ_2^p. From the property of superposition of HPPPs, Φ^p is also a HPPP with density $p\lambda$.

[2]Note that if links were selected based on link distance-related criteria, Φ_1 and Φ_2 would not be independent and their superposition would not be a HPPP. However, for the sake of tractability, we limit the present study to a HPPP of interferers.

5.1.2 Channel Model

We assume that all nodes use the same transmit power equal to unity. The channel impairments are composed of path-loss and fast fading. The path-loss is modeled by the standard power law $l(r) = r^{-\alpha}$ where r is the link distance and α is the path-loss exponent. The magnitude of the fast fading is assumed to be Rayleigh-distributed. Therefore, the corresponding power gain G is exponentially distributed with rate parameter 1. It follows that the received power for a link with distance r can be expressed as $Gr^{-\alpha}$.

Node mobility is assumed to be low enough so that node positions do not change significantly during a transmission. Therefore, the path-loss on any link is assumed to be fixed during any transmission. However, we still consider that the channel is slowly time-varying (either due to a changing environment or to the motion of nodes). To model this, we use the slot-by-slot block-fading channel, defined as follows [13]. Fast fading during a slot is assumed to be constant on any link. However, fading levels in different slots on the same link are assumed to be independent and fading levels on different links in any two time slots are also assumed to be independent.

5.1.3 Interference Correlation Model

In an IBFD network, all nodes can transmit and receive at the same time. Therefore, each node in Φ^p transmits at the same time as O and M and thus causes interference at both their receivers. Let X be a node in Φ^p and let $r = \|XO\|$ be the distance from X to O and let us define in the same way $z = \|XM\|$. Given $\|OM\| = d$, we have the following relationship (known as Al Kashi's theorem)

$$z = \left(r^2 + d^2 - 2rd\cos(\varphi)\right)^{\frac{1}{2}} \tag{5.1}$$

where $\varphi = (\hat{XOM})$. The configuration of those three nodes is illustrated in figure 5-1, in which solid lines are communicating links and dashed lines are the interfering links. The relation above implies that the interference levels at O and M are correlated. The analysis developed in the remainder of this chapter takes this correlation into account.

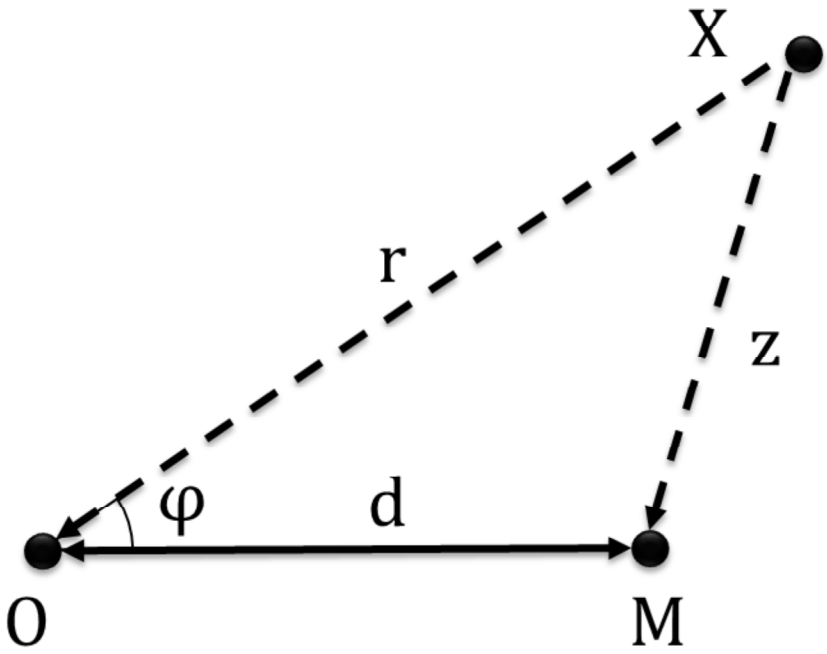

Figure 5-1: Geometric representation of the relative positions of O, M and an interferer X.

In the next section, we determine the joint distribution of the SIRs at O and M during an IBFD two-way transmission.

5.2 Two-Way Transmission with Ideal Self-Interference Cancellation

In this section, we assume that SIC is ideal at each node, so that no residual self-interference remains in the decoding stage of each receiver.

5.2.1 Joint Distribution of the Signal to Interference Ratios on a Link

For any $X_n \in \Phi^p$, where n is a unique numeral index, we can define $l_O(X_n)$ the path-loss between O and X_n. Also, for a given time slot, we define G_{O,X_n} the squared fading coefficient of the channel between O and X_n. We define $l_M(X_n)$ and G_{M,X_n} in the same way. Finally, we denote $G_{O,M}$ the squared fading coefficient of the channel from M to O in a given time slot and keep the notation $\|OM\| = d$ defined in the previous section. By reciprocity of the

wireless channel, we have that $G_{O,M} = G_{M,O} = G$. Then, the SIRs γ_O at O and γ_M at M in a given time slot can be expressed as

$$\begin{aligned} \gamma_O &= \frac{Gd^{-\alpha}}{\sum_{X_n \in \Phi^p} G_{O,X_n} l_O\left(X_n\right)} \\ \gamma_M &= \frac{Gd^{-\alpha}}{\sum_{X_n \in \Phi^p} G_{M,X_n} l_M\left(X_n\right)} \end{aligned} \tag{5.2}$$

We observe in the above that γ_O and γ_M are dependent because of the fading coefficient G which is the same in both numerators and because of the set of interferers Φ^p which is the same in both denominators. This dependence is entirely characterized by their joint Complementary Cumulative Distribution Function (CCDF), which can be expressed as

$$\begin{aligned} &\bar{F}\left(\theta_O, \theta_M\right) = \mathbb{P}\left(\gamma_O > \theta_O, \gamma_M > \theta_M\right) \\ &\overset{(a)}{=} \mathbb{P}\Bigg(G_{O,M} > \theta_O d^{\alpha} \sum_{X_n \in \Phi^p} G_{O,X_n} l_O\left(X_n\right), \\ &G_{O,M} > \theta_M d^{\alpha} \sum_{X_n \in \Phi^p} G_{M,X_n} l_M\left(X_n\right)\Bigg) \\ &\overset{(b)}{=} \mathbb{P}\Bigg(G_{O,M} > \max\Bigg(\theta_O d^{\alpha} \sum_{X_n \in \Phi^p} G_{O,X_n} l_O\left(X_n\right), \\ &\theta_M d^{\alpha} \sum_{X_n \in \Phi^p} G_{M,X_n} l_M\left(X_n\right)\Bigg)\Bigg) \end{aligned} \tag{5.3}$$

where (a) follows from the definition of the SIRs at O and M given in (5.2). The expression in (b) is difficult to develop further; however, the following lower bound can be obtained.

$$\begin{aligned} &\bar{F}\left(\theta_O, \theta_M\right) \geq \\ &\mathbb{P}\Bigg(G_{O,M} > d^{\alpha} \sum_{X_n \in \Phi^p} \max\Big(\theta_0 G_{O,X_n} l_O\left(X_n\right), \\ &\theta_M G_{M,X_n} l_M\left(X_n\right)\Big)\Bigg) \triangleq \underline{\bar{F}}\left(\theta_O, \theta_M\right) \end{aligned} \tag{5.4}$$

The above lower bound follows from the inequality $\max\left(\sum_{i\in\mathcal{I}} a_i, \sum_{i\in\mathcal{I}} b_i\right) \leq \sum_{i\in\mathcal{I}} \max\left(a_i, b_i\right)$ which is true when the terms of each sum are all positive, with equality if and only if $a_i = b_i, \forall i \in \mathcal{I}$.

Now let us define, for any $X_n \in \Phi^p$, the random variable H_n defined as

$$H_n = \max\left(\theta_0 G_{O,X_n} l_O\left(X_n\right), \theta_M G_{M,X_n} l_M\left(X_n\right)\right) \tag{5.5}$$

Using the definition in (5.5), the lower bound $\underline{\bar{F}}\left(\theta_O, \theta_M\right)$ can be developed as follows.

$$\begin{aligned}
\underline{\bar{F}}\left(\theta_O, \theta_M\right) &= \mathbb{P}\left(G_{O,M} > d^\alpha \sum_{X_n\in\Phi^p} H_n\right) \\
&\overset{(a)}{=} \mathbb{E}\left\{e^{-d^\alpha \sum_n H_n}\right\} \\
&\overset{(b)}{=} \exp\left(-\int_{\mathbb{R}^2} \left(1 - g\left(x\right)\right) \Lambda\left(dx\right)\right)
\end{aligned} \tag{5.6}$$

In the above, expression (a) follows from the definition of the CCDF of an exponentially distributed random variable with rate parameter 1. Expression (b) is obtained by recognizing in (a) the Probability Generating Functional (PGFL) of an HPPP [29]. In the resulting two-dimensional integral, x is a point of the two-dimensional space $\mathbb{R}^2$, while the function $\Lambda\left(dx\right)$ is the intensity measure of the HPPP Φ^p and can be thought of as the expected number of nodes in the region $dx \subset \mathbb{R}^2$. Also, $g\left(x\right) = \mathbb{E}\left\{e^{-d^\alpha H_n} | X_n \equiv x\right\} = L_{H_n}\left(d^\alpha | X_n \equiv x\right)$ is the Laplace Transform of H_n, conditioned on X_n being fixed at the position $x \in \mathbb{R}^2$, evaluated at the value d^α. The function $g\left(x\right)$ can be developed as follows (a proof is provided in appendix A).

$$\begin{aligned}
g\left(x\right) = &\frac{1}{1 + d^\alpha \theta_M l_M\left(x\right)} - \frac{1}{1 + d^\alpha \theta_M l_M\left(x\right) + \frac{\theta_M l_M(x)}{\theta_O l_O(x)}} \\
&\frac{1}{1 + d^\alpha \theta_O l_O\left(x\right)} - \frac{1}{1 + d^\alpha \theta_O l_O\left(x\right) + \frac{\theta_O l_O(x)}{\theta_M l_M(x)}}
\end{aligned} \tag{5.7}$$

We can further develop the lower-bound in (5.6) by changing the integral to polar co-

ordinates according to $x \rightarrow (r, \varphi)$ where $r = \|x\|$ and $\varphi = \arg(x)$. From (5.1), we have that $l_O(x) = r^{-\alpha}$ and $l_M(x) = (r^2 + d^2 - 2rd\cos(\varphi))^{-\frac{\alpha}{2}}$. Then, tedious but straightforward algebraic manipulations allow to express $1 - g(x)$ as

$$f(r,\varphi) = 1 - g(x) = f_1(r) + f_2(r,\varphi) = \frac{d^\alpha \theta_O}{d^\alpha \theta_O + r^\alpha} + \frac{\frac{\theta_M}{\theta_O} d^\alpha \theta_M r^\alpha}{\left(d^\alpha \theta_M + \frac{\theta_M}{\theta_O} r^\alpha + (r^2 + d^2 - 2rd\cos(\varphi))^{\frac{\alpha}{2}}\right)} \frac{1}{\left(d^\alpha \theta_M + (r^2 + d^2 - 2rd\cos(\varphi))^{\frac{\alpha}{2}}\right)} \tag{5.8}$$

Given that $\Lambda(dx) = p\lambda dx = p\lambda r dr d\varphi$, we obtain the following expression for $\underline{\bar{F}}(\theta_O, \theta_M)$.

$$\begin{aligned} \underline{\bar{F}}(\theta_O, \theta_M) &= \exp\left(-2p\lambda \int_0^{+\infty} \int_0^{\pi} r f(r,\varphi)\, dr d\varphi\right) \\ &= \exp\left(-2p\lambda\pi \int_0^{+\infty} r f_1(r)\, dr\right) \\ &\exp\left(-2p\lambda \int_0^{+\infty} \int_0^{\pi} r f_2(r,\varphi)\, dr d\varphi\right) \end{aligned} \tag{5.9}$$

From [29], we have

$$\begin{aligned} \int_0^{+\infty} r f_1(r)\, dr &= \int_0^{+\infty} \frac{d^\alpha \theta_O r}{d^\alpha \theta_O + r^\alpha} dr \\ &= \frac{1}{2}\pi d^2 \theta_O^\delta \delta \csc(\pi\delta) \end{aligned} \tag{5.10}$$

where $\delta = \frac{2}{\alpha}$.

Regarding the double integral on $f_2(r,\varphi)$, the variable substitution $t = \frac{r}{d}$ and a few

manipulations lead to the form

$$
\begin{aligned}
&2\int_0^{+\infty}\int_0^{\pi} r f_2(r,\varphi)\,dr d\varphi = \\
&2\frac{d^2}{\theta_O}\int_0^{+\infty}\int_0^{\pi} \frac{t^{\alpha+1}d\varphi}{\left(1+\frac{t^{\nu}}{\theta_O}+\frac{(1+t^2-2t\cos(\varphi))^{\frac{\alpha}{2}}}{\theta_M}\right)} \\
&\frac{dt}{\left(1+\frac{(1+t^2-2t\cos(\varphi))^{\frac{\alpha}{2}}}{\theta_M}\right)} \\
&= d^2 C(\theta_O,\theta_M)
\end{aligned}
\tag{5.11}
$$

Therefore, we have the following final expression for $\underline{\bar{F}}(\theta_O,\theta_M)$.

$$
\underline{\bar{F}}(\theta_O,\theta_M) = e^{-p\lambda d^2 \Psi \theta_O^{\delta}} e^{-p\lambda d^2 C(\theta_O,\theta_M)} \tag{5.12}
$$

where $\Psi = \pi^2 \delta \csc(\pi\delta)$.

Remark 2 *The above expression shows that the joint CCDF is the product of two factors. The first factor $e^{-p\lambda d^2 \Psi \theta_O^{\delta}}$ is equal to the marginal CCDF of γ_O [29]. Therefore, from Bayes's law, we conclude that $e^{-p\lambda d^2 C(\theta_O,\theta_M)}$ is a lower bound on the conditional CCDF of γ_M given that $\gamma_O > \theta_O$. The dependence between γ_M and γ_O is thus entirely described by the function $C(\theta_O,\theta_M)$.*

Unfortunately, the double integral in $C(\theta_O,\theta_M)$ cannot be brought into closed form. Nevertheless, considering that $t^2 \approx 1+t^2-2t\cos(\varphi)$, the integral in $C(\theta_O,\theta_M)$ can be reasonably

approximated as follows (a proof is provided in appendix B).[3]

$$
\begin{aligned}
C\left(\theta_O,\theta_M\right) &\approx \frac{2\pi}{\theta_O}\int_0^{+\infty}\frac{t^{\alpha+1}dtd\varphi}{\left(1+t^{\alpha}\left(\frac{1}{\theta_O}+\frac{1}{\theta_M}\right)\right)\left(1+\frac{t^{\alpha}}{\theta_M}\right)} \\
&= \pi^2\delta^2\,\mathrm{csc}\left(\pi\delta\right){}_2F_1\left(1+\delta,1,2,\frac{\theta_M}{\theta_M+\theta_O}\right) \\
&\left(\frac{\theta_M}{\theta_M+\theta_O}\right)\left(\frac{\theta_M\theta_O}{\theta_M+\theta_O}\right)^{\delta} \\
&\approx \tilde{C}\left(\theta_O,\theta_M\right) \triangleq \\
&\pi^2\delta\,\mathrm{csc}\left(\pi\delta\right)\frac{\theta_M\left(\left(\delta-1\right)\left(\frac{\theta_M}{\theta_M+\theta_O}\right)^{\delta}\theta_O^{\delta}+\theta_M^{\delta}\right)}{\theta_M+\theta_O}
\end{aligned}
\tag{5.13}
$$

where ${}_2F_1\left(a,b,c,z\right)$ is the Gauss Hypergeometric function.

Therefore, using $\tilde{C}\left(\theta_O,\theta_M\right)$, we can obtain a closed form approximation of the lower bound of the joint CCDF of γ_O and γ_M,[4] which we will refer to as $\bar{F}^a$ in the remainder.

In the next section, we use the above results to derive performance metrics for IBFD two-way transmissions.

5.2.2 Joint Success Probability

In the case where Gaussian signalling is used, a transmission can be defined as successful if its information rate (in bit/s) is smaller than the capacity of the channel [13]. Within the system model defined in the previous section, path-loss and fading are constant during a whole transmission. Therefore, the capacity of a channel with bandwidth B for a transmission from M to O can be defined as $C_{M\to O} = B\log_2\left(1+\gamma_O\right)$. The capacity $C_{O\to M}$ is simply obtained by substituting γ_O with γ_M. Let us define $\mathcal{T}$ the target spectral efficiency of a transmission (in bit/s/Hz). The information rate of transmission from M to O is then given by $B\mathcal{T}$. Following this definition, the joint probability of success of the two-way

[3]Note that two successive approximations are used. The first concerns the denominator in the double integral defining $C\left(\theta_O,\theta_M\right)$. The second concerns the Gauss Hypergeometric function. Details are provided in appendix B.

[4]One can note that the approximation of the lower bound may not behave as a lower bound of the actual joint CCDF.

transmission between O and M can therefore be expressed as

$$\begin{aligned} P_{tw} &= \mathbb{P}\left(B\mathcal{T}_{M\to O} < C_{M\to O}, B\mathcal{T}_{O\to M} < C_{O\to M}\right) \\ &\overset{(a)}{=} \mathbb{P}\left(\gamma_O > 2^{\mathcal{T}_{M\to O}} - 1, \gamma_M > 2^{\mathcal{T}_{O\to M}} - 1\right) \\ &\overset{(b)}{=} \bar{F}\left(\beta_O, \beta_M\right) \end{aligned} \tag{5.14}$$

where $\beta_O = 2^{\mathcal{T}_{M\to O}} - 1$ and $\beta_M = 2^{\mathcal{T}_{O\to M}} - 1$, which we both refer to as "receiver thresholds" in the remainder of this chapter. In the above, (a) is obtained by developing the capacity terms, then (b) follows by recognizing in (a) the joint CCDF of γ_O and γ_M. This result indicates that $\underline{\bar{F}}$ and $\bar{F}^a$ derived in the previous section can be applied to the probability of success of a two-way transmission between O and M.

In figure 5-2, given $\alpha = 4$ and $p = 1$, we plot $\underline{\bar{F}}\left(\beta_O, \beta_M\right)$ given by (5.12) against β_O for $\beta_M = 8$dB and compare it to simulated data. The method proposed in [29] is used to accurately model a HPPP deployment in the simulation. In the legend, "Approximate" denotes $\bar{F}^a$ and "Lower-Bound" denotes $\underline{\bar{F}}$. Finally, "Simulated" denotes the simulated data. We observe an excellent agreement between simulated and theoretical curves, which also appeared using different parameter values, and therefore validates the results presented in the previous sections.

Remark 3 *Due to the homogeneity and infinity of the interferer set Φ^p, the deployment model considered in the analysis is symmetric with respect to O and M (i.e O and M are interchangeable). Therefore, the joint CCDF of γ_O and γ_M is symmetric with respect to θ_O and θ_M. Numerical evaluation reveals that the lower bound in (5.12) and its approximation using the Hypergeometric function in (5.13) are symmetric with respect to θ_O and θ_M. However, the more simple approximation $\bar{F}^a$ defined in (5.13) exhibits a slight asymmetry.*

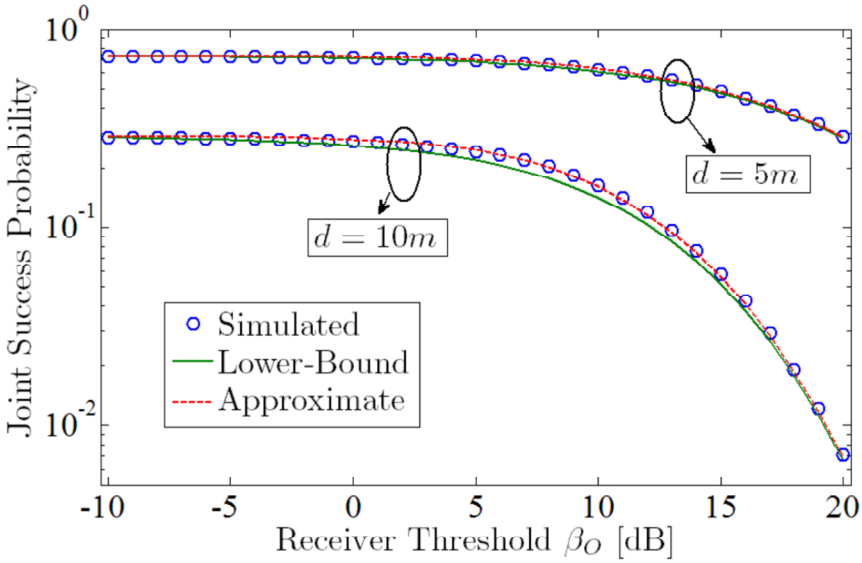

Figure 5-2: Join success probability of a two-way transmission against β_O given $\beta_M = 8$ dB, for various link distances in the case of ideal SIC.

5.3 Two-Way Transmission with Imperfect Self-Interference Cancellation

In this section, we consider that each node only cancels out partially the signal it emits, so that a non-negligible residual self-interference exists at its receiver due to reflections of the transmitted signal in the environment.

5.3.1 Joint Distribution of the SIRs and Two-Way Spectral Efficiency

Let us denote S_O and S_M the post-cancellation self-interference power (also known as residual self-interference power) at O and M, respectively. In this case, the SIRs γ_O and γ_M in a given time slot are expressed as

$$\gamma_O = \frac{Gd^{-\alpha}}{S_O + \sum_{X_n \in \Phi^p} G_{O,X_n} l_O(X_n)} \qquad (5.15)$$
$$\gamma_M = \frac{Gd^{-\alpha}}{S_M + \sum_{X_n \in \Phi^p} G_{M,X_n} l_M(X_n)}$$

Through a development similar to the case with ideal self-interference cancellation, we

obtain that their joint CCDF accepts the following lower bound.

$$\begin{aligned}
&\bar{F}_{SI}\left(\theta_O,\theta_M\right) \geq \underline{\bar{F}}_{SI}\left(\theta_O,\theta_M\right) \triangleq \\
&\mathbb{P}\Bigg(G > d^{\alpha}\sum_{X_n\in\Phi^p}\max\Big(\theta_O G_{O,X_n} l_O\left(X_n\right), \\
&\theta_M G_{M,X_n} l_M\left(X_n\right)\Big) + d^{\alpha}\max\left(S_O\theta_O, S_M\theta_M\right)\Bigg) \\
&= e^{-d^{\alpha}\max\left(S_O\theta_O,S_M\theta_M\right)} \\
&\mathbb{E}\left\{e^{-d^{\alpha}\sum_{X_n\in\Phi^p}\max\left(\theta_O G_{O,X_n} l_O(X_n),\theta_M G_{M,X_n} l_M(X_n)\right)}\right\} \\
&= e^{-d^{\alpha}\max\left(S_O\theta_O,S_M\theta_M\right)}\underline{\bar{F}}\left(\theta_O,\theta_M\right)
\end{aligned} \tag{5.16}$$

Similarly to the ideal SIC case, we can define the lower bound $\underline{\bar{F}}_{SI}$ and the approximation $\bar{F}^a_{SI}$ of $\bar{F}_{SI}$.

Because reflections in the environment experience multi-path propagation (i.e backscattering), a certain fraction of each slot is reserved for the estimation of the corresponding channel (referred to as the backscatter channel). To model this, any given slot is divided into two phases. A first phase lasting T_{SI} seconds is used by all nodes for Self-Interference Estimation (SIE). The second phase, lasting $T_{slot} - T_{SI}$ seconds, is used for two-way communication.

Given that a fraction $\rho_{SI} = \frac{T_{SI}}{T_{slot}}$ of each slot is not used for data transmission, the two-way spectral efficiency of a link in the network is given by

$$\mathcal{S}_{SI} = p\left(1-\rho_{SI}\right)\left(\mathcal{T}_{M\to O}+\mathcal{T}_{O\to M}\right)\bar{F}_{SI}\left(\beta_O,\beta_M\right) \tag{5.17}$$

We can then define the lower bound $\underline{\mathcal{S}}_{SI}$ and the approximation $\mathcal{S}^a_{SI}$ of $\mathcal{S}_{SI}$, where $\bar{F}_{SI}$ is replaced by $\underline{\bar{F}}_{SI}$ and $\bar{F}^a_{SI}$, respectively.

Remark 4 *Given a set of constraints on a two-way transmission between O and M (e.g outage probability, information rate, etc.), let us assume that there exist an optimal target spectral efficiency $\mathcal{T}^*_{M\to O}$ for the transmit direction from M to O. Then, by symmetry of the deployment model with respect to O and M, the optimal target spectral efficiency for the*

opposite transmit direction (i.e from O to M) is the same (i.e $\mathcal{T}^*_{O\to M} = \mathcal{T}^*_{M\to O} = \mathcal{T}^*$*). Note that this result holds only if both transmit directions are subject to the same constraints. This important observation simplifies the feasible solution set for the optimization of the two-way spectral efficiency.*

In the next subsection, we describe in more details the self-interference estimation (SIE) process and how the residual self-interference power is related to other system parameters.

5.3.2 Residual Self-Interference Model

During the SIE phase, each node needs to perform two operations, successively.

The first is to cancel the line-of-sight (LoS) component of the self-interference between its transmitter and receiver front-ends. This operation is straightforward as the signal is very strong and the characteristics of the channel are hardware-dependent and already known [31]. Therefore, the process is immediate and does not take any noticeable time.

The second step is to cancel the self-interference due to reflections in the environment. This step is more challenging and requires the estimation of the backscatter channel. That is, each node during the SIE phase transmits a control signal which, when picked up by its own receiver front-end, provides channel state information regarding the reflection-induced self-interfering signal.[5] The reflections have a much lower power than the LoS component and are affected by the interference from other nodes performing the same SIE process (an illustration of the situation is provided in figure 5-3). We assume in the following that the whole duration of the SIE phase of any slot is used by each node to estimate the backscatter channel.

One may note that the estimation of the backscatter channel can be modelled using simple adaptations of the conventional channel estimation framework. The estimate (e.g, at node O) of the complex backscatter channel coefficient in a given slot can be expressed as $\hat{h}_O = h_O - e_O$ where h_O is the true channel coefficient and e_O is the estimation error.

Given a bandwidth B, a receiver can collect a maximum of $L_{SI} = BT_{SI}$ samples during the SIE phase. For tractability, let us consider the simple case in which, for each node, the

[5] It is assumed that the LoS component of the control signal used for channel sounding is perfectly cancelled by the receiver front-end.

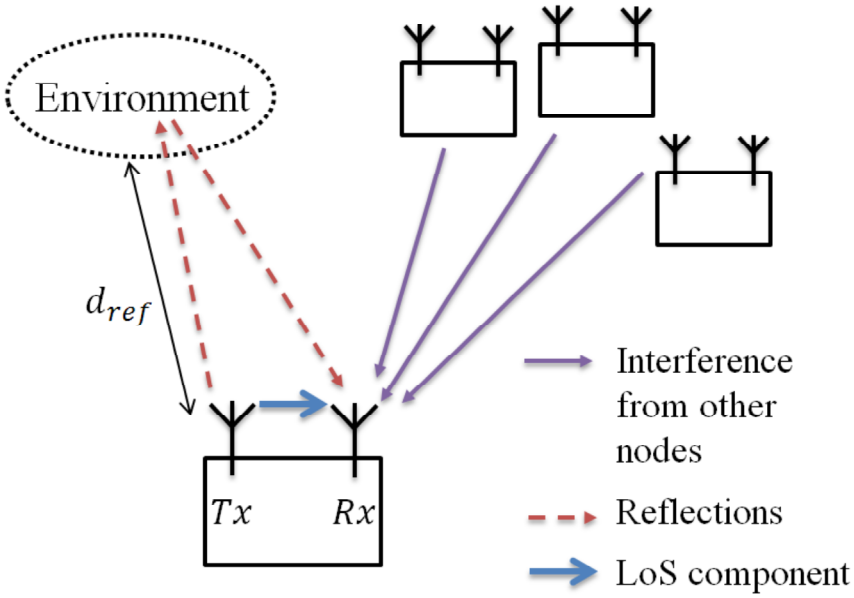

Figure 5-3: Illustration of the interference situation at the receiver front-end of a given node during the SIE phase.

reflections can be approximated as originating from a single reflector located d_{ref} meters away and having a reflection coefficient ϵ_{ref}.[6] Then, estimating the backscatter channel is equivalent to estimating a channel with a path-loss exponent 2α between the receiver front-end and a source with power ϵ_{ref} located at a distance d_{ref}. In these conditions, from [56], we have that the variance σ_e^2 of the error of a Minimum Mean Square Error (MMSE) channel estimator can be expressed by

$$\sigma_e^2 = \frac{1}{1 + \frac{L_{SI}}{\Psi\left(1+\hat{d}_{ref}^{2\alpha}\right)p\lambda}} \tag{5.18}$$

where $\hat{d}_{ref} = \epsilon_{ref}^{\frac{1}{2\alpha}} d_{ref}$.

Using this model and given that $h_O = \hat{h}_O + e_O$, it follows that the SIRs at O and M will be given by (5.15) with $S_O = S_M = \sigma_e^2 \epsilon_{ref} d_{ref}^{-2\alpha} = \sigma_e^2 \hat{d}_{ref}^{-2\alpha}$.

In figure 5-4, we plot $\underline{\bar{F}}_{SI}(\beta_O, \beta_M)$ given by (5.16) against $\beta = \beta_O = \beta_M$ for various values of ρ_{SI}. The MAC parameter is fixed to $p = 1$ and the numerical values of the other constants used for the comparison are given in table 5.1.

[6]Note that this model can be adapted to approximate the case of multiple sources of reflections with a mean distance to the node equal to d_{ref} and a mean reflection coefficient ϵ_{ref}.

Table 5.1: Simulation Parameters

Parameter	Symbol	Value
Bandwidth	B	500 kHz
Slot duration	T_{slot}	2 ms
Path-loss exponent	α	4
Node density	λ	10^3 node/km^2
Distance to reflector	$\hat{d}_{ref}$	5 m

We observe a satisfying agreement between simulation and theory. Results logically show that as ρ_{SI} decreases, less samples become available for estimating the backscatter channel, thus leading to higher self-interference and lower two-way transmission success probability.

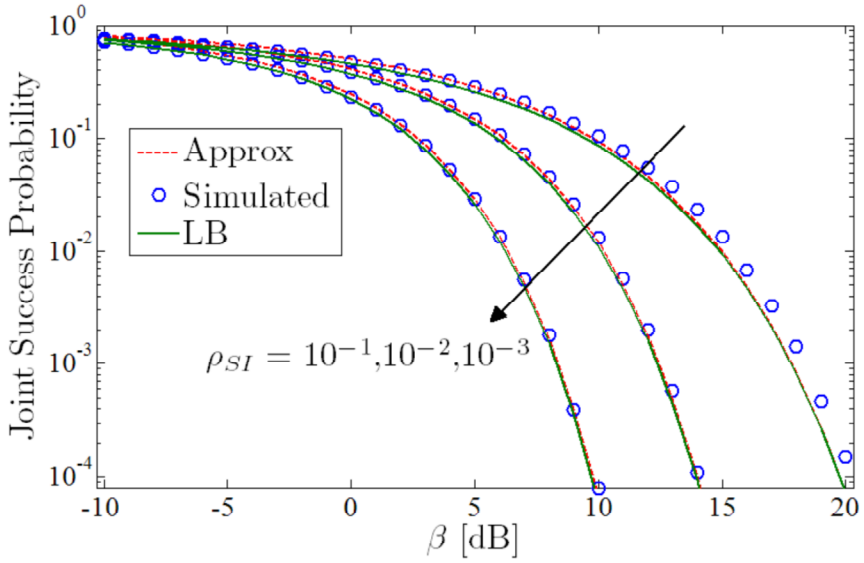

Figure 5-4: Join success probability of a two-way transmission against $\beta_O = \beta_M = \beta$ for various link distances in the case of imperfect SIC.

In figure 5-5, we plot the contour of $\underline{\mathcal{S}}_{SI}$ and $\mathcal{S}^a_{SI}$. The parameters used as input are given in table 5.1, $d = 10$ meters, $p = 1$ and $\rho_{SI} = 0.1$. We observe as expected that $\underline{\mathcal{S}}_{SI}$ is symmetric with respect to β_O and β_M. Also, it admits a single maximum located on the line $\beta_O = \beta_M$. Plots for different set of parameters consistently confirmed these two results, which illustrate earlier deductions based on the geometric properties of the deployment model. It is noteworthy that the approximation $\mathcal{S}^a_{SI}$ shows very similar results with the

lower bound, especially regarding the position of the maximum. This encourages the use of its simple expression for further numerical analysis.

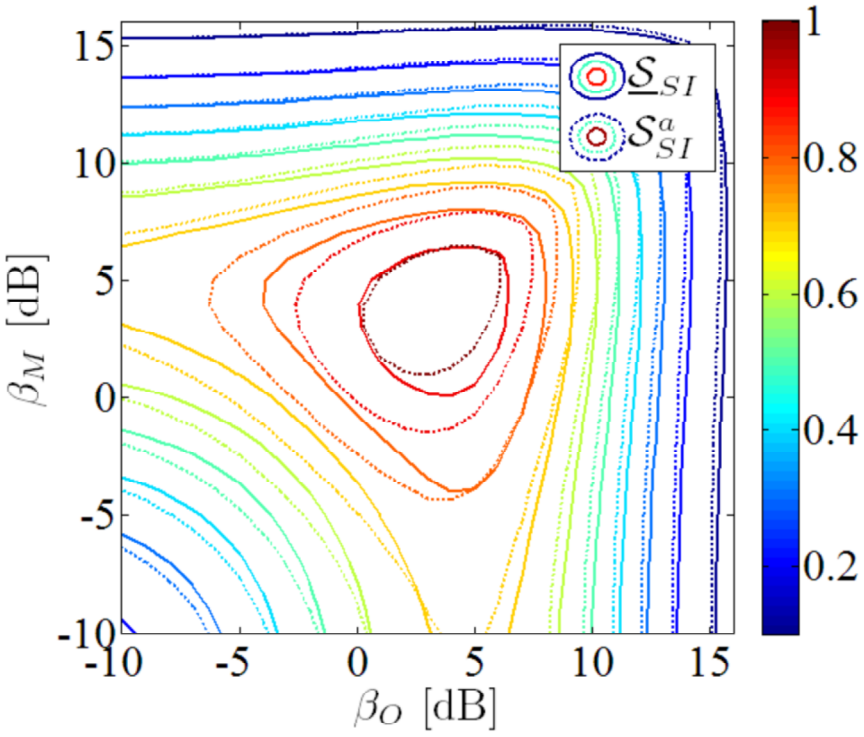

Figure 5-5: Contour plot of $\mathcal{S}_{SI}$ given by (5.17) against the receiver thresholds β_O and β_M.

In the following section, we present a detailed performance comparison of IBFD and IBHD for the case of two-way transmissions in an ad hoc network.

5.4 In Band Full-Duplex vs In Band Half-Duplex

5.4.1 In-Band Half-Duplex Performances

In this subsection, we characterize the joint distribution of γ_O and γ_M during a two-way transmission in the case of an IBHD ad hoc network. Let us consider the same system model as described in section II. As in the IBFD case, we assume that all nodes in the network are arranged by pairs (i.e, links). The MAC protocol allows a fraction p of these pairs to be active during a given frame. However, IBHD operation necessitates to allocate the two transmit directions (from O to M and from M to O) to different resources. Without

loss of generality, in the following we consider a time-division based system. Therefore, each frame is divided into two equal slots. During the first slot, for all pairs of nodes, transmissions take place in a given direction (i.e, from M to O). Transmissions in the opposite direction (i.e, from O to M) then follow during the second slot (see figure 5-6 for an illustration).

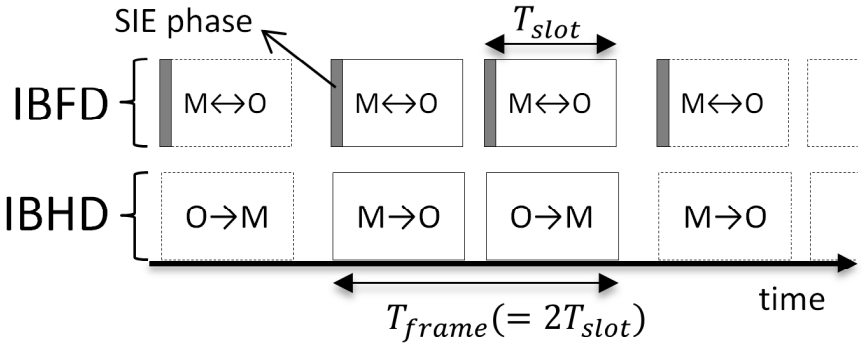

Figure 5-6: Illustration of the frame structure used for the comparison of IBHD and IBFD, for a given link O, M. The direction of arrows indicate the transmit direction.

Consequently, the two-way spectral efficiency in a IBHD network is expressed as follows.

$$\mathcal{S}_{HD} = p\frac{\mathcal{T}_{M\to O} + \mathcal{T}_{O\to M}}{2}\bar{F}\left(\beta_O, \beta_M\right) \tag{5.19}$$

where the factor $\frac{1}{2}$ appears due to each transmission only using half the duration of a frame. In the remainder, the two-way spectral efficiency for the IBFD case will be denoted as $\mathcal{S}_{FD}$, so as to distinguish it from the IBHD case.

From the independent thinning property of HPPPs, the interferer set during each slot is an HPPP with intensity $p\lambda/2$. Assuming that M transmits to O during the first slot, we denote the corresponding interferer set as Φ_O^p. Then, the interferer set during the second slot is denoted as Φ_M^p. We consider two cases in the following: a) channel variant within a frame and b) channel invariant within a frame.

Case of Time-Variant Channel In the case of time-varying channel, the channel model considered is exactly the same as the one described in section II. That is, a slot-by-slot block-fading channel is assumed, such that the fading levels on a same link in two successive time slots are independent. Therefore, γ_O and γ_M are independent and their joint

CCDF can be simply expressed as follows [29].

$$\bar{F}_{var}(\theta_O, \theta_M) = e^{-\frac{p\lambda}{2} d^2 \Psi \theta_O^{\delta}} e^{-\frac{p\lambda}{2} d^2 \Psi \theta_M^{\delta}} \tag{5.20}$$

Case of Time-Invariant Channel In the case of time-invariant channel, we assume that the fading levels on a given link during a frame remains constant. Therefore, as in the IBFD case, we have equal fading levels on the link between O and M during both slots of a frame (i.e $G_{O,M} = G_{M,O} = G$). In this case, similarly to the derivation in (5.3), the joint CCDF of γ_O and γ_M is given by

$$\bar{F}_{invar}(\theta_O, \theta_M) = \mathbb{P}\left(G > d^{\alpha} \max\left(\theta_O I_O, \theta_M I_M\right)\right) \tag{5.21}$$

In the above expression, I_O and I_M are the interference power levels at O and M during the first and second slots of a given frame, respectively. Note that I_O and I_M are not only identically distributed but also independent, unlike in the IBFD case. This independence actually complicates the derivation of a closed form expression for $\bar{F}_{invar}(\theta_O, \theta_M)$, since it is not possible anymore to recognize the PGFL of a single HPPP in its expression. Nevertheless, for the case $\alpha = 4$, the distribution of I_O and I_M can be written in closed form (see eq.(3.23) in [29]) and, consequently, $\bar{F}_{invar}$ can be written as a simple integral as follows.

$$\begin{aligned} \bar{F}_{invar}(\theta_O, \theta_M) &= \mathbb{P}\left(I_O < \frac{G}{d^{\alpha}\theta_O}, I_M < \frac{G}{d^{\alpha}\theta_M}\right) \\ &= \int_0^{+\infty} F_{I_O}\left(\frac{g}{d^{\alpha}\theta_O}\right) F_{I_M}\left(\frac{g}{d^{\alpha}\theta_M}\right) e^{-g} dg \end{aligned} \tag{5.22}$$

where

$$F_{I_O}(z) = F_{I_M}(z) = 1 - erf\left(\frac{\pi^2 p\lambda}{8\sqrt{z}}\right) \tag{5.23}$$

In figure 5-7, we compare IBFD and IBHD in terms of $\max_p \mathcal{S}$, given that $\beta_O = \beta_M = \beta$. That is, for each value of β, we plot the result of the maximization of the two-way spectral efficiency over p. The invariant parameters are set as in table 5.1 and $\rho_{SI} = 0.1$. Note that

we do not assume here that nodes are aware of the coherence time of the channel, therefore, in the case of IBFD, the SIE process is performed in each slot. Three main observations can be made from this figure. 1) IBFD with ideal SIC outperforms IBHD in all the tested scenarios. 2) If the link distance is short enough, IBFD with imperfect SIC achieves a higher maximum spectral efficiency than IBHD (even with time-invariant channel within a frame). 3) However, IBHD still outperforms IBFD when β is large enough, given any link distance d.

We thus conclude that the viability of IBFD in ad hoc networks is not a clear cut and will depend on several factors (e.g type of application[7], link distance, etc.).

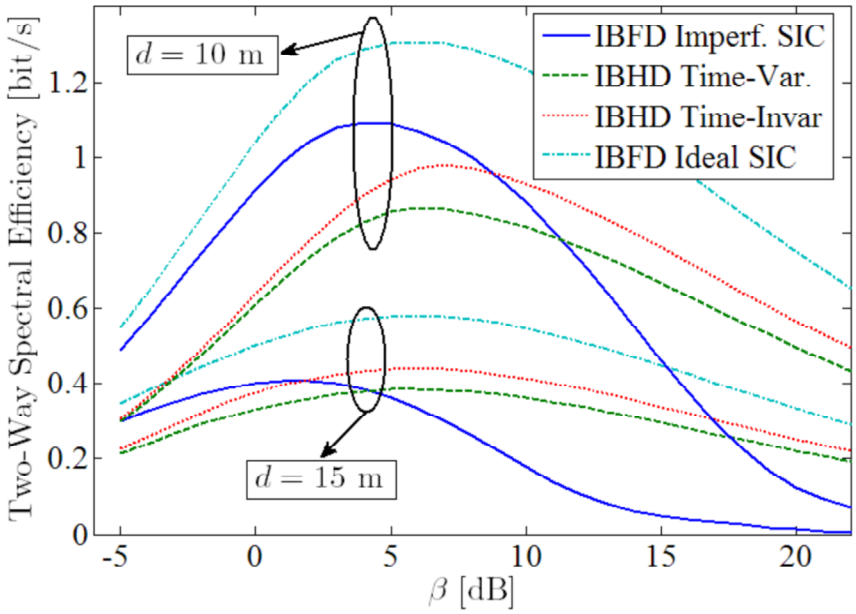

Figure 5-7: Comparison of the two-way spectral efficiency of the IBFD and IBHD cases, against the receiver threshold β.

In the next subsection, we investigate in more details the influence of various system parameters on the potential spectral efficiency gain of IBFD technology applied to ad hoc networks.

[7]Applications using only high target rates will not benefit from IBFD.

5.4.2 Analytical Performance Comparison

In this subsection, we determine the conditions in which IBFD outperforms IBHD in terms of two-way spectral efficiency, given that p is optimal. For tractability, the case of IBHD with time-varying channel within a frame is used for comparison.

In a first time, we consider the case of IBFD with ideal SIC. The approximation $\bar{F}^{a}_{FD}(\beta_O, \beta_M)$ is used to obtain a simple analytical formula. Also, we restrict our study to the case $\beta_O = \beta_M = \beta$. In this case, $\bar{F}^{a}_{FD}(\beta) = e^{-p\lambda d^2 \Psi \kappa \beta^{\delta}}$ where $\kappa = \frac{3}{2} + \frac{(\delta-1)}{2^{\delta+1}}$.

One can note that in both IBFD and IBHD cases, the two-way spectral efficiency can be written in the form $\mathcal{S}(p) = c_1 p e^{-c_2 p}$. This function admits a single maximum for $p = \frac{1}{c_2}$. From this result, we deduce that for IBFD, the optimal p, denoted p^{*}_{FD}, is given by $p^{*}_{FD} = (\lambda d^2 \Psi \kappa \beta^{\delta})^{-1}$. For the case of IBHD, we have similarly $p^{*}_{HD} = (\lambda d^2 \Psi \beta^{\delta})^{-1}$. Replacing p by p^{*}_{FD} and p^{*}_{HD} in the expressions of $\mathcal{S}_{FD}$ and $\mathcal{S}_{HD}$, respectively, leads the inequality $\mathcal{S}_{FD} > \mathcal{S}_{HD}$ to be equivalent to $\kappa < 2$, which is true for all positive α. We conclude that IBFD with ideal SIC can always outperforms IBHD, provided that optimal MAC is employed.

In the case of IBFD with imperfect SIC, p^{*}_{FD} does not take a simple closed form. Nevertheless, assuming p^{*}_{HD} is used in the IBHD case, the condition for $\mathcal{S}_{FD} > \mathcal{S}_{HD}$ is then equivalent to

$$p\lambda d^2 \Psi \beta^{\delta} e^{-d^{\nu} S\beta - p\lambda d^2 \Psi \kappa \beta^{\delta}} > \frac{e^{-1}}{2(1-\rho_{SI})} \tag{5.24}$$

which is better understood by means of numerical analysis. In figure 5-8, we plot the maximum β satisfying (5.24) against α for various $\hat{d}_{ref}$ and p. We observe that for high reflection levels (i.e low $\hat{d}_{ref}$), contrarily to what may be expected, IBFD does not outperforms IBHD in environment with high α (i.e $\alpha > 4$), no matter the value of p. This is due to the impact of the residual self-interference. However, for low reflection level (and thus, low residual self-interference), the range of values of β over which IBFD outperforms IBHD expands linearly (in decibel scale) with α, with a slope proportional to $\hat{d}_{ref}$. Also, we note that IBFD benefits more from low values of p when α is low and benefits more from high values of p

when α is large. This observation confirms the intuition that IBFD benefits more from the increased spatial reuse created by a higher path-loss exponent than IBHD does.

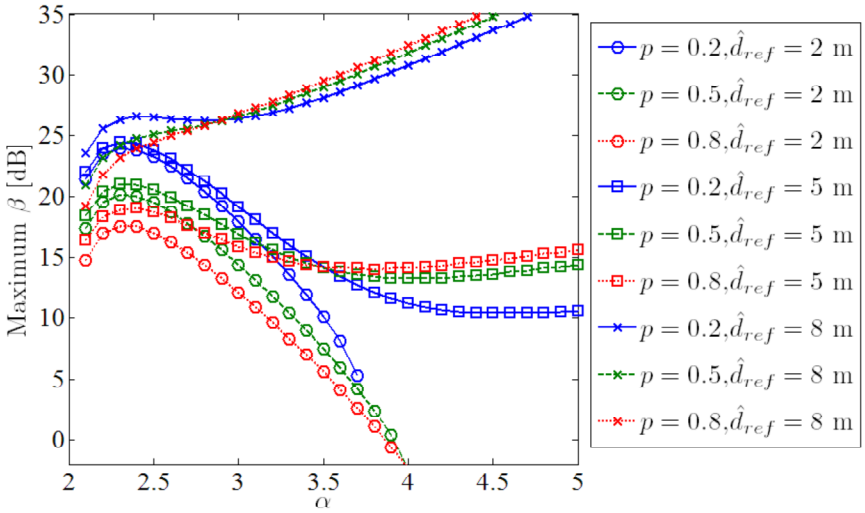

Figure 5-8: Maximum β satisfying (5.24) against the path-loss exponent α.

5.5 Conclusion

In this chapter, we presented an in-depth stochastic analysis of two-way transmissions in an IBFD ad hoc network. IBFD radios can transmit and receive at the same time on the same frequency band. Applied to ad hoc networks, this technology has two main effects each with opposite influences on the performance: on one hand, the average network throughput could be doubled (since nodes transmit twice more often); on the other, the interference in the network is doubled. In this work, we analyzed this trade-off, which has so far been overlooked in the literature. Firstly, we determined a tight lower bound on the joint probability of success of a two-way transmission in an IBFD ad hoc network. Both cases of ideal and imperfect Self-Interference Cancellation (SIC) were investigated. We then compared the performances of an IBFD transmission to the half-duplex case and determined the environmental and network conditions in which IBFD technology provides the best spectral efficiency. Our theoretical results, confirmed by comparison to simulated data, provide key insights regarding the design of two-way transmissions in IBFD ad hoc networks, which can be summarized as follows. 1)IBFD with ideal SIC can always outperform In-Band Half

Duplex (IBHD), provided optimal MAC parametrization. 2) When imperfect SIC is considered in environments with high reflection levels, an increasing path-loss exponent leads to a deterioration of IBFD performances, which is quickly outperformed by IBHD. 3) On the contrary, in environments with low reflection levels, IBFD with imperfect SIC benefits from the reduced inter-node interference of the high path-loss exponent regime and, in this case, outperforms IBHD over a large range of target transmission rates.

Chapter 6

Conclusion

In this thesis, we have presented a stochastic analysis of various medium access control and communication mechanisms in wireless ad hoc networks. The analysis was based mathematically on the theory of multidimensional point processes. The mechanisms under study included a half-duplex single handshake, half-duplex multiple successive handshakes as well as a full-duplex two-way communication. The numerous closed form expressions derived enable to relate network and environment parameters to network performances. Their numerical analysis provided important practical insights regarding medium access control design and performance optimization in wireless ad hoc networks. In more details, the contribution of each chapter of the thesis was as follows.

In chapter 2, we analyzed the probability of success of a transmission (one-way and handshake) to the k-th nearest neighbour in an ad hoc network modelled by a single homogeneous Poisson Point Process in which nodes employ the Slotted-ALOHA MAC protocol (without and with acknowledgement, respectively). The proposed approach enables to derive spatially averaged network performances at the routing level while tackling directly the dependency between both transmit directions in handshakes. We compared the developed close-form formula with computer simulation results and concluded that our results can find applications in the joint quantitative study of some MAC and routing protocols. Notably, exploiting the notion of neighbour index, we confirmed through our results the intuitive fact that imperfect feedback in handshakes is only negligible for transmissions to/from the closest neighbour.

Nevertheless, the use of the single HPPP as a deployment model limits the tractability of the theoretical results obtained by mathematical analysis. Therefore, in order to study the more complex four-way handshake, we opted for a more tractable HPPP-based model.

Then, in chapter 3, we presented a stochastic analysis a simple medium access control scheme including a random test followed by a four-way handshake (one control handshake without spatial reservation and one traffic handshake). This combination of contention mechanisms which recently appeared in the literature had so far been studied only by means of simulation. Our new mathematical framework takes into account time-varying channel impairments, interference, distinct decoding requirements for each packets as well as imperfect feedback. All our results were confirmed by comparison to simulated data and led us to two general conclusions. In the presence of fading uncorrelated between traffic and control handshakes, we observe the following. 1) Optimal contention is achieved by designing control packets decodable even in the presence of strong interference. 2) The impact of imperfect feedback on performances in an interference-limited mobile ad hoc network is not negligible.

An other aspect which is of importance in a four-way handshake is the potential use of diversity in the transmission of control packets. This subject was treated in the next chapter. Indeed, in chapter 4, keeping the same system model as in chapter 3 but assuming error-free feedback for tractability, we obtained a closed form expression of the mean effective link throughput (MELT) for the case with control packet diversity implemented through multiple frequency bands in a block-fading channel. Our results, confirmed by comparison to simulated data, provided the following important insights regarding contention in mobile ad hoc networks. In the presence of uncorrelated fading between control and traffic handshakes and given a fixed transmit-energy constraint: 1) as the diversity order increases, the diversity gain becomes counterbalanced by the loss due to increased control packet duration; hence the existence of an optimal diversity order value. 2) The design of MELT-optimal decoding requirements for the control packets is strongly influenced by the order of the control packet diversity.

Taking into account the development of new technologies, we also presented in chapter 5 an in-depth stochastic analysis of two-way transmissions in an IBFD ad hoc network.

IBFD radios can transmit and receive at the same time on the same frequency band. Applied to ad hoc networks, this technology has two main effects each with opposite influences on the performance: on one hand, the average network throughput could be doubled; on the other, the interference inherent to ad hoc deployments is doubled. In this chapter, we analyzed this trade-off, which has so far been overlooked in the literature. Firstly, we determined a tight lower bound and a tractable yet accurate approximation of the joint probability of success of a two-way transmission in an IBFD ad hoc network. Both cases of ideal and imperfect SIC were investigated. We then compared the performances of an IBFD transmission to the half-duplex case and determined the environmental and network conditions in which IBFD technology provides the best spectral efficiency. Our theoretical results, confirmed by comparison to simulated data, provided key insights regarding the design of two-way transmissions in IBFD ad hoc networks, which can be summarized as follows. Assuming optimal MAC parametrization: 1) IBFD with ideal SIC always outperform In-Band Half Duplex (IBHD), 2) nevertheless, IBFD with imperfect SIC outperforms IBHD over a large range of target information rates in environments with low path-loss exponent, even in the presence of high levels of residual self-interference. 3) On the contrary, in environments with large path-loss exponents, the performance of IBFD with imperfect SIC is very sensitive to variations in the level of residual self-interference. We conclude that self-interference from reflections in the environment is particularly problematic for indoor applications using IBFD two-way transmissions but does not represent a key limiting factor in open, free space environments.

There are several problems which have not been investigated in our study and remain open for future research. Noteworthy research directions include the investigation of the impact of multiple antenna techniques and various channel models on the mechanisms studied in the present thesis. Also, it is of great interest to expand the study of network mechanisms to more complex networks (e.g multi-tiered network, heterogeneous deployments, etc.) so as to provide relevant theoretical insights for the development of future generations of wireless networks.

Appendix A

Proofs for Chapter 2

A.1

In this appendix, we provide the proof of (2.3). From [30] (eq.(4)), we have

$$L_I(s) = \left(\frac{d}{B^d - A^d} \int_A^B x^{d-1} L_G\left(sx^{-\alpha}\right) dx \right)^k \tag{A.1}$$

The Laplace transform of the squared fading is given by

$$L_G(s) = \frac{1}{1+s} \tag{A.2}$$

Replacing the above in (A.1), leads to the integral given by

$$\begin{aligned} J &= \int_A^B \frac{x^{d-1} dx}{1 + sx^{-\alpha}} \\ &= \int_A^B u(x)\, dx \\ &= \int_0^B u(x)\, dx - \int_0^A u(x)\, dx \end{aligned} \tag{A.3}$$

Note that through the variable substitution $t = 1 - \left(\frac{x}{y}\right)^{\alpha}$, each of the integrals in the right-hand side of the last line of (A.3) can also be expressed as

$$\int_0^y u(x)\,dx = \frac{y^d \int_0^1 (1-t)^{\frac{d}{\alpha}} \left(1 - \frac{1}{1+sy^{-\alpha}}t\right)^{-1} dt}{\alpha\left(1+sy^{-\alpha}\right)} \tag{A.4}$$

where y takes the value A or B. One can recognize in (A.4) Euler's integral transform for the Gauss hypergeometric function[43], given by (A.5).

$$F(a,b,c,z) = \frac{\int_0^1 t^{b-1}(1-t)^{c-b-1}(1-zt)^{-a}\,dt}{B(b,c-b)} \tag{A.5}$$

where $B(a,b)$ is the Beta function and $F(a,b;c;z)$ denotes the Gauss hypergeometric function. It then follows that

$$\int_0^y u(x)\,dx = \frac{y^d F\left(1,1,2+\frac{d}{\alpha},\frac{1}{1+sy^{-\alpha}}\right)}{(\alpha+d)\left(1+sy^{-\alpha}\right)} \tag{A.6}$$

Then, one can use the following identity for $z = \frac{sx^{-\alpha}}{1+sx^{-\alpha}}$ to relate the above result to the function $\Omega(s,X)$ as defined earlier in the paper

$$\begin{aligned}&\frac{F\left(1,1,2+\frac{d}{\alpha},1-z\right)(1-z)^{\frac{d}{\alpha}}}{1+\frac{d}{\alpha}} = \\ &F\left(1,1,1-\frac{d}{\alpha},z\right)(1-z) - B\left(1-\frac{d}{\alpha},1+\frac{d}{\alpha}\right)\left(\frac{z}{1-z}\right)^{\frac{d}{\alpha}}\end{aligned} \tag{A.7}$$

Using (A.7) and (A.6) in (A.1) leads to the final result, which completes the proof.

A.2

In this appendix we provide the proof of (2.5). We first notice from the properties of the Gauss Hypergeometric function that for $c-a-b<0$, we have [43]

$$\lim_{z\to 1^-} \frac{F(a,b,c,z)}{(1-z)^{c-a-b}} = \frac{\Gamma(c)\,\Gamma(a+b-c)}{\Gamma(a)\,\Gamma(b)} \tag{A.8}$$

Then, using (2.4), let us rephrase $A^d\Omega(s,A)$ as

$$A^d\Omega(s,A) = A^d f(s,A)\left(1-\frac{s}{s+1A^\alpha}\right)^{-\frac{d}{\alpha}} - A^d$$
$$- B\left(1-\frac{d}{\alpha},1+\frac{d}{\alpha}\right)s^{\frac{d}{\alpha}} \tag{A.9}$$

where $f(s,A) = F\left(1,1,1-\frac{d}{\alpha},\frac{s}{1A^\alpha+s}\right)\left(1-\frac{s}{s+1A^\alpha}\right)^{1+\frac{d}{\alpha}}$ We observe that by setting $z=\frac{s}{s+1A^\alpha}$ and $a=1,b=1,c=1-\frac{d}{\alpha}$, we obtain easily the limit of $f(s,A)$ for A converging toward zero from (A.8). The final result then follows as

$$\lim_{A\to 0^+} A^d\Omega(s,A) = 0 \tag{A.10}$$

which completes the proof.

A.3

In this appendix we provide the proof of (2.6). From [29] (section 3.7.1), we have

$$L_{I_{\mathbb{R}^d/\mathcal{B}(O,x)}}(s) =$$
$$e^{-\lambda c_d \mathbb{E}_G\left\{s^{\frac{d}{\alpha}}G^{\frac{d}{\alpha}}\gamma\left(1-\frac{d}{\alpha},sGx^{-\alpha}\right)-x^d\left(1-e^{-sGx^{-\alpha}}\right)\right\}} \tag{A.11}$$

where $\gamma(n,x)$ denotes the lower incomplete gamma function. Let us rephrase part of the above expression as follows.

$$\mathbb{E}_G\left\{G^{\frac{d}{\alpha}}\gamma\left(1-\frac{d}{\alpha},sGx^{-\alpha}\right)\right\} =$$
$$\int_0^{+\infty}\frac{1}{\Gamma(1)}t^{\frac{d}{\alpha}}\gamma\left(1-\frac{d}{\alpha},tsx^{-\alpha}\right)e^{-1t}dt \tag{A.12}$$

The above integral can be solved by replacing initially the incomplete lower gamma function by its equivalent involving the Kummer's confluent hypergeometric function.[43] That

is,

$$\gamma\left(1-\frac{d}{\alpha},tsx^{-\alpha}\right)=\frac{e^{-tsx^{-\alpha}}M\left(1,2-\frac{d}{\alpha},tsx^{-\alpha}\right)}{\left(1-\frac{d}{\alpha}\right)\left(tsx^{-\alpha}\right)^{\frac{d}{\alpha}-1}} \tag{A.13}$$

which is valid only for $tsx^{-\alpha}>0$. Then, replacing (A.13) into (A.12) reveals an integral form of the Gauss Hypergeometric function given by

$$F\left(a,b,c,z\right)=\frac{1}{\Gamma\left(b\right)}\int_{0}^{+\infty}e^{-t}t^{b-1}M\left(a,c,tz\right)dt \tag{A.14}$$

which is valid only for $b>0$. Therefore, it follows that

$$\begin{aligned}&\mathbb{E}_G\left\{G^{\frac{d}{\alpha}}\gamma\left(1-\frac{d}{\alpha},sGx^{-\alpha}\right)\right\}=\\&\frac{\left(sx^{-\alpha}\right)^{1-\frac{d}{\alpha}}F\left(1,2,2-\frac{d}{\alpha},\frac{sx^{-\alpha}}{1+sx^{-\alpha}}\right)}{\left(1-\frac{d}{\alpha}\right)\left(1+sx^{-\alpha}\right)^{2}}\\&=\frac{zs^{-\frac{d}{\alpha}}x^{d}}{\left(1-\frac{d}{\alpha}\right)}F\left(1,2,2-\frac{d}{\alpha},z\right)(1-z)\end{aligned} \tag{A.15}$$

where $z=\frac{sx^{-\alpha}}{1+sx^{-\alpha}}$. Note that using the same notation, we have

$$\mathbb{E}_G\left\{1-e^{-sGx^{-\alpha}}\right\}=1-(1-z) \tag{A.16}$$

Using the recurrence relations of the Hypergeometric function, one can obtain the following identity

$$F\left(1,b,c,t\right)=\frac{c-1}{b-1}\left(\frac{F\left(1,b-1,c-1,t\right)}{t}-\frac{1}{t}\right) \tag{A.17}$$

which, by setting $b=2$, $c=2-\frac{d}{\alpha}$ and $t=z=\frac{sx^{-\alpha}}{1+sx^{-\alpha}}$ lead us to

$$\begin{aligned}&\mathbb{E}_G\left\{G^{\frac{d}{\alpha}}\gamma\left(1-\frac{d}{\alpha},sGx^{-\alpha}\right)\right\}=\\&s^{-\frac{d}{\alpha}}x^{d}\left(F\left(1,1,1-\frac{d}{\alpha},z\right)-1\right)(1-z)\end{aligned} \tag{A.18}$$

Replacing (A.18) and (A.16) into (A.11) we obtain

$$L_{I_{\mathbb{R}^d/\mathcal{B}(O,x)}}(s) = \exp\left(-\lambda c_d x^d \left(F\left(1,1,1-\frac{d}{\alpha},z\right)(1-z)-1\right)\right) \tag{A.19}$$

which can be expressed as a function of $\Omega(s,x)$ as defined in (2.4) and thus completes the proof.

A.4

In this appendix, we prove that the p.m.f in (2.7) satisfies the normalization condition. That is, we aim to prove that

$$S_k = \sum_{n=1}^{\infty} \mathcal{F}(n,k) = 1 \tag{A.20}$$

To do so, we start by reordering the double sum above into

$$S_k = \sum_{l=0}^{k-1} \sum_{n=l+1}^{\infty} \binom{k-1}{l} \binom{n+k-l-2}{k-1} \frac{\beta_d^l (1-\beta_d)^{n+k-2l-2}}{(2-\beta_d)^{n+k-l-1}} \tag{A.21}$$

which is obtained simply by interverting sum indexes after making the term $\min(n,k)$ disappear. Then, sorting terms and using the change of index $n = n' + l + 1$, we obtain

$$S_k = \frac{1}{1-\beta_d} \left(\frac{1-\beta_d}{2-\beta_d}\right)^k \sum_{l=0}^{k-1} \binom{k-1}{l} \left(\frac{\beta_d}{1-\beta_d}\right)^l \sum_{n=0}^{\infty} \binom{n+k-1}{n} \left(\frac{1-\beta_d}{2-\beta_d}\right)^n \tag{A.22}$$

Using the binomial theorem and recognizing the series expansion of the function $(1-x)^{-k}$ in the second sum, we can transform the above into

$$S_k = \frac{1}{1-\beta_d}\left(\frac{1-\beta_d}{2-\beta_d}\right)^k \frac{1}{(1-\beta_d)^{k-1}}(2-\beta_d)^k = 1 \tag{A.23}$$

which completes the proof, for all $k \geq 1$.

A.5

In this appendix we provide a justification for the approximation of $\Omega(s,X)$ provided in (2.33). Let us define $z = \frac{sX^{-\alpha}}{1+sX^{-\alpha}}$. We can then define the single-variate version of $\Omega(s,X)$

$$\begin{aligned}\Omega(z) &= F\left(1,1,1-\frac{d}{\alpha},z\right)(1-z)-1 \\ &- B\left(1-\frac{d}{\alpha},1+\frac{d}{\alpha}\right)\left(\frac{z}{1-z}\right)^{\frac{d}{\alpha}}\end{aligned} \tag{A.24}$$

which is strictly positive on $]0,1[$ and such that $\Omega(0)=0$. Now let us define

$$g(z) = \left((1-z)^{-\frac{d}{\alpha}} - \left(\frac{z}{1-z}\right)^{\frac{d}{\alpha}} - 1\right) B\left(1-\frac{d}{\alpha},1+\frac{d}{\alpha}\right) \tag{A.25}$$

Note that $g(z)$ and $\Omega(z)$ have same value at 0 and, from (A.8), same limit at 1^-. Now let us define $h(z) = \frac{\Omega(z)-g(z)}{\Omega(z)}$. Since $h(z)$ is a strictly decreasing positive function on $]0,1[$, its maximum is

$$h(0) = \lim_{z\to 0^+} h(z) = 1 - B\left(1-\frac{d}{\alpha},1+\frac{d}{\alpha}\right)\left(1-\frac{d}{\alpha}\right) \tag{A.26}$$

which can be obtained using l'Hospital's rule. Consequently, we conclude that $g(z)$ can be seen as a lower bound of $\Omega(z)$ with a relative difference to the actual function at most equal to $h(0)$. As an example, for $d=2$, $\alpha=4$ and $\rho=1$ we have $h(0)\approx 0.21$. Thus, practically $g(z)$ may be used as a reasonable approximation of $\Omega(z)$.

A.6

In this appendix we give a description of the simulations. Let us consider first the "single HPPP" model. We assume the MAC layer splits the nodes into two independent HPPPS: one for active transmitters, one for silent nodes. This actually models well the impact of the MAC protocol Slotted-ALOHA (see [5]). We select randomly among the silent nodes an intended receiver (denoted Rx) and assume its nearest neighbour as intended transmitter (denoted Tx). That is, we condition the system on the nearest neighbour of Rx being a transmitter. We run a Monte-Carlo simulation using the same channel model as in [29] and record the interference power at Rx. Then, in a different simulation for the "HPPP+1" model, we record the interference power at the center of a HPPP of same intensity as the transmitter set in the first simulation.

Appendix B

Proofs for Chapter 3

B.1

In this appendix, we provide a proof for the integral in (3.7). Through some algebraic manipulations, we can express the integrand $g(t)$ as

$$\frac{\bar{P}_{fwt->D}\theta_D r^{\alpha} t^{\alpha(n+l)+1}}{\left(t^{\alpha}+\theta_{fwt}r^{\alpha}\right)^{n+l}\left(t^{\alpha}+\theta_D r^{\alpha}\right)}+\frac{\sum_{i=0}^{n+l-1}\binom{n+l}{i}\left(\theta_{fwt}r^{\alpha}\right)^{n+l}t^{\alpha i+1}}{\left(\theta_{fwt}r^{\alpha}\right)^{i}\left(t^{\alpha}+\theta_{fwt}r^{\alpha}\right)^{n+l}} \tag{B.1}$$

Let us consider the integral $J(y)$ with general parameters u, v, w satisfying $u-\alpha(v+w)<-1$.

$$J(y)=\int_0^y \frac{t^u dt}{\left(t^{\alpha}+\theta_{fwt}r^{\alpha}\right)^{v}\left(t^{\alpha}+\theta_D r^{\alpha}\right)^{w}} \tag{B.2}$$

Recognizing $J(y)$ as the integral form of a well-known function, we have the following development.

$$
\begin{aligned}
J &= \frac{y^{u+1}}{\alpha\left(y^{\alpha}+\theta_{fwt}r^{\alpha}\right)^{v}\left(y^{\alpha}+\theta_{D}r^{\alpha}\right)^{w}}\int_{0}^{1}\frac{(1-s)^{\frac{u+1}{\alpha}-1}\,ds}{\left(1-z_{fwt}s\right)^{v}\left(1-z_{D}s\right)^{w}} \\
&\overset{(a)}{=} \frac{y^{u+1}F_{1}\left(1,v,w,\frac{u+1}{\alpha}+1,z_{fwt},z_{D}\right)}{(u+1)\left(y^{\alpha}+\theta_{fwt}r^{\alpha}\right)^{v}\left(y^{\alpha}+\theta_{D}r^{\alpha}\right)^{w}} \\
&\overset{(b)}{=} \begin{cases} \dfrac{F_{1}\left(\frac{u+1}{\alpha},1+\frac{u+1}{\alpha}-v-w,w,1+\frac{u+1}{\alpha},\frac{y^{\alpha}}{y^{\alpha}+\theta_{fwt}r^{\alpha}},\frac{\theta_{D}r^{\alpha}-\theta_{fwt}r^{\alpha}}{\theta_{D}r^{\alpha}+\theta_{D}r^{\alpha}\theta_{fwt}r^{\alpha}y^{-\alpha}}\right)}{(u+1)\left(\theta_{fwt}r^{\alpha}\right)^{v-\frac{u+1}{\alpha}}(\theta_{D}r^{\alpha})^{w}\left(1+\theta_{fwt}r^{\alpha}y^{-\alpha}\right)^{-\frac{u+1}{\alpha}}} & \theta_{fwt}\leq\theta_{D} \\ \dfrac{F_{1}\left(\frac{u+1}{\alpha},v,1+\frac{u+1}{\alpha}-v-w,1+\frac{u+1}{\alpha},\frac{\theta_{fwt}r^{\alpha}-\theta_{D}r^{\alpha}}{\theta_{fwt}r^{\alpha}+\theta_{D}r^{\alpha}\theta_{fwt}r^{\alpha}y^{-\alpha}},\frac{y^{\alpha}}{y^{\alpha}+\theta_{D}r^{\alpha}}\right)}{(u+1)\left(\theta_{fwt}r^{\alpha}\right)^{v}(\theta_{D}r^{\alpha})^{w-\frac{u+1}{\alpha}}(1+\theta_{D}r^{\alpha}y^{-\alpha})^{-\frac{u+1}{\alpha}}} & \theta_{fwt}\geq\theta_{D} \end{cases}
\end{aligned}
\tag{B.3}
$$

In the above, the first line follows from the variable substitution $u = 1-\left(\frac{t}{y}\right)^{\alpha}$ and the definition of $z_{fwt} = \frac{y^{\alpha}}{y^{\alpha}+\theta_{fwt}r^{\alpha}}$ and $z_{D} = \frac{y^{\alpha}}{y^{\alpha}+\theta_{fwt}r^{\alpha}}$. Then (a) is obtained by recognizing the integral form of the Appell hypergeometric function F_1 in the first line (see equation (16.15.1) in [18]).

Appendix C

Proofs for Chapter 4

C.1

In this appendix,we provide the proof for (5.7). For a given fixed position x of X_n, H_n is the maximum of two independent random variables. Therefore, its Cumulative Probability Function (CDF) is given by the product of their marginal CDFs as follows.

$$F_{H_n}(h) = \left(1 - e^{-\frac{h}{\theta_O l_O(x)}}\right)\left(1 - e^{-\frac{h}{\theta_M l_M(x)}}\right) \tag{C.1}$$

Taking the derivative of the above with respect to h trivially leads to the probability density function $f_{H_n}(h)$ of H_n given by

$$\begin{aligned} f_{H_n}(h) = & \frac{e^{-\frac{h}{\theta_O l_O(x)}}\left(1 - e^{-\frac{h}{\theta_M l_M(x)}}\right)}{\theta_O l_O(x)} \\ & + \frac{e^{-\frac{h}{\theta_M l_M(x)}}\left(1 - e^{-\frac{h}{\theta_O l_O(x)}}\right)}{\theta_M l_M(x)} \end{aligned} \tag{C.2}$$

Then, calculating $\mathbb{E}_{H_n}\left\{e^{-d^{\psi}H_n}\right\}$ leads to an integral of the form $\int e^{-hQ}dh$, where Q is independent of h, which can be solved easily and directly leads to the final result.

C.2

In this appendix, we provide the proof of equation (5.13). Proving the final result is equivalent to solving a special case of the integral $\int_0^\infty \frac{t^u}{(t^\alpha+A)^v(t^\alpha+B)^w}$ where $A > B$. To proceed, let us first consider the finite integral $J(y)$ defined as follows.

$$J(y) = \int_0^y \frac{t^u}{(t^\alpha + A)^v (t^\alpha + B)^w} \tag{C.3}$$

Through the variable substitution $s = 1 - \frac{t^\alpha}{y^\alpha}$ and a few simple manipulations, one may express $J(y)$ in the following form

$$\begin{aligned} J(y) = \frac{y^{u+1}}{\alpha} \frac{1}{(A + y^\alpha)^v (B + y^\alpha)^w} \\ \int_0^1 \frac{(1-s)^{\frac{u+1}{\alpha}-1} ds}{\left(1 - \frac{y^\alpha}{A+y^\alpha} s\right)^v \left(1 - \frac{y^\alpha}{B+y^\alpha} s\right)^w} \end{aligned} \tag{C.4}$$

In the above equation, one can recognize the integral form of the Hypergeometric Appell's function given by

$$\begin{aligned} F_1(a, b_1, b_2, c, z_1, z_2) = \frac{\Gamma(c)}{\Gamma(a)\Gamma(c-a)} \\ \int_0^1 \frac{s^{a-1}(1-s)^{c-a-1} ds}{(1-z_1 s)^{b_1} (1-z_2 s)^{b_2}} \end{aligned} \tag{C.5}$$

Then, using the following transformations of the F_1 function (see [18], equation (16.16.8)),

$$\begin{aligned} &F_1(a; b_1, b_2; c; z_1, z_2) = \\ &(1-z_1)^{-b_1}(1-z_2)^{-b_2} F_1\left(c-a; b_1, b_2; c; \frac{z_1}{z_1-1}, \frac{z_2}{z_2-1}\right) \\ &= (1-z_1)^{-a} F_1\left(a; c-b_1-b_2, b_2; c; \frac{z_1}{z_1-1}, \frac{z_2-z_1}{1-z_1}\right) \end{aligned} \tag{C.6}$$

we can express $J(y)$ as

$$J(y) = \frac{F_1\left(\frac{u+1}{\alpha}, v, 1+\frac{u+1}{\alpha}-v-w, 1+\frac{u+1}{\alpha}, \frac{A-B}{A+ABy^{-\alpha}}, \frac{y^{\alpha}}{y^{\alpha}+B}\right)}{(u+1)A^{v}B^{w-\frac{u+1}{\alpha}}\left(1+By^{-\alpha}\right)^{-\frac{u+1}{\alpha}}} \tag{C.7}$$

Then, letting y tend to infinity in the above and using the property that $F_1(a, b_1, b_2, c, z, 1)$ is equal to the product ${}_2F_1(a, b_2, c, 1)\,{}_2F_1(a, b_1, c-b_2, z)$ of two Gauss hypergeometric ${}_2F_1$ functions together with the identity ${}_2F_1(a, b; c; 1) = \frac{\Gamma(c)\,\Gamma(c-a-b)}{\Gamma(c-a)\,\Gamma(c-b)}$ if $c-a-b > 0$, we obtain the following limit.

$$\lim_{y\to+\infty} J(y) = \frac{\Gamma\left(1+\frac{u+1}{\alpha}\right)\Gamma\left(v+w-\frac{u+1}{\alpha}\right){}_2F_1\left(\frac{u+1}{\alpha}, v, v+w, 1-\frac{B}{A}\right)}{(u+1)\,\Gamma(v+w)\,A^{v}B^{w-\frac{u+1}{\alpha}}} \tag{C.8}$$

Then, from [18] (equation (15.4.23)), we note that for $c-a-b < 0$ the Gauss Hypergeometric function ${}_2F_1(a, b, c, z)$ can be reasonably approximated by $1+\frac{\Gamma(c)\Gamma(a+b-c)}{\Gamma(a)\Gamma(b)}\left((1-z)^{c-a-b}-1\right)$. Then using this last approximation and substituting $v = 1$, $w = 1$, $u = \alpha+1$, $A = \frac{1}{\theta_O}+\frac{1}{\theta_M}$ and $B = \frac{1}{\theta_M}$ in the above, we obtain the final result, which completes the proof.

Bibliography

[1] Norman Abramson. The aloha system: Another alternative for computer communications. In *Proceedings of the November 17-19, 1970, Fall Joint Computer Conference*, AFIPS '70 (Fall), pages 281–285, New York, NY, USA, 1970. ACM.

[2] G. Alfano, M. Garetto, and E. Leonardi. New insights into the stochastic geometry analysis of dense csma networks. In *INFOCOM, 2011 Proceedings IEEE*, pages 2642–2650, April.

[3] J.G. Andrews, R.K. Ganti, M. Haenggi, N. Jindal, and S. Weber. A primer on spatial modeling and analysis in wireless networks. *Communications Magazine, IEEE*, 48(11):156 –163, november 2010.

[4] Weng Chon Ao and Kwang-Cheng Chen. Bounds and exact mean node degree and node isolation probability in interference-limited wireless ad hoc networks with general fading. *Vehicular Technology, IEEE Transactions on*, 61(5):2342–2348, 2012.

[5] F. Baccelli, B. Blaszczyszyn, and P. Muhlethaler. An aloha protocol for multihop mobile wireless networks. *Information Theory, IEEE Transactions on*, 52(2):421 – 436, feb. 2006.

[6] F. Baccelli, Bartlomiej Blaszczyszyn, and P. Muhlethaler. Stochastic analysis of spatial and opportunistic aloha. *Selected Areas in Communications, IEEE Journal on*, 27(7):1105–1119, 2009.

[7] F. Baccelli, Bartlomiej Blaszczyszyn, and P. Muhlethaler. Stochastic analysis of spatial and opportunistic aloha. *Selected Areas in Communications, IEEE Journal on*, 27(7):1105–1119, September.

[8] Jan Beutel, Kay Römer, Matthias Ringwald, and Matthias Woehrle. Wireless sensor network deployments. In G. Ferrari, editor, *Sensor Networks: Where Theory Meets Practice*, Heidelberg, 2009. Springer.

[9] G. Bianchi. Performance analysis of the ieee 802.11 distributed coordination function. *Selected Areas in Communications, IEEE Journal on*, 18(3):535 –547, march 2000.

[10] Thomas Bourgeois and Shigeru Shimamoto. Stochastic analysis of handshake-type mechanisms in uniformly random wireless ad hoc networks. In *Global Communications Conference (GLOBECOM), 2013 IEEE*, pages 158–163, Dec 2013.

[11] Yegui Cai, F.R. Yu, Jun Li, Yifeng Zhou, and L. Lamont. Mac performance improvement in uav ad-hoc networks with full-duplex radios and multi-packet reception capability. In *Communications (ICC), 2012 IEEE International Conference on*, pages 523–527, June 2012.

[12] Yegui Cai, F.R. Yu, Jun Li, Yifeng Zhou, and L. Lamont. Medium access control for unmanned aerial vehicle (uav) ad-hoc networks with full-duplex radios and multi-packet reception capability. *Vehicular Technology, IEEE Transactions on*, 62(1):390–394, Jan 2013.

[13] G. Caire, Giorgio Taricco, and Ezio Biglieri. Optimum power control over fading channels. *Information Theory, IEEE Transactions on*, 45(5):1468–1489, 1999.

[14] Wenli Chen, N. Jain, and S. Singh. Anmp: ad hoc network management protocol. *Selected Areas in Communications, IEEE Journal on*, 17(8):1506–1531, Aug 1999.

[15] W. Crowther, R. Rettberg, D. Walden, S. Ornstein, and E Heart. A system for broadcast communication: reservation-aloha. In *Hawaii International Conference on System Sciences*, 1973.

[16] D.J. Daley and D. Vere-Jones. *An Introduction to the Theory of Point Processes*. Springer Series in Statistics, 1988.

[17] Haichuan Ding, Shaodan Ma, Chengwen Xing, Zesong Fei, Yiqing Zhou, and C.L.P. Chen. Analysis of hybrid arq in ad hoc networks with correlated interference and feedback errors. *Wireless Communications, IEEE Transactions on*, 12(8):3942–3955, 2013.

[18] NIST Digital Library of Mathematical Functions. http://dlmf.nist.gov/, Release 1.0.8 of 2014-04-25. Online companion to [43].

[19] Weihuang Fu and D.P. Agrawal. Capacity of hybrid wireless mesh networks with random aps. *Mobile Computing, IEEE Transactions on*, 12(1):136–150, Jan 2013.

[20] R.K. Ganti, J.G. Andrews, and M. Haenggi. High-sir transmission capacity of wireless networks with general fading and node distribution. *Information Theory, IEEE Transactions on*, 57(5):3100–3116, 2011.

[21] Y. George and I. Bergel. The spectral efficiency of slotted csma ad-hoc networks with directional antennas. *Wireless Communications, IEEE Transactions on*, 11(10):3799 –3809, october 2012.

[22] J.C. Haartsen. The bluetooth radio system. *Personal Communications, IEEE*, 7(1):28–36, Feb 2000.

[23] Z.J. Haas, M. Gerla, D.B. Johnson, C.E. Perkins, M.B. Pursley, M. Steenstrup, C.-K. Toh, and J.F. Hayes. Guest editorial wireless ad hoc networks. *Selected Areas in Communications, IEEE Journal on*, 17(8):1329–1332, Aug 1999.

[24] M. Haenggi. Routing in ad hoc networks - a wireless perspective. In *Broadband Networks, 2004. BroadNets 2004. Proceedings. First International Conference on*, pages 652–660, 2004.

[25] M. Haenggi. A geometric interpretation of fading in wireless networks: Theory and applications. *Information Theory, IEEE Transactions on*, 54(12):5500–5510, 2008.

[26] M. Haenggi. Outage, local throughput, and capacity of random wireless networks. *Wireless Communications, IEEE Transactions on*, 8(8):4350–4359, 2009.

[27] M. Haenggi. Diversity loss due to interference correlation. *Communications Letters, IEEE*, 16(10):1600–1603, 2012.

[28] M. Haenggi. The local delay in poisson networks. *Information Theory, IEEE Transactions on*, 59(3):1788–1802, 2013.

[29] M. Haenggi and R. K. Ganti. Interference in large wireless networks. *Foundations and Trends in Networking*, (2):127 –248, 2009.

[30] M. Haenggi and S. Srinivasa. Modeling interference in finite uniformly random networks. *Proc. International Workshop on Information Theory for Sensor Networks (WITS'07)*, 2007.

[31] S. Hong, J. Brand, Jung Choi, M. Jain, J. Mehlman, S. Katti, and P. Levis. Applications of self-interference cancellation in 5g and beyond. *Communications Magazine, IEEE*, 52(2):114–121, February 2014.

[32] H. Inaltekin, Mung Chiang, H.V. Poor, and S.B. Wicker. On unbounded path-loss models: effects of singularity on wireless network performance. *Selected Areas in Communications, IEEE Journal on*, 27(7):1078–1092, September.

[33] A. Iwata, Ching-Chuan Chiang, Guangyu Pei, M. Gerla, and Tsu-Wei Chen. Scalable routing strategies for ad hoc wireless networks. *Selected Areas in Communications, IEEE Journal on*, 17(8):1369–1379, Aug 1999.

[34] E. T. Jaynes. Information theory and statistical mechanics. *Physical Review*, 106:620 – 630, May 1957.

[35] E. T. Jaynes. Information theory and statistical mechanics. *Physical Review*, 108:171 – 191, Oct. 1957.

[36] M. Kaynia, F. Fabbri, R. Verdone, and G.E. Oien. Analytical study of the outage probability of aloha and csma in bounded ad hoc networks. In *Wireless Conference (EW), 2010 European*, pages 544 –550, april 2010.

[37] D. Kim, S. Park, H. Ju, and D. Hong. Transmission capacity of full-duplex based two-way ad-hoc networks with arq protocol. *Vehicular Technology, IEEE Transactions on*, PP(99):1–1, 2014.

[38] M. Levorato and M. Zorzi. On the performance of ad hoc networks with multiuser detection, rate control and hybrid arq. *Wireless Communications, IEEE Transactions on*, 8(6):2938–2949, 2009.

[39] C.R. Lin and Jain-Shing Liu. Qos routing in ad hoc wireless networks. *Selected Areas in Communications, IEEE Journal on*, 17(8):1426–1438, Aug 1999.

[40] Hui Ma, R. Vijayakumar, S. Roy, and Jing Zhu. Optimizing 802.11 wireless mesh networks based on physical carrier sensing. *Networking, IEEE/ACM Transactions on*, 17(5):1550–1563, Oct 2009.

[41] S. Malik, P. Jacquet, and C. Adjih. On the throughput capacity of wireless multi-hop networks with aloha, node coloring and csma. In *Wireless Days (WD), 2011 IFIP*, pages 1–6, Oct.

[42] D.A. Maltz, J. Broch, J. Jetcheva, and D.B. Johnson. The effects of on-demand behavior in routing protocols for multihop wireless ad hoc networks. *Selected Areas in Communications, IEEE Journal on*, 17(8):1439–1453, Aug 1999.

[43] F. W. J. Olver, D. W. Lozier, R. F. Boisvert, and C. W. Clark, editors. *NIST Handbook of Mathematical Functions*. Cambridge University Press, New York, NY, 2010.

[44] Theodore S. Rappaport. *Wireless Communications: Principles and Practice*. IEEE Press, Piscataway, NJ, USA, 1st edition, 1996.

[45] E.M. Royer and Chai-Keong Toh. A review of current routing protocols for ad hoc mobile wireless networks. *Personal Communications, IEEE*, 6(2):46–55, Apr 1999.

[46] S.P. Smith. Threshold validity for mutual neighborhood clustering. *Pattern Analysis and Machine Intelligence, IEEE Transactions on*, 15(1):89 –92, jan 1993.

[47] S. Srinivasa and M. Haenggi. Distance distributions in finite uniformly random networks: Theory and applications. *Vehicular Technology, IEEE Transactions on*, 59(2):940 –949, feb. 2010.

[48] K. Stamatiou and M. Haenggi. Random-access poisson networks: Stability and delay. *Communications Letters, IEEE*, 14(11):1035–1037, 2010.

[49] Guobao Sun, Fan Wu, Xiaofeng Gao, and Guihai Chen. Phed: Pre-handshaking neighbor discovery protocols in full duplex wireless ad hoc networks. In *Global Communications Conference (GLOBECOM), 2012 IEEE*, pages 584–590, Dec 2012.

[50] Guobao Sun, Fan Wu, Xiaofeng Gao, Guihai Chen, and Wei Wang. Time-efficient protocols for neighbor discovery in wireless ad hoc networks. *Vehicular Technology, IEEE Transactions on*, 62(6):2780–2791, July 2013.

[51] S. Toumpis and A.J. Goldsmith. New media access protocols for wireless ad hoc networks based on cross-layer principles. *Wireless Communications, IEEE Transactions on*, 5(8):2228 –2241, aug. 2006.

[52] R. Vaze. Throughput-delay-reliability tradeoff with arq in wireless ad hoc networks. *Wireless Communications, IEEE Transactions on*, 10(7):2142–2149, 2011.

[53] R. Vaze and R.W. Heath. Transmission capacity of ad-hoc networks with multiple antennas using transmit stream adaptation and interference cancellation. *Information Theory, IEEE Transactions on*, 58(2):780–792, 2012.

[54] R. Vaze, K.T. Truong, S. Weber, and R.W. Heath. Two-way transmission capacity of wireless ad-hoc networks. *Wireless Communications, IEEE Transactions on*, 10(6):1966–1975, 2011.

[55] Zhiguo Wan, Kui Ren, Bo Zhu, B. Preneel, and Ming Gu. Anonymous user communication for privacy protection in wireless metropolitan mesh networks. *Vehicular Technology, IEEE Transactions on*, 59(2):519–532, Feb 2010.

[56] Yueping Wu, R.H.Y. Louie, and M.R. McKay. Analysis and design of wireless ad hoc networks with channel estimation errors. *Signal Processing, IEEE Transactions on*, 61(6):1447–1459, March 2013.

[57] Shugong Xu and T. Saadawi. Does the ieee 802.11 mac protocol work well in multihop wireless ad hoc networks? *Communications Magazine, IEEE*, 39(6):130–137, 2001.

[58] Weiyi Zhao and Jiang Xie. Domain: A novel dynamic location management solution for internet-based infrastructure wireless mesh networks. *Parallel and Distributed Systems, IEEE Transactions on*, 24(8):1514–1524, Aug 2013.

[59] Lidong Zhou and Z.J. Haas. Securing ad hoc networks. *Network, IEEE*, 13(6):24–30, Nov 1999.

List of academic achievements

Category	
Articles in refereed journals	○Thomas Bourgeois, Shigeru Shimamoto, "Outage and Density of Transport of Four-Way Handshaking with Imperfect Feedback in a Mobile Multi-Hop Ad Hoc Network", IEICE Transactions on Communications, Vol.E97-B,No.12,pp.-,Dec. 2014. (forthcoming) ○Thomas Bourgeois, Shigeru Shimamoto, "Stochastic Analysis of Random Ad Hoc Networks with Maximum Entropy Deployment", International Journal on Wireless and Mobile Networks, Volume 6. Number 3, June 2014
Presentations at International conferences	○ Thomas Bourgeois, Shigeru Shimamoto, "Stochastic analysis of handshake-type mechanisms in uniformly random wireless ad hoc networks," Global Communications Conference (GLOBECOM), 2013 IEEE , vol., no., pp.158,163, 9-13 Dec. 2013 Thomas Bourgeois, Shigeru Shimamoto, "Stochastic analysis of Multi-slot ALOHA in poisson networks," Personal Indoor and Mobile Radio Communications (PIMRC), 2013 IEEE 24th International Symposium on , vol., no., pp.2082,2088, 8-11 Sept. 2013 Thomas Bourgeois, Shigeru Shimamoto, "Accirate subgraph probabilities in a Random Geometric Graph and application to cooperative multihop ad-hoc networks," Global Communications Conference (GLOBECOM), 2012 IEEE , vol., no., pp.506,511, 3-7 Dec. 2012